Modelling of hydrological extremes and rice irrigation optimization for decision support in Central Vietnam

Dissertation zur Erlangung des Doktorgrades an der
Fakultät für Angewandte Informatik der
Universität Augsburg

vorgelegt von

DANG **Quang Thinh**

2018

Erstes Gutachten: Prof. Dr. Harald Kunstmann
Zweites Gutachten: Prof. Dr. Peter Fiener

Tag der mündlichen Prüfung: 19. October 2018

Acknowledgements

The completion of this dissertation could not have been accomplished without the assistance and support of many people and institutions. I would therefore like to kindly offer my sincere thanks to all of them.

Firstly, I would like to express my heartfelt gratitude to my supervisor, Prof. Dr. Harald Kunstmann for accepting me as his PhD student working at the Institute of Meteorology and Climate Research, Karlsruhe Institute of Technology (KIT/IMK-IFU), for his patience and immense knowledge. Furthermore, you offered me a topic on the hydrological impact study which is of paramount importance and necessity for my country. It is my extreme privilege to do the research under your excellent supervision and constant support. Dear Prof. Kunstmann, what I have learned from you is not only the scientific knowledge, but also the dedication to the science.

Besides my supervisor, I am deeply indebted to my day-to-day advisor Dr. Patrick Laux for his fundamental role in my doctoral research. You gave me an opportunity to come to IMK-IFU and introduced me to Prof. Kunstmann. You are the pioneer on the novel direction to deal with my topic and you provided me with every bit of guidance, assistance, and expertise that I needed to carry out my research. You always provided me generous supports both in science and daily life during my stay in Garmisch-Partenkirchen. You motivated and challenged me with your encouragements and trust and you kept me going and raised me up during the most difficult times when doing my research. For me you are much more than a great advisor and I simply cannot express how much I own you and how much I highly appreciate things you have done for me. What I learned in working with you would undoubtedly continue to influence my career in years to come.

I would also like to sincerely thank Dr. Rui Pedroso at Institute for Technology and Resources Management in the Tropics and Subtropics (ITT), Cologne University of Applied Sciences for his great assistance and kind helps. I am very grateful for your contributions of time, ideas and great support in the development of the irrigation optimization model. The provision of the model coding facilitated the completion of this study. I will also never forget your presence and great time we had during field

visits.

Content

List of Figures

List of Tables

Abstract

Central Vietnam is characterized by a complex climatology, which in combination with the sparse hydrometeorological observation network, creates a challenge in the quantification of projected hydrological extremes under a changing climate. In the region, farmers report increasing damages on agriculture caused by extreme floods and drought conditions. Particularly during the summer-autumn rice season, water is often insufficient to irrigate the entire rice production areas, and thus significantly affecting rice productivity. Therefore, scientifically sound information on the expected future hydrological extremes as well as water-efficient agricultural strategies are urgently required for sustainable water resources management.

In this thesis a complex hydrometeorological modelling chain is employed to investigate the impact of climate change on future hydrological extremes in the Vu Gia - Thu Bon (VGTB) river basin, Central Vietnam. The modelling chain consists of six Global Circulation Models (GCMs) (CCAM, CCSM, ECHAM3, ECHAM5, HadCM3Qs, and MRI), six Regional Climate Models (RCMs) (CCAM, MM5, RegCM, REMO, HadRM3P and MRI), six bias correction (BC) approaches (linear scaling, local intensity scaling, power law transform (monthly), empirical and gamma quantile mapping, and power law transform), the fully distributed hydrological Water Flow and Balance Simulation Model (WaSiM) which was calibrated for the VGTB basin using two different calibration approaches, and extreme values analysis.

The nonlinear parameter estimation tool PEST, which is based on the Gauss-Marquardt-Levenberg method, was combined with the distributed hydrological model WaSiM. Confidence bounds for all estimated parameters of the WaSiM model were developed based on a covariance analysis. A reasonable quality of fit between modelled and observed runoffs was achieved showing the reasonable performance of the WaSiM model in this region.

Both bias corrected and raw RCM data are used as input for the WaSiM to simulate flows for the VGTB basin. To derive high flow and low flow frequency curves for the control (baseline) period (1980-1999) and the future periods 2011-2030, 2031-2050, and 2080-2099, the generalized extreme value (GEV) distribution is fitted to the annual

maxima/minima of the simulated continuous discharge series. Permutation tests are developed and applied to the observed discharge series (1980-1999) to quantify the uncertainties related to the relatively small size to estimate the GEV distribution. Results show that the GEV fits based on sample size of n = 20 can partially be considered as robust.

Due to limitations in the performance of the BC methods, the delta change approach was applied to facilitate extreme flow analysis as required for hydrological decision support. The results exhibit a remarkable variation among the different climate scenarios. As indicated by the majority of the discharge projections, a tendency towards increased high flows and decreased low flows is concluded. The results highlight challenges in using current GCM/RCMs in combination with state-of-the-art BC methods for local impact studies on both high and low flows.

A second central objective of this PhD dissertation was the development and application of an integrated hydrological-irrigation modelling system to optimize irrigation strategies for a typical rice irrigation system in Central Vietnam. The modelling system comprises WaSiM to simulate the inflow to a reservoir and an irrigation model, which optimizes the rice irrigation technology, i.e. *Alternate Wetting and Drying* (AWD) or *Continuous Flooding* (CF), the rice irrigation area and the irrigation scheduling under given water constraints.

Irrigation strategies are derived based on different initial water levels in the reservoir at the beginning of the cropping season as well as different maximum water releases. The simulation results show that the initial level of water in the reservoir is crucial: water levels of less than 90% do not provide sufficient water to irrigate the entire cropping area, whereas a level of 70% restricts the cropping area to 75% under current design maximum outflow of 0.3 m^3/s. AWD is able to reduce the water irrigation input, ranging from 4% to 10% and reduce the number of irrigation events compared to CF. The adoption of AWD, which has been not popular in Central Vietnam therefore, has the potential to save more water and may help to increase the profit of the farmers. However, the benefits of AWD can only be achieved after significant investment in the canal system and the reservoir outlet.

The impact of the different computing environments on the solutions of the integrated model is estimated, since the robustness of the optimization results (performance variability) is crucial for decision support. Only limited performance variability due to the computing environment is finally found, giving confidence in the robustness of the model for decision support.

Prior to the application and the transfer of the model to similar irrigation schemes

in other regions, the model must be further validated by field experiments under various conditions.

Zusammenfassung

Zentralvietnam weist eine komplexe Klimatologie auf, die zusammen mit einem spärlichen hydrometeorologischen Beobachtungsnetzwerk eine Herausforderung für die Quantifizierung der projizierten hydrologischen Extreme unter einem sich verändernden Klima darstellt. Landwirte berichten über agrarwirtschaftliche Schäden, die in dieser Region zunehmend durch extreme Hochwasser- und Dürreereignisse hervorgerufen werden. Insbesondere während der Reisanbausaison im Sommer und Herbst wird der Reisertrag signifikant von unzureichender Bewässerung der Ackerflächen durch Wasserknappheit beeinflusst. Deshalb sind wissenschaftlich fundierte Erkenntnisse über zukünftige hydrologische Extremereignisse sowie eine wasserwirtschaftliche Strategie für ein nachhaltiges Wasserressourcenmanagement dringend erforderlich.

In dieser Arbeit wird eine komplexe hydrometeorologische Modellkette eingesetzt, um die Auswirkungen des Klimawandels auf zukünftige hydrologische Extremereignisse im Vu Gia - Thu Bon (VGTB) Flusseinzugsgebiet in Zentralvietnam zu untersuchen. Die Modellkette besteht aus 6 globalen Zirkulationsmodellen (GCMs) (CCAM, CCSM, ECHAM3, ECHAM5, HadCM3Qs und MRI), 6 regionalen Klimamodellen (RCMs) (CCAM, MM5, RegCM, REMO, HadRM3P und MRI), 6 Bias Korrekturverfahren (BCs) (lineare Skalierung, lokale Intensitätsskalierung, Power Law Transformation (monatlich), empirisches und Gamma-Quantil-Mapping, und Power Law Transformation) und einem flächenverteilten hydrologischen Abflussmodell (WaSiM), das für das VGTB-Einflussgebiet mit 2 verschiedenen Kalibrieransätzen kalibriert und deren Output zur Extremwertanalyse verwendet wurde.

Parameterschätzung im WaSiM und seine Evaluierung von WaSiM ist ein weiterer Aspekt dieser Arbeit. Das nichtlineare Parameterschätz-Tool PEST, das auf der Gauss-Marquardt-Levenberg-Methode basiert, wurde mit dem hydrologischen Modell WaSiM kombiniert. Vertrauensgrenzen für alle geschätzten Parameter des WaSiM-Models wurden mittels der Kovarianzanalyse abgeschätzt. Das hohe Maß an Übereinstimmung zwischen den modellierten sowie den beobachteten Abflüssen zeigt, dass die Anwendung des WaSiM Models in der Region zu guten Anwendungsergebnissen geführt hat.

Für die Abflusssimulation des VGTB-Beckens wurden Rohdaten und Bias-korrigierte Klimadaten als Eingangsvariablen für WaSiM verwendet. Um Wiederkehrwahrscheinlichkeiten für hohe und niedrige Abflüsse für den Kontroll-zeitraum (Baseline, 1980-1999) und die zukünftigen Perioden 2011-2030, 2031-2050 und 2080-2099 zu erreichen, wird die verallgemeinerte Extremwertverteilung (GEV) auf die jährlich simulierten Ablfussmaxima und -minima angepasst. Aufgrund der Tatsache, dass die vorliegenden Datenreihen relativ kurz und zur Bestimmung der GEV Verteilung für die Quantifizierung von Unsicherheiten ungeeignet sind, werden Permutationstests anhand der beobachteten Abfulssraten (1980-1999) durchgeführt. Die Ergebnisse zeigen, dass die angepassten GEV´s auf Basis einer Stichprobengröße von n = 20 als bedingt robust angesehen werden können.

Um die in der hydrologischen Entscheidungsunterstützung erforderliche Analyse von Abflussextremen zu erleichtern, wird aufgrund der Einschränkungen der BC Methoden der Delta-Ansatzes angewendet. Die Ergebnisse weisen eine bemerkenswerte Variation zwischen den verschiedenen Klimaszenarien auf. Wie auch von der Mehrzahl der Abflussprojektionen angedeutet wird eine Tendenz zu höheren Hochwasser- und verminderten Niedrigwasserabflüssen gefolgert. Diese Ergebnisse unterstreichen die Herausforderungen bei der Nutzung aktueller GCMs und RCMs in Kombination mit geeigneten BC-Methoden für lokale Wirkungsstudien von Hoch- und Niedrigwasser-abflüssen.

Ein weiteres zentrales Ziel dieser Dissertation ist die Entwicklung und Anwendung eines integrierten hydrologischen Systems zur Optimierung von Bewässerungsstrategien für ein typisches Reisbewässerungssystem in Zentralvietnam. Das Modellierungssystem besteht aus WaSiM, das den Zufluss zu einem Reservoir simuliert, und einem landwirtschaftlichen Bewässerungsmodell, programmiert mittels des General Algebraic Modeling System (GAMS). Dadurch kann die Reisbewässerungstechnologie, d.h. abwechselnde Bewässerung und Austrocknung (Alternate Wetting and Drying, AWD) oder kontinuierliche Flutung (Continuous Flooding, CF), die Reisbewässerungsfläche und die Bewässerungsplanung unter den gegebenen Verhältnissen der Wasserverfügbarkeit optimiert werden.

Bewässerungsstrategien werden aufgrund unterschiedlicher Anfangswasser-spiegel des Reservoirs zu Beginn der Erntezeit sowie unterschiedlicher maximaler Wasserabgaben abgeleitet. Die Simulationsergebnisse zeigen, dass vor allem der Anfangswasserspiegel im Reservoir entscheidend ist: Wasserstände von weniger als 90% liefern nicht ausreichend Wasser, um die gesamte Anbaufläche zu bewässern. Bei einem aktuellen maximalen Abfluss von 0.3 m^3/s beschränkt ein Wasserstand von 70% die Anbaufläche auf 75%. Im Vergleich zu CF können die Anzahl der Bewässerungsereignisse durch AWD reduziert werden. Ebenfalls mindert sich durch

AWD der Bewässerungseintrag zwischen 4% und 10%. Obwohl die Einführung von AWD in Zentalvietnam nicht weit verbreitet ist, hat sie Potenzial zur Einsparung von Wasser und könnte so den Profit der Landwirte steigern. Allerdings können die Vorteile von AWD erst nach einer umfassenden Investition in das Kanalsystem und den Reservoirauslass erreicht werden.

Schließlich wird auch der Einfluss der verschiedenen Rechenumgebungen (Windows, Linux, Mac) auf die Ergebnisse des integrierten Modells untersucht, da die Robustheit der Optimierungsergebnisse (Leistungsvariabilität) ausschlaggebend für die landwirtschaftliche Entscheidungsunterstützung ist. Es wird gezeigt, dass die Rechenumgebung nur eine begrenzte Leistungsvariabilität hervorruft, wodurch die Robustheit des Modells für die Entscheidungsunterstützung bestätigt werden kann.

Vor der Anwendung und der Übertragung des Modells auf ähnliche Bewässerungsanlagen in weiteren Regionen muss das Modell durch Feldversuche unter verschiedenen Bedingungen weiter validiert werden.

Chapter 1

Introduction

1.1 Motivation

Vietnam is largely exposed to risks from natural disasters. On average, Vietnam is hit by 7 typhoons/tropical cyclones annually which affect primarily the Northern and Central coast regions (UNDP, 2007). As a consequence, there has been losses of life during climatic extreme events during the last decades. Additionally, damages caused by natural disasters to the country's economy of which agricultural production accounts for 21% of the share output is tremendous (Nguyen et al., 2010). The annual average economic losses (2005-2014) from natural risks in Vietnam range between 1.0% and 1.5% of the country's *Gross Domestic Product* (GDP). Of which damages caused by floods is approximately 2,300 million US$ and accounts for 0.5% of the country capital stock and have an increasing tendency (UN, 2015).

Meanwhile, Vietnam is ranked amongst the top severely affected countries world-wide by climate change and is likely to have an increased exposure to extreme events (IPCC, 2007; MONRE, 2012; IPCC, 2013). By 2100, the average temperature is expected to increase by approximately 2.2°C - 3.1°C; dry season rainfall will likely decrease whereas seasonal rainfall is likely to increase by approximately 20% by 2070 (MONRE, 2012). According to the *Fifth Global Assessment Report*, by 2050 about 40% of the global population is expected to be living in river basins that experience severe water stress, including many areas in Vietnam (UN, 2015). More frequent high intensity rainfall events in many regions of the world are projected due to a more dynamic atmosphere caused by global warming (e.g. Fiener et al., 2013). It is expected that both climate variability and climate change will continuously pose critical threats to Vietnam's economy and to agricultural production, which is a particular great water-dependent sector.

Vu Gia - Thu Bon (VGTB) is the largest river basin in Central Vietnam in terms of mean annual flow. Climate in the basin is mainly driven by the South Asia

Monsoon and has an uneven distribution of rainfall, both in time and space. The number of hydrometeorological stations in the basin is limited with most stations situated at low elevations. Due to its high coastal exposure, the VGTB basin is frequently affected by natural disasters which often exacerbate their intensities in regions of complex topography. On the one hand, the region is affected by risks of flood events in the wet seasons, often induced by typhoons/tropical cyclones coming from the East Sea or originating in the Pacific Ocean and accompanied by heavy rains. Results of trend analysis based on observation data show that there is a significant increase in winter rainfall during past decades (Souvignet et al., 2014). On the other hand, the region also faces severe low flow and drought conditions in the dry seasons. Compared to other regions in Vietnam, the South Central Coast area is at high risks of water shortages and floods (IMHEN and UNDP, 2015). The latest climate projections indicate that precipitation extremes related to the monsoon are very likely to increase in Southeast Asia (Vu et al., 2017). Under the projected changes of monsoon rainfalls, changes in both high and low flows are expected as a consequence.

Although hydrological extremes under a changing climate are of great relevance for water management and climate change adaptation (Hoang et al., 2016), only few insights on how climate change will impact the occurrence and magnitude of future high/low flows in the VGTB region have been gained so far. Notably, there were earlier studies focusing on the changes in annual and monthly flows in Vietnam in general and in the VGTB region in particular, but they are not widely available. These studies mostly rely on uncorrected climate data derived from one single *Global Circulation Model* (GCM) and/or one statistical downscaling method exclusively (e.g. IMHEN, 2010; IMHEN and UNDP, 2015). In addition, a vast majority of lumped hydrological models were employed in these studies due to their simplicity and ease of use, but no fully spatially distributed hydrological model has been available so far for the VGTB region.

In the VGTB basin, agriculture plays an important role and accounted for an average of 31% GDP of the region between 2000 and 2010. Major economic activities and over 50% of the workforce are employed in the agricultural sector (ICEM, 2008). However, fragmented and smallholder farming systems associated with weak technical infrastructure and low crop productivity due to the cultivation dependent on nature are dominant. The prevailing irrigation practice is *Continuous Flooding* (CF), although the water-saving irrigation technology of *Alternate Wetting and Drying* (AWD) has been introduced and officially integrated into the guidelines for rice irrigation across Quang Nam province by the *Department of Agriculture and Rural Development* (DARD). There is only limited knowledge on the performance of AWD in comparison to CF in the VGTB basin and across Central Vietnam in general. Most of studies on the application of AWD is tested in small field trials only and no systematic and

consolidated efforts are undertaken until now. Very few studies have looked at the adoption AWD for an entire rice irrigation system. The reasons for reluctance of the wide adoption of AWD may vary, but can be summarized as:

- Farmers traditionally believe that ponded water is required at all stages of rice growing to obtain high yields.

- Farmers have little incentive to reduce water use as a water pricing system is not in place. In fact, farmers only pay a small fee for the water withdrawal service (i.e. fee for management, protection and maintenance of tertiary canals). This fee is applied per cropping area (ha) per season instead of per amount of supplied water.

- AWD may cause potential problems with rodent, particularly when the soil is dried.

- The higher water requirement for AWD compared to CF at the beginning of each irrigation event; this may lead to temporary water shortages, if all fields are prepared at the same time.

- Farmers prefer to store water in the fields (CF practice) instead of drying out the field for some time under AWD due to unreliable irrigation water.

Agriculture is the most sensitive and vulnerable sector due to climate variability and climate change amongst others in the VGTB basin. Rice is the most important staple crop and is predominantly grown in the region, but rice production is unstable. The abundance of rainwater results in vast inundation posing severe threads in the maintenance of the level of rice productivity in wet seasons (e.g. flood events in 1999, 2010, 2011, and 2013). In contrast, rice yield is relatively low due to water stress during the cropping period, particularly for the SA rice season. Exchanging with local stakeholders revealed water shortage at the end of recent SA rice seasons becomes more severe and frequent. This consequently may lead to crop failures or low crop productivity. For example, rice productivity in the dry season 2008 was only 50% of expected productivity due to insufficient irrigation water (S. Nguyen, 2015, personal communication). Expected changes in frequencies and severity of droughts, as well as heavy precipitation events are projected, which may cause more adverse effects on agricultural production in the VGTB basin (Laux et al., 2013). In addition, increasing water stress due to rapid population growth (1.26% during 2000-2010), the deterioration of water quality and increasing demand for competitive sectors resulted from socio-economic development will exacerbate the problem of water shortage for agricultural irrigation in the VGTB basin.

Hence, an improved understanding of possible changes in extreme high and low flows caused by climate change for the VGTB basin is of paramount impor-

tance, especially to improve decision support in water resources management and water-related risk mitigation. Future changes in high and low flows should be quantified and made widely available. Based on this information, particular responses and adaptation measures may be required. More specifically, scientifically sound decisions on efficient usage of irrigation water are demanded, e.g. the adoption of water-saving AWD irrigation technology to sustain crop productivity in dry conditions as well as to eliminate the effect of increasing water scarcity in the VGTB region. This is in line with the development strategy of socio-economy by 2025 and the view towards 2030 determined by the local provincial governments in Central Vietnam.

1.2   The Vu Gia - Thu Bon basin

The Vu Gia - Thu Bon river basin is located in Central Vietnam. The basin has a total area of 10,350 km^2 and encompasses the entire Quang Nam province, Da Nang city and a small part (approximately 500 km^2) of the Kon Tum province. The basin is surrounded by high mountain ranges to the North, the West and the South and faces the East Sea to the East. The elevation of the VGTB ranges from sea level to approximately 2600 m above sea level. The area of interest for hydrological simulations in this study has a size of 3213.5 km^2 within the upper part of the Thu Bon river. The outlet of the study area is located at Nong Son station, where discharge measurements are available (Figure 1.1).

1.2.1   Climate

The climate in the VGTB basin is characterized by two distinct seasons: a strong monsoonal rainy season with typhoons occurring from September to December and the dry season from January to August (Souvignet et al., 2014). Rainfall is unevenly distributed over the basin and has a strong orographic component ranging from 2000 mm in the flood plains to over 4000 mm in the mountainous regions. Annual mean rainfall is about 2500 mm. Heavy rain is typically caused by typhoons, tropical depressions, and cold airs. Rainfall in the wet season amounts up to 60-80% of the total annual rainfall, the remainder during dry season rainfall. The historical 1-day maximum rainfall is 667mm on 3rd November 1999; it was followed by a historical flood event in Central Vietnam. Figure 1.2 shows the mean seasonal and annual rainfall measured at selected gauging stations in the VGTB basin. Annual mean temperature varies between 23° and 26°C and decreases from the coast to the mountains. The maximum temperature can reach values above 35°C during June and July, whereas the minimum temperature can fall below 15°C in January. Annual mean potential evatranspiration ranges between 800 mm in the mountains up to 1500 mm in the coastal plain. In the wet season, the relative humidity is 85-88% in the lowlands and 90-95% in high elevation areas, while
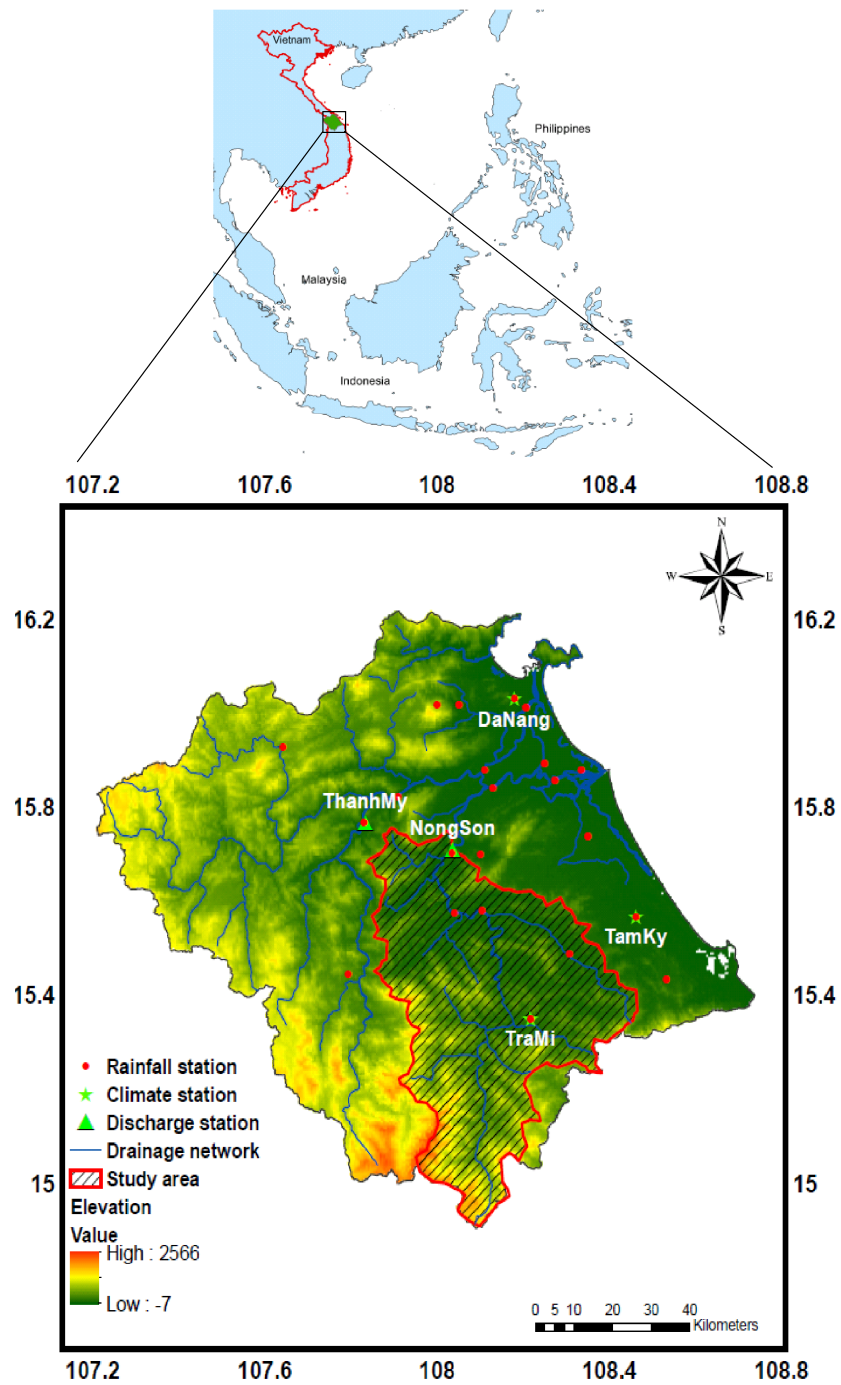
Figure 1.1: Vu Gia - Thu Bon basin. The shaded area represents the upper Thu Bon river basin, which is the considered area for hydrological simulations.

during the dry season this is below 80% and 80-85%, respectively.
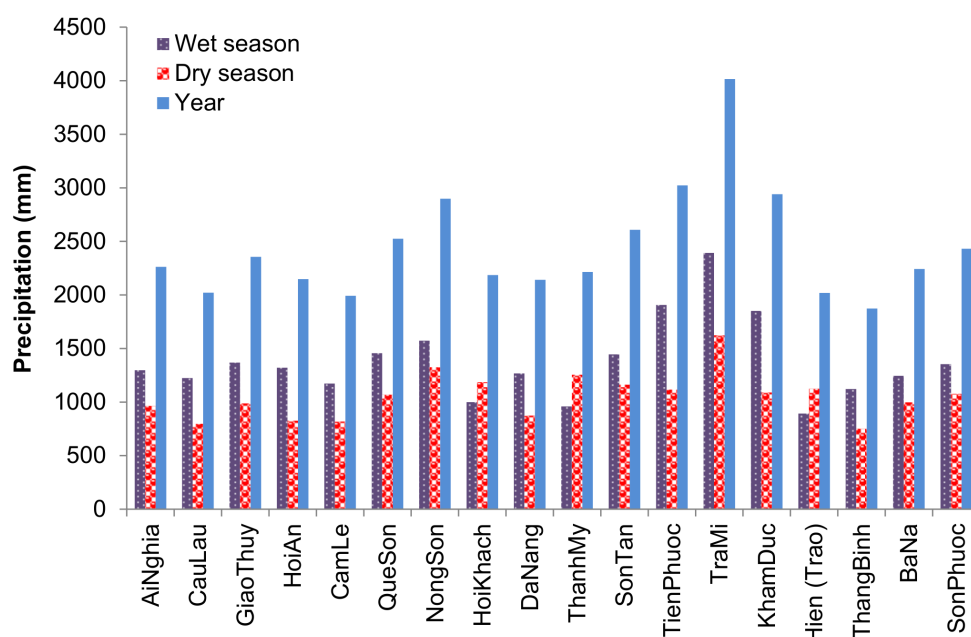
Figure 1.2: Mean seasonal and annual rainfall at different stations in VGTB basin (1977-2012).

1.2.2 Hydrology

VGTB is one of the five largest river basins of Vietnam in terms of flow volume (Souvignet et al., 2014). Thu Bon and Vu Gia are the two main rivers of the VGTB drainage network. The Vu Gia originates from the mountains in the South-West of Quang Nam and includes three major tributaries, namely Song Cai, Song Bung and Song Con. The Vu Gia river mainly flows from the West to the East before tuning North in the direction of Da Nang then pours into Han estuary. The Thu Bon river originates from the South-East slopes of Ngoc Linh range at an altitude of over 2500 m a.s.l. It drains from the South to the North and changes the direction to West-East before joining the East Sea at Cua Dai estuary. The Thu Bon river has a total length of 198 km measuring from its source to the estuary while this is about 204 km for the Vu Gia river. Similarly to rainfall, river flows in the VGTB basin are unevenly distributed (Figure 1.3).

In the VGTB basin, the differences between high flows and low flows are significant. While the flow in the wet season amounts to nearly 65% the total annual water, the flow in the dry season is responsible for only 35%. The mean annual discharges during the period 1976-2012 observed at Nong Son station (Thu Bon river) and Thanh My
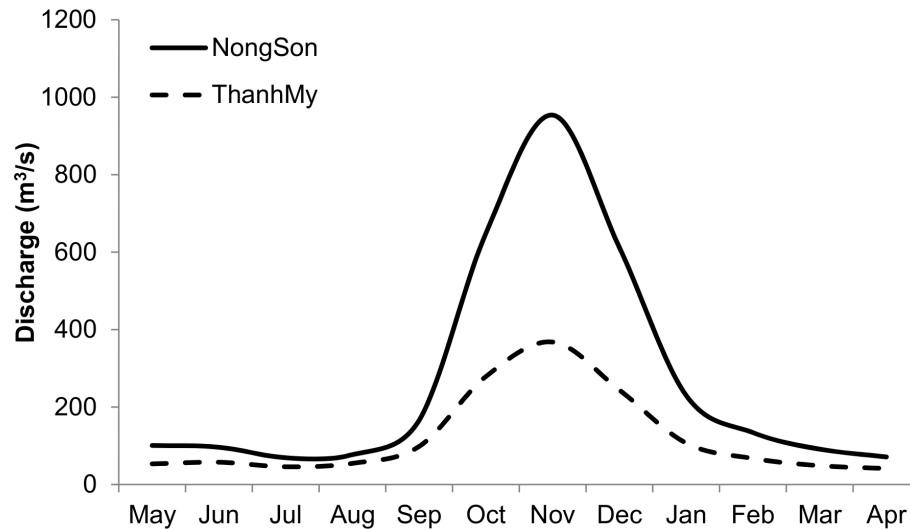
Figure 1.3: Mean monthly flows measured in VGTB basin (1976-2012). The location of the two stations is referred to Figure 1.1.

station (Vu Gia river) are 282.8 m^3/s and 128.6 m^3/s, respectively. Maximum mean monthly flow (often occurs in November) measured at Nong Son accounts for 29% of the total mean annual flow volume of Thu Bon river, whereas this value is 25% for Vu Gia river measured at Thanh My. In contrast, minimum monthly flow accounts for 1-3% of the annual total flow volume and mainly concentrates in April. The largest flow and smallest flow that have been recorded at Nong Son were 10,600 m^3/s in November, 2007 and 14.6 m^3/s in August, 1977, respectively. High rainfall intensity and small buffer areas (mid-stream) as well as large river slopes mainly attribute to the flooding in the low lying area. Flooding lasts relatively long (2-5 days) due to the strong tidal influence in the downstream area of the basin. The basin is expected to suffer from increasing frequency and severity of hydroclimate-related extremes such as typhoons, floods and droughts (Souvignet et al., 2014; Ho et al., 2011; Sheffield and Wood, 2008).

1.2.3   Land use and land cover

The VGTB basin consists of three distinct landscape types, i.e. the uplands, the midlands, and the lowlands (Fink et al., 2013). A combination of natural and production forests is dominant in the uplands and accounts for over 48% of the land cover. The lowlands are mainly characterized by irrigated rice paddies and short-term perennial crops including sugarcane, cotton, sesame, and tobacco. Annual crops and irrigated paddy rice are predominantly prevailing in the narrow valleys in the midland and in alluvial areas along rivers. Total rice land and cash crops land is approximately 15%, while shrub land is 33%. Open water and residential area is 0.2% and 0.5%, respectively. Figure 1.4 shows the landuse map of the VGTB river basin.
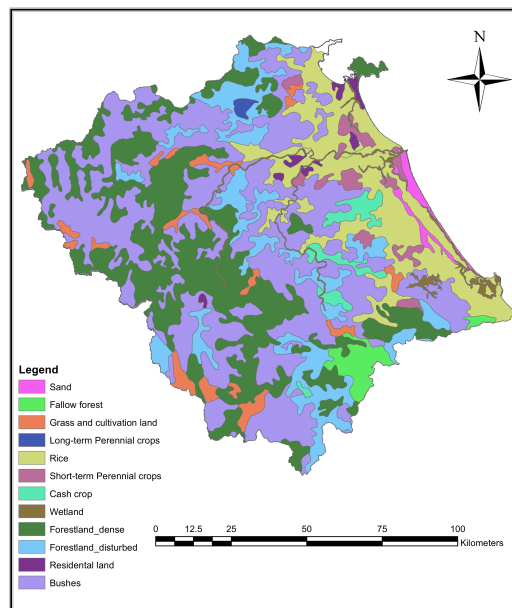
Figure 1.4: Land use in the VGTB basin.

1.2.4   Soil

Acrisols soil including Ferralic, Humic and Plinthic is the dominant soil group, covering most of the uplands and midlands in the VGTB basin. The other main soil group is Fluvisols, mainly found in the midlands and lowlands of the VGTB basin. Silty soil and alluvial soil present in the low-lying area along rivers, while sandy soil and sand dune are prevailing along the coast. Figure 1.5 shows the soil map of the VGTB river basin.
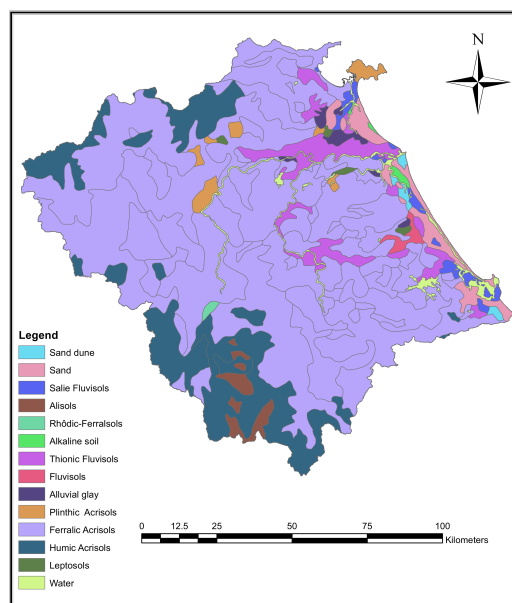
Figure 1.5: Soil types in the VGTB basin.

1.2.5   Irrigation infrastructure and selection of a typical local rice irrigation scheme for modeling

In the VGTB basin, a large number of small-scale reservoirs have been built to store water in response to an increasingly unstable water supply for irrigation. In total, there are 73 reservoirs with the volume range between $1x10^6m^3$ and over $2x10^6m^3$. There are 757 irrigation schemes, of which 518 are weirs and 179 are pumping stations (ADB, 2011). The reservoirs are capable of providing irrigation water for 17,048 ha, accounting for about 42.5% of the total demand area. However, the actual irrigated area reaches less than 50% of its designed capacity due to insufficient irrigation systems. The shortage of local financial investments is the main cause for the incomplete irrigation scheme from headworks to field levels. Additionally, most of headworks and main canals have been deteriorated and silted. The poor operation and inadequate maintenance and management lead to deterioration of the systems (ICEM, 2008).

The Que Trung rice irrigation scheme, located in Nong Son district, Quang Nam province, is selected as a typical irrigation system in the VGTB basin for modelling. The irrigation system includes a reservoir (Trung Loc) and an associated canal system for irrigation. Water for irrigation is taken from the reservoir with the designed volume capacity of $1.85x10^6m^3$. The reservoir consists of a concrete dam of 331m in length and 27.4m in height. Water is diverted to the canal scheme for irrigation via one submerged conduit running beneath the dam and controlled by a valve. The reservoir outlet is designed to release a maximum of 0.3 m^3/s of water in order to irrigate up to 145 ha of rice during the SA season. The decision of the total irrigated area strongly depends on the initial level of the reservoir before the dry season and seasonal climate forecast outlook. On average the reservoir is filled up with approximately 75% of its designed capacity before the SA season. This fact frequently leads to water shortages towards the end of the SA season and poses risks on the rice production.

1.3   Research questions

Based on the problems in the VGTB region, derived from literature review and personal communications with local stakeholders, the following research questions are derived:

- Are climate information obtained by GCMs and RCMs suitable to derive reliable and robust hydrometeorological extreme values for the VGTB basin?

- What are the expected impacts of projected future climate change on high and low flows in the VGTB basin?

- Can we reliably model the interactions between water availability and agricultural

irrigation?

- How can we provide scientific sound joint hydrological and economical information for decision support of agricultural management (irrigated area for cropping, irrigation technology and irrigation schedules)?

1.4 Research objectives

The objectives of this thesis accordingly are:

- To investigate the performance of the fully distributed hydrological model WaSiM in the VGTB basin.

- To develop and apply methods that allow optimized irrigation strategies and schedules in terms of water efficiency under different scenarios of water availability in the summer-autumn rice season.

- To investigate the performance of different bias correction methods for GCM/RCM-derived rainfall and temperature.

- To assess the potential impact of projected climate change on high and low flows in the VGTB basin.

1.5 Innovation of the thesis

The innovation of the thesis is summarized as follows:

- Set up and application of a fully distributed hydrological model in Central Vietnam under weak technical infrastructure for the first time. In addition, the nonlinear parameter estimation tool PEST was combined with the distributed hydrological model WaSiM for automatic parameter estimation.

- Confidence ellipses for the estimated hydrological model parameters are developed using a covariance analysis.

- Development of an irrigation optimization model under limited water conditions to provide scientific sound decision support for agricultural management. In close interactions with local stakeholders, the model has been developed and applied to optimize irrigation water for the Que Trung irrigation scheme (Central Vietnam) to derive improved irrigation strategies.

- The impact of different computing environments on the solution of integrated hydrological-irrigation optimization model is estimated to investigate the robustness of the model for decision support.

- Application of a complex hydrometeorological modelling chain to assess the impact of climate change on hydrological extremes and to develop feasible solutions for hydrological decision support.

1.6   Structure of the thesis

This thesis is organized in six chapters. Chapter 1 provides general introduction to the study area. The chapter also includes objectives and research questions. Chapter 2 deals with data availability for the research. Hydrological modelling for the Vu Gia - Thu Bon basin is discussed in Chapter 3. Chapter 4 describes the integrated hydrological-irrigation optimization simulations for a rice scheme in the VGTB basin. Chapter 5 concentrates on impact of climate change on hydrological extremes in the VGTB basin. The key results as well as general conclusions and recommendations are summarized in Chapter 6.

The core parts of this thesis are presented in the two publications:

- Quang Thinh Dang, Patrick Laux, Harald Kunstmann (2017). Future high and low-flow estimations for Central Vietnam: A hydro-meteorological modelling chain approach. Hydrological Sciences Journal, 62(11):1867-1889.

- Quang Thinh Dang, Rui Pedroso, Patrick Laux, Harald Kunstmann (2018). Development of an integrated hydrological-irrigation optimization modeling system for a typical rice irrigation scheme in Central Vietnam. Agricultural Water Management, 208(2018):193-203.

A further co-authored and peer-reviewed publication related to the Vu Gia - Thu Bon river basin is:

- Maxime Souvignet, Patrick Laux, Jim Freer, Hannah Cloke, Quang Thinh Dang, Thuc Tran, Johannes Cullmann, Alexandra Nauditt, Wolfgang-Albert Flugel, Harald Kunstmann, and Lars Ribbe (2014): Recent climatic trends and linkages to river discharge in Central Vietnam. Hydrological Processes, 28(4):1587-1601.

Chapter 2

Data

The Vu Gia - Thu Bon basin has a sparse hydro-meteorological observation network. Most gauging stations are located in the lowlands, and only few are installed in higher altitudes where the accessibility is limited. There are only three climate stations (Da Nang, Tam Ky and Tra Mi) within the VGTB basin, of which only Tra Mi station is situated in the Thu Bon catchment. Climate variables measured at the observation stations comprise rainfall, temperature, relative humidity, wind speed, and solar radiation. There are nine hydrological stations, however, discharges in m^3/s are only measured at Nong Son station and Thanh My station. The observational lengths are not consistent for all hydro-meteorological stations. Most stations continuously recorded their measurements in 1976, except for Da Nang station (records started in 1931). Table 2.1 lists the hydro-meteorological stations in the VGTB basin.

2.1 Station observations and reanalysis climate data

Two types of historical climate data are employed. The first one is observed daily rainfall from 20 hydro-meteorological stations within the VGTB basin (Table 2.1). The second one is downscaled WRF-ERA40 reanalysis data covering the entire domain of the VGTB basin (Laux et al., 2013). The RCM WRF has been driven by ERA40 reanalysis data of the European Centre for Medium-Range Weather Forecasting (Uppala et al., 2005). It is obtained through the project Land Use and Climate Change Interactions in Central Vietnam (LUCCi). The considered WRF-ERA40 reanalysis data comprise daily temperature, relative humidity, windspeed and global radiation with a spatial resolution of 5 km and from 1971 to 2000. This downscaled WRF-ERA40 reanalysis data are used as a model derived pseudo reality and a proxy for observations due to the sparse observation network in the region as well as missing observation data for wind, humidity, and radiation. Observed precipitation data and the ERA40 reanalysis data are used for calibration and validation of the hydrological model.

Table 2.1: Hydro-meteorological stations in the VGTB basin. P: Precipitation, T: Temperature, RH: Relative Humidity, R: Radiation, W: Windspeed, Q: Discharge and WL: Water level.

ID	Station	Location Lon E.	Location Lat N.	Variable	Recording period
1	Ai Nghia	108.12	15.88	P, WL	1976-2012
2	Cau Lau	108.28	15.85	P, WL	1976-2012
3	Giao Thuy	108.13	15.85	P, WL	1976-2012
4	Hoi An	108.33	15.87	P, WL	1976-2012
5	Tam Ky	108.50	15.55	P, RH, T, W, R	1977-2012
6	Cam Le	108.20	16.00	P	1976-2012
7	Que Son	108.10	15.70	P	1977-2012
8	Nong Son	108.03	15.70	P, WL, Q	1976-2012
9	Hoi Khach	107.82	15.82	P, WL	1976-2012
10	Da Nang	108.18	16.03	P, RH, T, W, R	1931-2012
11	Thanh My	107.83	15.77	P, WL, Q	1976-2012
12	Hiep Duc	108.03	15.57	P, WL	1976-2012
13	Tien Phuoc	108.30	15.48	P	1977-2012
14	Tra Mi	108.25	15.33	P, RH, T, W, R	1977-2012
15	Kham Duc	107.78	15.43	P	1976-2012
16	Hien (Trao)	107.65	15.59	P	1976-2012
17	Thang Binh	108.35	15.74	P	1977-1995
18	Vinh Dien	108.25	15.89	P, WL	1977-1988
19	Ba Na	108.00	16.02	P	1977-1995
20	Son Phuoc	108.05	16.02	P	1978-1994

2.2   River flow data

Daily measured river flow data from 1976 to 2012 at Nong Son hydrological station are available. This is the only station in the upper Thu Bon river for which long-term daily flows are observed. The quality of the flow data has been checked for homogeneity and consistency in an earlier study (Souvignet et al., 2014). Thus, data from this station are used for calibration and validation of the hydrological model and for extreme value analysis.

2.3   Climate projections

Global circulation models (GCMs) are considered to be state-of-the-art and most intensively used data sources to estimate possible future climate changes (Dobler et al., 2012b). However due to its too coarse resolutions to be directly applicable for climate change impact studies (e.g. Chiew et al., 2010; Sunyer et al., 2012; Chen et al., 2012; Khazaei et al., 2012), outputs from GCMs need to be downscaled to finer resolutions to

bridge the gap between regional and local scale processes (Fowler et al., 2007). These limitations are particular of importance in regions of complex orography and regions of highly heterogeneous land cover, where land–atmosphere interactions are difficult to model (Bordoy and Burlando, 2013). Most commonly used approaches of downscaling include dynamical downscaling (using regional climate models, RCMs) and statistical downscaling. Apart from statistical downscaling, which inherently corrects for the biases between large scale and local scale information, a promising alternative is the dynamical downscaling method based on RCMs. Dynamical downscaling is computationally expensive and therefore its output is not generally available for many regions (Prudhomme et al., 2003; Chen et al., 2012). RCMs can provide regional climate data at horizontal resolutions of 10km or less, and are capable of describing climate feedbacks at the regional scales (IPCC, 2013). RCMs are a crucial data source required in hydrological applications, especially for hydrological decision-making in response to a changing climate.

Recently, the *Representative Concentration Pathways* (RCPs) (van Vuuren et al., 2011) scenarios have replaced *Special Report on Emission* (SRES) (Nakicenovic et al., 2000) emission scenarios, widening the range of climate change scenarios. The dynamic downscaled data under the new RCP scenarios (e.g. the Coordinated Regional Climate Downscaling Experiment (CORDEX) data) has been available for many parts of the globe (e.g the European and the African). However, there has not been regional climate model data available for download for the Southeast Asia domain (CORDEX-SEA) so far. There is only one GCM-RCM combination available for the historical period for East Asia (CORDEX-EA), i.e. the HadGEM2-AO – HadGEM3-RA combination based on RCP4.5 and RCP8.5 (a medium to low scenario and a high radiative-forcing scenario assuming a stabilization and increase of radiative forcing by 2100, respectively) (Riahi et al., 2011; Hoang et al., 2016). For projected future time slices, only 1 GCM in combination with 4 RCMs (RegCM_v4, SNU_MM5, SNU_WRF_v3, YSU-RSM_v3) and two scenarios are available, while their corresponding historical experiments are not available.

Due to insufficient RCP-driven CORDEX data for this region, it is necessary to rely on data from a consorted downscaling experiment for Vietnam based on the former SRES scenarios A1B and A2 to quantify the model-inherent uncertainties for hydrological decision support. Albeit the concept of the SRES and the new RCP scenarios is different, some scenarios can be expected to lead to similar consequences for the climate projections. Applying the A1B and A2 scenarios, possible climate changes due to a radiative forcing in the range between 6 and 8 W/m^2 is expected to be covered (Figure 2.1).

In this PhD dissertation, a number of climate projections for the VGTB basin are

employed for the hydrological impact study. Daily rainfall and temperature data used in this study are derived from simulations of ensembles of six selected GCMs including CCAM, CCSM, ECHAM3, ECHAM5, HadCM3Qs (consisting of four different realizations HadCM3Q0, HadCM3Q10, HadCM3Q11, and HadCM3Q13) and MRI.
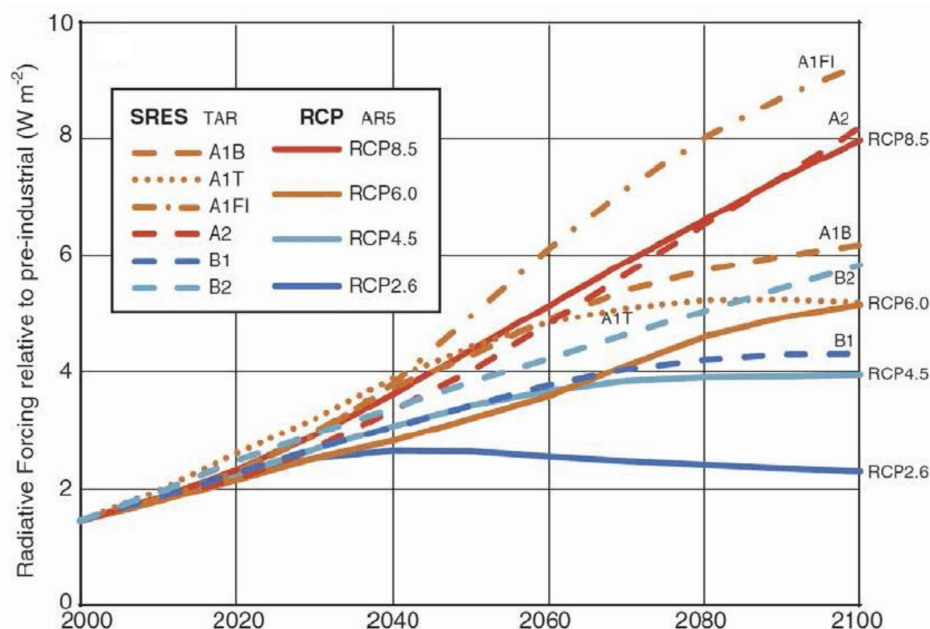
Figure 2.1: Radiative forcing until 2100 according to different SRES and RCP scenarios (IPCC, 2013)

All these six GCMs are forced with SRES emission scenario A1B while only three models (CCAM, CCSM, and ECHAM3) are forced with the A2 emission scenario. These climate variables are subsequently downscaled using six RCMs including CCAM, RegCM, MM5, REMO, HadRM3P and MRI to derive regional climate projections and made available for this study by the Vietnamese National University (VNU).

Of all combinations, the RCMs of CCAM and MRI are forced with the same originated source GCMs of CCAM and MRI, respectively. RegCM and MM5 models are forced with the CCSM model. The REMO model is forced with ECHAM3 while the HadRM3P model is forced with ECHAM5, HadCM3Q0, HadCM3Q10, HadCM3Q11 and HadCM3Q13. Altogether, ten GCM/RCM combinations are considered and they are shown in Table 2.2. The time slice from 1980 to 1999 is used as the baseline period (control run) whereas the periods: 2011-2030, 2031-2050 and 2080-2099 are considered as future climate scenarios. More detailed information about the climate projection data can be found in (Ngo et al., 2014).

The horizontal resolution of all considered RCMs is between 20 km and 36 km and is coarser than the downscaled WRF-ERA40 reanalysis (e.g. pseudo-reality in this study).

The Distance-Weighted Average (DWA) remapping method is employed to interpolate time series for precipitation and temperature from the coarser climate simulations to the grid of the high-resolution climate simulations derived by WRF (5 km). The DWA approach looks for the nearest four neighbors and calculates the weights as a function of the distance. The 5 km-interpolated GCM/RCM data are subsequently used in the hydrometeorological modeling chain which will be described later in the methodology section.

Table 2.2: Climate projections for the VGTB basin

No.	GCM	RCM	Resolution	Climate scenario	
				A1B	A2
1	CCAM	CCAM	25km, daily	2011-2030 2031-2050 2080-2099	2011-2030 2031-2050 2080-2099
2	CCSM	RegCM	36km, daily	2011-2030 2031-2050 2080-2099	2011-2030 2031-2050 2080-2099
3	CCSM	MM5	36km, daily	2011-2030 2031-2050	2011-2030 2031-2050
4	ECHAM3	REMO	36km, daily	2011-2030 2031-2050	2011-2030 2031-2050
5	ECHAM5	HadRM3P	25km, daily	2011-2030 2031-2050	
6	HadCM3Q0	HadRM3P	25km, daily	2011-2030 2031-2050	
7	HadCM3Q10	HadRM3P	25km, daily	2011-2030 2031-2050	
8	HadCM3Q11	HadRM3P	25km, daily	2011-2030 2031-2050	
9	HadCM3Q13	HadRM3P	25km, daily	2011-2030 2031-2050	
10	MRI	MRI	20km, daily	2080-2099	

2.4 Agricultural data

Information on agricultural data in the Que Trung rice cropping area in the VGTB basin was collected through field surveys in 2014 & 2015. The data include rice cropping seasons, annual land area allocated for rice cropping, annual rice yields, rice prices and local rice irrigation practices. In addition, information on an existing irrigation system including irrigation water amount for rice cropping and information on a reservoir is obtained. These data are exclusively gathered during personal interviews with local agricultural managers in March 2015.

Chapter 3

Hydrological modelling for the Vu Gia - Thu Bon basin

3.1   Introduction

Hydrological modelling is the state-of-the art tool for simulating the hydrologic processes e.g. transformation of rainfall to runoff. The structure of hydrological models range from relatively simple to complex and the preliminary differences between them are the input data requirements and the way of transferring input to output. Great efforts have been put in the model development, however, so far no model can be assumed to be universal and most models are not able to describe the full range of natural dynamics (Cullmann et al., 2011). Only the most crucial components of the water cycle are usually taken into account in the runoff generation, because of the complexity of the rainfall-runoff process (Wagner, 2008). Hydrological models are usually classified in three major groups, including empirical (black-box), lumped conceptual and distributed physically-based models. Nowadays, a great number of models applied in practice belong to the empirical black-box and lumped conceptual models due to their simplicity and less parameters required for calibration (Raymond, 2009).

In the Vu Gia - Thu Bon basin, Central Vietnam, the majority of hydrological models applied are lumped or semi-distributed hydrological models such as the Mike11 from Danish Hydraulics Institute (DHI) and the HEC-HMS from US Army Corps of Engineers. So far, no fully spatially distributed hydrological model is available for the region. The hydrological model applied in this thesis is the WaSiM model developed by (Schulla, 2012). The following sections present details about the used model, data requirements, model set up, and model calibration.

3.2   Methodology

3.2.1   Hydrological model WaSiM: Introduction

WaSiM (Water Balance Simulation Model) is a fully distributed hydrological water balance model. The model simulates the surface and sub-surface processes in the hydrologic cycle (Schulla, 2012). The model mainly applies process-based algorithms for various components, while conceptual approaches are employed where physical parameters are difficult to obtain (Kunstmann et al., 2006). The model is spatially differentiated and supports both continuous and event-based rainfall-runoff simulations. WaSiM was developed at the ETH Zürich by (Schulla, 1997), and the model has been widely used in catchments in European countries (e.g. Klok et al., 2001; Verbunt et al., 2003; Jasper et al., 2004; Cullmann et al., 2006; Kunstmann et al., 2006; Warscher, 2014; Smiatek and Kunstmann, 2016). The model has also been applied in semi-arid regions (e.g. Jung, 2006; Ahrends et al., 2008; Wagner, 2008; Kasei, 2009). However, its applicability in the tropical climate basins such as the Vu Gia-Thu Bon, Central Vietnam has not been documented yet.

Being a modular structured model, the utility of the WaSiM model features (modules) depends on specific conditions of the study area, the availability of input data and desired outputs. Unnecessary modules can be deactivated to reduce the computational expenses (e.g. glacier and snow module can be deselected in this study due to the tropical climate area). The main model components are described below (Schulla, 2012; Wagner, 2008).

Potential and actual evapotranspiration WaSiM provides a number of approaches for calculating the potential evapotranspiration such as Penman-Monteith, methods after Hamon, Wending and Haude. In this study, the potential evapotranspiration is estimated using the Penman-Monteith approach (Penman, 1978). This method, besides meteorological variables, requires additional data such as a crop resistance, which depends on the pressure head in the root zone, the percentage of the soil covered by the crop (LAI), effective height of the vegetation and the soil water content threshold below that the reduction of transpiration starts. To determine the real evapotranspiration, potential evaporation is reduced first by the amount of water equal to interception storage. A further reduction is conducted depending on the actual suction of the soil considering plant and soil physiological properties.

Interception Interception represents the part of precipitation intercepted by the canopy, which is formed by the vegetation above the ground surface. A simple bucket approach is applied to account for the interception storage of vegetation layers and the ground level. The maximum interception storage capacity is a function of the degree of vegetation coverage (a function of LAI) and maximum height of water at

the leaf surfaces. The potential evaporation rate is assumed for the extraction rate of
water out of the interception storage by evaporation. No evaporation will occur at the
soil component if the water amount in the storage is sufficient and the storage content
is reduced by the potential evaporation. If the storage content is smaller than the
potential rate, the remaining rate will be taken from the soil.

Infiltration and generation of surface runoff When the soil is saturated or when
the precipitation intensity exceeds infiltration capacities, excess precipitation feeds
directly surface runoff. The amount of water infiltrated into the soil serves as an upper
boundary condition for the water fluxes in the unsaturated soil. It is calculated from
a combination of the infiltration equation by Green and Ampt and the saturation
time estimation by Peschke (Jasper et al., 2004; Kleinn et al., 2005; Kunstmann et al.,
2006). The WaSiM model uses the Richards equation, i.e. infiltration is considered in
the calculation of the Richards equation for the unsaturated zone.

Flow and interflow in the unsaturated zone The vertical fluxes of water within
the unsaturated soil zone are calculated with a finite difference scheme for the discrete
Richards equation.

$$\frac{\partial \Theta}{\partial t} = \frac{\partial q}{\partial z} = \left(-k\left(\Theta\right) \cdot \frac{\partial \Psi\left(\Theta\right)}{\partial z} \right) \tag{3.1}$$

where Θ is the water content [m^3/m^3], t is the time [s], k is the hydraulic conductivity
[m/s], Ψ is the hydraulic head as sum of suction ψ and geodetic altitude h [m], q is the
specific flux [m/s], z is the vertical coordinate [m], and β is the local slope angle.
The parameterization of the dependence of the hydraulic head and hydraulic conduc-
tivity on soil moisture content is done by applying method after (Van Genuchten,
1980).

$$k_{s,z} = k_s \cdot k_{rec}^z \tag{3.2}$$

$k_{s,z}$ is the saturated hydraulic conductivity within depth z [m/s], k_s is the saturated
hydraulic conductivity at the soil surface [m/s], k_{rec} is the recession constant [-], and z
is the depth [m].
Interflow is generated for soil layer m according to

$$q_{ifl} = k_s\left(\theta_m\right) \cdot \Delta z \cdot d_r \cdot \tan\beta \tag{3.3}$$

q_{ifl} is the interflow [m^3/s], k_s is the saturated hydraulic conductivity [m/s], θ_m is the
water content in the specific layer m [-], Δz is the layer thickness [m], d_r is the scaling
parameter used to consider river density [-], β is the local slope angle. Groundwater
recharge in WaSiM is defined as the remaining vertically percolating water.
The linear storage approaches are employed for the concentration of grid-based runoff

to catchment runoff, which requires the calibration of the respective recession constants for direct flow and interflow, K_d and K_i. The runoff component Q_t at time t is a result of the runoff component Q_{t0} at the previous time t_0 and the corresponding recession constants K.

$$Q_t = Q_{t0} \cdot e^{\frac{-\Delta t}{K}} \tag{3.4}$$

with $\Delta t = t - t_0$

Baseflow in the saturated zone Baseflow is calculated as exfiltration from the groundwater into the river surface water. Exfiltration is calculated using the hydraulic gradient and the colmation at the river bed. The baseflow can only be generated when the difference between groundwater table and river bed is positive. Infiltration of surface water into groundwater occurs if the difference between groundwater table and river bed is negative. In the WaSiM model version using Richards' equation, an integrated two-dimensional groundwater model is dynamically coupled to the unsaturated zone to calculate the fluxes between unsaturated zone and groundwater. If the model is run without the groundwater module, baseflow is calculated in a conceptual way (WaSiM version using Topmodel approach).

$$Q_B = Q_0 \cdot k_s \cdot e^{\left[\left(h_{gr} - h_{geo,0}\right)/k_B\right]} \tag{3.5}$$

Q_B is the base flow [m/s], Q_0 is the scaling factor for base flow [-], k_s is the saturated hydraulic conductivity [m/s], h_{gr} is the ground water table [m a.s.l], $h_{geo,0}$ is the geodetic altitude of the soil surface [m a.s.l] and k_B is the recession constant for base flow [m].

3.2.2   Hydrological model WaSiM: Set up for the upper Vu Gia - Thu Bon basin

Preprocessed climate data
The required meteorological input data for the hydrological WaSiM model include precipitation, temperature, relative humidity, solar radiation and wind speed. Prior to inputing into the model, these data need to be interpolated onto the predefined regular model grid resolution (500m). The methods available for interpolation within WaSiM model are described below, following (Schulla, 2012):

- Inverse Distance Weighting (IDW): This is a widely used and easy to implement interpolation method (Wagner et al., 2012). The method uses all stations within a specified search radius for the interpolation. Weights are calculated and assigned to the stations in inverse proportion to the square of the distances from the locations requiring an estimate to the stations. The method is suitable for variables which are not (strongly) dependent on elevation, or modelling the flat

area.

- Bilinear interpolation: This method is effective (less time consuming) when using equidistant data e.g. gridded data derived from meteorological model.

In this PhD dissertation, the IDW method is applied for interpolating station precipitation and the bilinear interpolation method is applied for temperature, global radiation, wind and relative humidity for the model calibration and validation periods. For the baseline and future hydrological model simulations the bilinear method is applied for the interpolation of all climate variables derived from GCM/RCM combinations. The interpolated data is 500m grid resolution.

Radiation and temperature are usually topographically dependent. Therefore adjustments are required to compensate for the shadowing effects in the mountainous areas. Sensible heat flux and air temperature depend on incoming shortwave radiation which is influenced by shading effects. An adjustment of radiation and temperature is implemented using an approach after (Oke, 1987). This method requires calculating a correction factor which depends on sunshine duration, empirical factor considering diffuse shortwave radiation, zenith and azimuth angles. This is done within the WaSiM model.

Land use data

Land use data used in this study are resampled to the 500m grid cell from the original 90m gridded land use data obtained from LUCCi project using the nearest-neighbor method. The land use statistic is originally available in 19 categories and to be aggregated into six main classes. Default parameters such as leaf-area index, rooting depth, and stomatal diffusion for these various classes are obtained from (Schulla and Jasper, 2000; Schulla, 2012). Figure 3.1 shows the landuse map for the upper Thu Bon basin.

Soil data

Soil texture data were derived from the Harmonized World Soil Database (HWSD), a raster soil database with the original grid cell resolution of 1km (FAO, 2012). The HWSD contains spatial soil mapping units (SMU) consisting of dominant and associated soils. A SMU includes one or more soils, often three or four soil types (Nelson et al., 2015). Initially, based on the coordinates of study domain, the matching soil mapping unit is obtained. This soil data was subsequently processed onto to 500m regular grid using the ArcGIS and Tanalys preprocessing analysis tools. The parameter required for the model e.g. the van Genuchten parameters were derived from Hodnett and Tomasella (2002). Other parameters including porosity, saturated soil moisture content, and wilting point of soil moisture content were obtained from Schulla (2012). Figure 3.2 shows the dominant soil mapping unit codes for the study area.
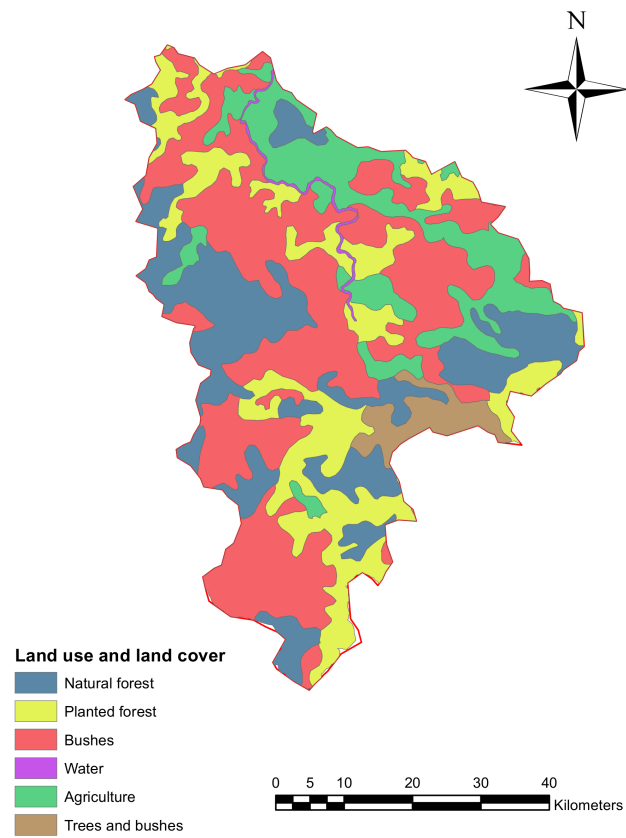
Figure 3.1: Landuse in the upper VGTB basin (the Thu Bon basin).
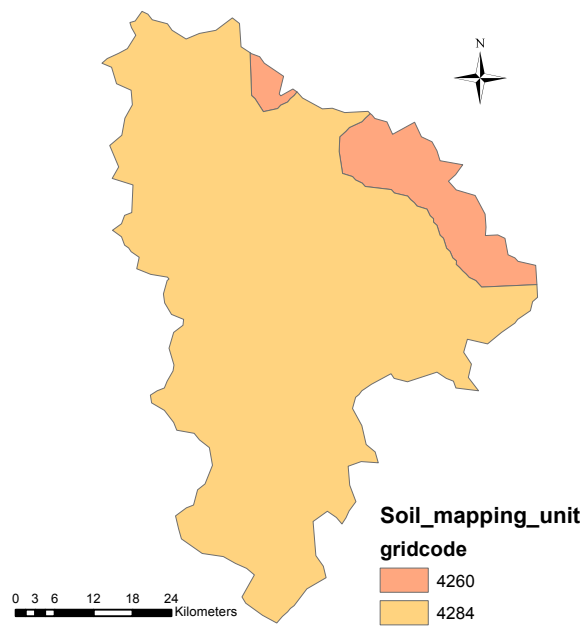
Figure 3.2: Soil type in the upper VGTB basin (4260: Clay, 4284: Silt loam).

Standard set up

In this study, a 24-hour model time step is selected due to the availability of daily observed data and daily reanalysis data. The horizontal resolution for the model set up is 500m grid cell. The vertical fluxes of water within the unsaturated soil zone are calculated with a finite difference scheme for the discrete Richards equation. Surface runoff, interflow, and base flow are determined at each model grid cell. The base-flow is aggregated over the catchment using a conceptual approach because reliable information on aquifers in the study area is not available. Total discharge is formed at the outlet gauge from superimposing three runoff components. Channel routing is applied to the total discharge based on hydraulic calculations of the flow velocities (the kinematic wave approach). Apart from meteorological data the model requires gridded information on topography, soil characteristics and land use. The settings and methods applied for the most important modules are shown in (Table 3.1).

Table 3.1: Module settings for the hydrological WaSiM model

Considered Module	Approach
Spatial interpolation of data	Inverse distance weighting and bilinear
Evapotranspiration	Penman-Monteith
Interception	Bucket approach
Unsaturated Zone	Infiltration Green-Ampt / Peschke Richards equation
Groundwater	Conceptual approach
Routing	Single linear storage / Kinematic wave

3.2.3   Performance criteria for the hydrological model

In order to evaluate the performance of the hydrological model WaSiM, several statistical measures are used. These criteria include the coefficient of determination (R^2), Nash-Sutcliffe efficiency (NSE), the root mean square error (RMSE) and the RMSE related to the data range, i.e. by applying a max-min normalization (NRMSE), and the percent bias (PBIAS).

The coefficient of determination denotes the strengths of the linear relationship between simulated and observed flows. R^2 ranges between 0 and 1.

$$R^2\,[-] = \left(\frac{\sum_{i=1}^{n} \left(Y_{i,obs} - \bar{Y}_{i,obs}\right)\left(Y_{i,sim} - \bar{Y}_{i,sim}\right)}{\sqrt{\sum_{i=1}^{n} \left(Y_{i,obs} - \bar{Y}_{i,obs}\right) \sum_{i=1}^{n} \left(Y_{i,sim} - \bar{Y}_{i,sim}\right)}} \right)^2 \tag{3.6}$$

where $Y^i obs$ is the ith day observed flow, $Y^i sim$ is the ith day simulated flow and *n* is the total number of days in the flow time series.

The NSE value indicates how well the observed data versus simulated results fit the 1:1 line (Nash and Sutcliffe, 1970). NSE values range from -∞ to 1, with values less than or very close to zero indicating a poor model performance and values equal to one indicating a perfect performance. It is in particular suitable for measuring the performance of high flows (Dobler et al., 2012a). NSE is expressed as follows:

$$NSE\,[-] = 1 - \frac{\sum_{i=1}^{n}\left(Y_{i,obs} - Y_{i,sim}\right)^2}{\sum_{i=1}^{n}\left(Y_{i,obs} - \bar{Y}_{i,obs}\right)^2} \tag{3.7}$$

RMSE is a non-biased performance criterion measuring the differences between simulated values and observed values. It punishes "outlines" by the square. A smaller value indicates better model performance (Chai and Draxler, 2014).

$$RMSE\,[-] = \sqrt{\frac{\sum_{i=1}^{n}(Y_{i,sim} - Y_{i,obs})^2}{n}} \tag{3.8}$$

Apart from the RMSE, the NRMSE is related to the range of the observed data.

$$NRMSE\,[-] = \frac{RMSE}{Y_{max} - Y_{min}} \tag{3.9}$$

Percent bias (PBIAS) is a measure for the total volume differences between simulated and observed flows. It is used to evaluate the long-term performance of the model simulations (Breuer et al., 2009). A positive value indicates model underestimation whereas a negative value indicates model overestimation (Gupta et al., 1999). A PBIAS of 0 represents a perfect fit.

$$PBIAS\,[\%] = \frac{\sum_{i=1}^{n}\left(Y_{i,obs} - Y_{i,sim}\right)}{\sum_{i=1}^{n} Y_{i,obs}} \cdot 100 \tag{3.10}$$

3.2.4 Parameter estimation tool PEST: Introduction

PEST Parameter estimation (Doherty, 2002) is a tool for automated model parameter estimation. This is a classical search method, widely used, and can be adapted to existing models (e.g. Kunstmann et al., 2006; Cullmann et al., 2011). For nonlinear parameter estimation, PEST uses the Gauss-Marquardt-Levenberg algorithm. This is an iterative estimation process that expects fewer model runs than any other estimation method (Doherty, 2002). However, the drawback of the method is that the algorithm might converge to a local minimum (Cullmann et al., 2011). PEST requires user specified parameter ranges and initial values to optimize the given

model. At the start of each iteration, the relationship between model parameters and model simulated values is linearized by the approximate expansion using the Taylor's theorem. Thus the calculation of the derivatives of all observations with respect to all parameters must be done. The iterative estimation process is briefly summarized as follows, following Doherty (2002), and Kunstmann et al. (2006).

Suppose that the function M which maps n-dimensional parameter space into the m-dimensional observation space is the representative of the relationship between parameters and model simulated outputs. It is required that this function is continuously differentiable with respect to all model parameters for which estimates are searched for. The corresponding set of discharges q_o derived from hydrological model using the set of parameters comprising the vector p_o is then:

$$q_o \left[m^3/s \right] = M(p_o) \tag{3.11}$$

The model output q corresponding to parameter vector p that is slightly different from vector p_o, can be approximated to (Taylor's theorem).

$$q \left[m^3/s \right] = q_o + J \cdot (p - p_o) \tag{3.12}$$

In which J is the Jacobian matrix (m rows, n columns) of M. J_{ij} is the derivative of the ith observation with respect to the jth parameter. The ultimate goal of the model calibration is to derive a set of parameter for which the model generated outputs are as close as possible to observed runoff. PEST does this by minimizing the objective function which is given by:

$$\Phi_{Discharge} \left[m^3/s \right] = \sum_{i=1}^{m} (w_i r_i)^2 \tag{3.13}$$

where r_i is the difference between the simulated discharge and observed discharge, w_i is the weight attached to the i's observation.
Equation 3.13 can be rewritten as,

$$\Phi_{Discharge} \left[m^3/s \right] = (q_{obs} - q_o - J \cdot (p - p_o))^t \cdot W \cdot (q_{obs} - q_o - J \cdot (p - p_o)) \tag{3.14}$$

superscript "t" denotes the transposed matrix, q_{obs} indicates the observed discharges and q_o the simulated discharges. W is a square matrix (m x m) whose entries w_{ij} are the squares of weights that account for the discrepancies contributed to the objective function of the observations. Observation with higher reliability should contribute larger weight to the objective function. A new estimate for the parameter p can be obtained by

$$p \left[- \right] = p_o + u \tag{3.15}$$

where u is the parameter upgrade vector

$$u[-] = (J^t \cdot W \cdot J)^{-1} \cdot J^t \cdot W \cdot (q_{obs} - q_o) \qquad (3.16)$$

superscript "-1" denotes the inverse matrix.

Let the gradient of the objective function Φ in parameter space be denoted by the vector g, which is defined as

$$g[-] = \frac{\partial \Phi}{\partial p_i} \qquad (3.17)$$

and which can be expressed as

$$g[-] = -2J^t \cdot W \cdot (q - q_o) \qquad (3.18)$$

Equation 3.16 rewritten by Marquardt (1963) and Levenberg (1944) then becomes

$$u[-] = (J^t \cdot W \cdot J + \alpha I)^{-1} \cdot J^t \cdot W \cdot (q_{obs} - q_o) \qquad (3.19)$$

where α is the Marquardt parameter and I is the (n x n) identity matrix. When α is high, the direction of u approaches that of negative of the gradient vector g, when α equals zero equation (3.17) becomes equation (3.14). For the initial optimization iterations, it is beneficial to assume a relatively high value of α. Then α is decreasing as the estimation process progresses and the optimum value of objective function is approached. To circumvent the round-off errors caused by the possibly great difference in magnitude of elements of Jacobian matrix (J), the scaling matrix S is introduced.

$$S_{ii}[-] = (J^t \cdot W \cdot J)_{ii}^{-0.5} \qquad (3.20)$$

At the first optimization, PEST will use the initial Marquardt lambda (denoted as $\lambda = \alpha S^t S$), provided by the user to get the objective function. A new λ is obtained by lowering the previous λ by a user-supplied factor. Then PEST tries the new λ to get a new objective function. If the corresponding objective function is lower, the λ is lowered yet again. If the objective function was raised by reducing λ below the initial λ, then λ is raised above its initial value. A new λ is formed by increasing the initial λ by the same user-supplied factor. If objective function was lowered, the λ is raised again. This procedure repeats until the minimum objective function is reached. A detailed information on how the PEST determines objective function is available in the PEST's manual (Doherty, 2002).

The sensitivity of each parameter with respect to all observations can be calculated (based on the Jacobian matrix) as follows.

$$s_i[-] = \frac{(J^t \cdot W \cdot J)_{ii}^{0.5}}{m} \qquad (3.21)$$

where m is the number of observations and i is the number of the parameter.

3.2.5 PEST: Coupling and communication to WaSiM

In general, PEST requires three input files for optimization of the WaSiM model's parameters. All these files are prepared in ASCII format. For a detailed description of these files it is referred to Doherty (2002):

- A *template file* consists of parameters needed to be optimized. This file is similar to the control file (contain parameters) of the WaSiM model but the values of parameters are replaced by variables (often as a sequence of characters) instead of fixed values.

- An *instruction file*. This file provides instructions to PEST on how to read the WaSiM model output files. The instruction file contains information on positions of simulated flows in WaSiM's output files. For every WaSiM model's output file containing model-generated information which is required a comparison with observations, an instruction file is provided accordingly.

- The *PEST control file*. This file provides information on parameters such as names and numbers of parameters cited in the template file, initial values of parameters, lower and upper bounds of parameter limits, incremental interval, and flow observation data. In addition, names and numbers of template files and instruction files are required for the PEST control file. Each pair of PEST template file - WaSiM input file (control file) and PEST instruction file - WaSiM output file has to be put in a line under "model input/output" section of the PEST control file. The model command line which supplies the command including path names for PEST to run the WaSiM model is also included. Figure 3.3 illustrates the coupling and communication between WaSiM and PEST.
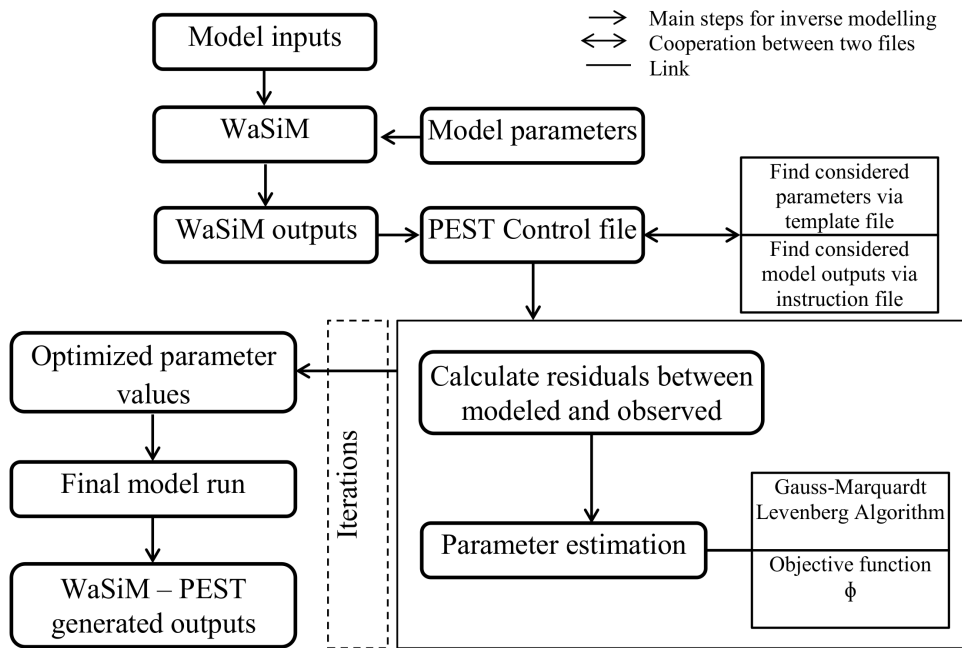
Figure 3.3: The flowchart for coupling between WaSiM and PEST

3.2.6   Calibration Procedure

The calibration of a hydrological model is a prerequisite for successfully applying to a specific catchment, especially for the weak infrastructure region where prior applications of the given model has not been done (Kunstmann et al., 2006; Cullmann et al., 2006). The main goal of the model calibration is to determine suitable parameter sets that result in satisfactory model performance under the specified conditions.

In this PhD thesis, the WaSiM model is calibrated and validated by continuous runoff simulations. A split sampling technique is used for the model calibration and validation. The period between 1976 and 1981 is used for model calibration, while two independent periods of 1982-1988 and 1995-2000 are used for model validation. One reason for the selection of these time periods was that the flow regime of the Thu Bon river was quite natural and was not disturbed by hydropower dams during these periods. Model simulated discharges are compared against discharges observed at Nong Son station. The model is calibrated using station precipitation and reanalysis data for temperature, relative humidity, wind speed and solar radiation (Laux et al., 2013). The geophysical parameters are extracted from the DEM, landuse, and soil maps. Other empirical parameters have to be calibrated. In total, six parameters have to be calibrated. The main calibration parameters for the VGTB basin are listed in Table 3.2.

In this PhD thesis, also an covariance analysis is conducted to obtained confidence bounds for estimated parameters. The covariance matrix is given by (following Press

Table 3.2: Main calibration parameters for WaSiM model

Parameter	Unit
Recession constant for direct runoff (k_d)	[h]
Recession constant for interflow (k_i)	[h]
Drainage density (d_r)	[m^{-1}]
Recession constant for saturated-hydraulic conductivity with depth (k_{rec})	[-]
Scaling factor for base flow (Q_0)	[-]
Recession constant for base flow (k_B)	[m]

et al. (1992) and Kunstmann et al. (2006)):

$$[Cov] \equiv [\alpha]^{-1} \tag{3.22}$$

with matrix $[\alpha]$, equal to one-half times the Hessian matrix

$$\alpha_{kl} \equiv \frac{1}{2}\frac{\partial^2 \chi^2}{\partial p_k p_l} \approx \sum_{i=1}^{N}\left[\frac{\partial y(x_i, p)}{\partial p_k} \cdot \frac{\partial y(x_i, p)}{\partial p_l}\right] \tag{3.23}$$

Cov is the two-dimensional projection of the n x n parameter covariance matrix; p is the two-dimensional vector of parameters; $k = 1, 2....M$; N is the data points (x_i, y_i). The uncertainty of the estimated parameters is quantified by the standard deviations which yielded from the square roots of the diagonals of the parameter covariance matrix. The uncertainty range is described by the standard deviations only in case the correlation between the estimated parameters is negligible. In case two parameters are correlated, the axes of the hyper-ellipsoid are rotated with respect to the parameter axes (Kunstmann et al., 2006).

Two-dimensional ellipses are most frequently used for describing the shape of confidence region. The confidence ellipses are defined as

$$\Delta\chi^2(p) = (p - p_{bestfit}) \cdot [Cov]^{-1} \cdot (p - p_{bestfit})^T \tag{3.24}$$

$\Delta\chi^2$: tabulated function depending on confidence level and number of degrees of freedom (number of parameters of interest) while $(p - p_{bestfit})$ is the change in parameters whose second component is the optimized parameter. Confidence ellipses for any combination of two parameters are obtained by applying Equation 3.24 to the covariance matrix and the estimated parameters $p_{bestfit}$.

The calibrated model parameters are obtained by two approaches: the trial-and-error procedure (manual approach) and the automatic parameter estimation tool PEST (Doherty, 2002). For the manual calibration, a combination of visual assessment and the

NSE is used to achieve optimal parameters by successively adjusting the most cru-
cial model parameters until modelled and observed discharges correspond well. Con-
versely, PEST tries to minimize an objective function that is represented by weighted
sum of squared difference between model-generated discharges and observed discharges
(Gauss-Marquardt Levenberg-approach). Boundaries for the parameters search are
provided to force the Gauss-Marquardt-Levenberg algorithm into the correct parame-
ter range. The results shown in this PhD thesis are based on the PEST approach.

3.3   Results and discussion

3.3.1   Model calibration

As mentioned in section 3.2.1, this is the first time that WaSiM is adapted and applied
for the VGTB basin. Accordingly, the calibration of the model is a crucial prerequisite
before an implementation for the hydrological impact analysis. This section presents
the results of the model calibration.

Values for estimated model parameters and the estimated uncertainty range (standard
deviation σ) of all estimated parameters derived from Equation 3.22 and Equation 3.23
are shown in Table 3.3.

Table 3.3: Main calibration parameters for WaSiM model including uncertainty ranges
(standard deviation σ) and parameter sensitivity (s) according to covariance analysis.

Parameter	Unit	Limits	Initial value	Optimized value	Standard deviation σ	Sensitivity s
k_d	[h]	10 - 100	15	30.6	1.6	8.8E+00
k_i	[h]	100 - 600	200	250	69.5	1.9E-01
d_r	[m^{-1}]	5.0 -30	20	12	2.8	5.4E+00
k_{rec}	[-]	0.1 - 1.0	0.5	0.8	-	-
Q_0	[-]	1.0 - 20	11	11.5	5.3	6.2E+01
k_B	[m]	0.01 - 0.99	0.9	0.96	0.2	2.4E+00

It can be seen that the uncertainty is relatively small for most of the estimated
parameters except for the recession constant of interflow which is about one order
of magnitude larger. Estimated values for all parameters are within the physical
reasonable ranges.

Figure 3.4 shows the confidence regions for the estimated recession constants for direct
runoff and interflow as obtained by the covariance analysis. The isolines show the
probabilities of 68.3% (red), 95.4% (blue) and 99.7% (green) that the true parameter

values fall within the corresponding confidence region. In this case, the correlation between the two calibrated parameters is negligible and k_d shows smaller confidence bounds than k_i. Figure 3.5 shows confidence regions for drainage density (d_r) and recession constant of direct runoff. As shown in the figure, it is rather an ellipse than a circle, parameters are a bit correlated.
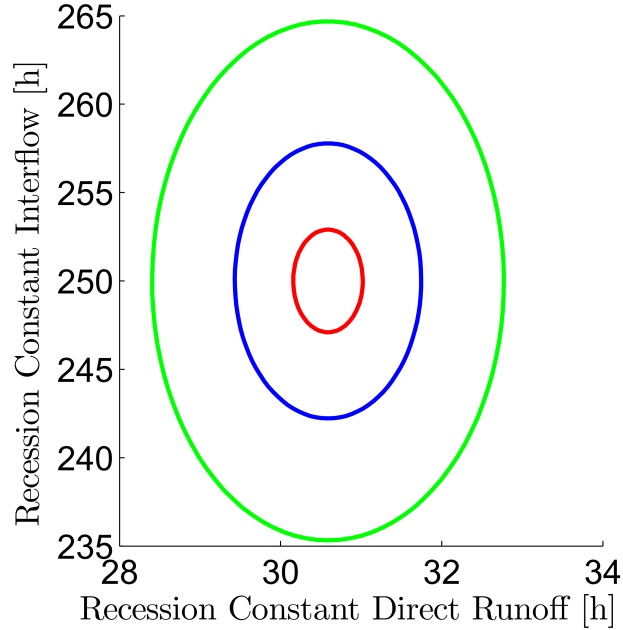
Figure 3.4: Confidence ellipses for estimated parameter k_d (recession constant for direct runoff) and k_i (recession constant for interflow). The isolines indicate the confidence regions 68.3% (red), 95.4% (blue) and 99.7% (green).

Apart form confidence ellipses, parameter sensitivities are also of a particular concern for the model performance as they quantify the influence on the performance. Values of parameter sensitivity in case of optimal parameters are calculated by Equation 3.21 and shown in Table 3.3. Of all estimated parameters, the sensitivity of the recession constant for interflow (k_i) has a lower value than that of other parameters indicating that the estimated value of this parameter is less reliable. This is consistent with the confidence ellipses which show larger confidence bounds for k_i than those of other parameters.

The results of the calibration of WaSiM model are provided in Table 3.4. It can be seen that NSE and R^2 are comparable for the two calibration approaches and are in a satisfying range. Values of RMSE and NRMSE are also in the same order of magnitude for both calibration approaches (manual calibration and PEST approach).
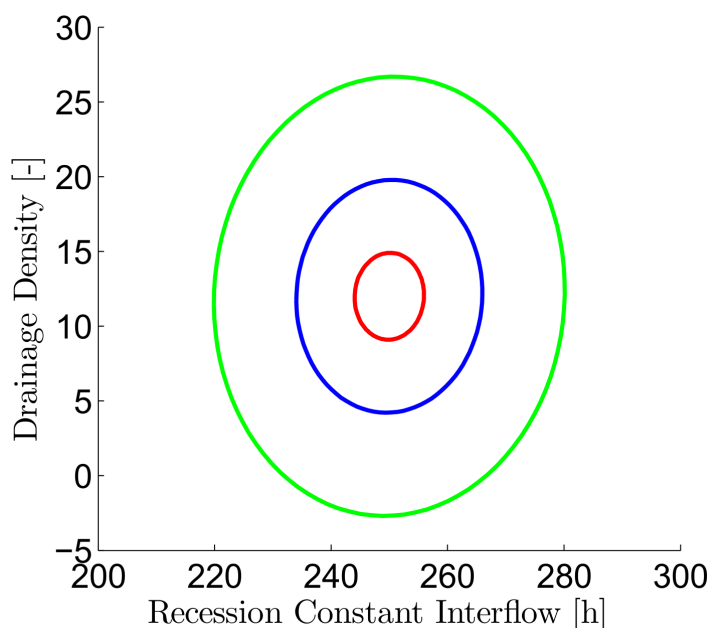
Figure 3.5: Confidence ellipses for estimated parameter d_r (drainage density) and k_i (recession constant for interflow). The isolines indicate the confidence regions 68.3% (red), 95.4% (blue) and 99.7% (green).

Table 3.4: Values of performance criteria for calibration of the hydrological model WaSiM.

Calibration (1976 - 1981)					
Criteria	NSE	R^2	PBIAS (%)	RMSE	NRMSE
Manual	0.84	0.84	-0.6	194	0.031
PEST	0.83	0.85	-0.2	197	0.032

Figure 3.6 shows the modelled and observed daily time series of Nong Son station for the model calibration (1976-1981).

A visual inspection indicates that the simulated flows match the observations reasonably well despite a slight underestimation of some flood peaks (Figure 3.6). The slight underestimation of the flow peaks can be observed for both calibration strategies. According to the performance criteria in Table 3.4, no remarkable differences between the two calibration strategies can be observed. Differences between modelled and observed flows are probably due to a small number of precipitation stations within the study area of interest. Additionally, the interpolation method applied in this complex orography conditions may lead to considerable errors in precipitation input to the model, thereby contributing further to this small mismatch.
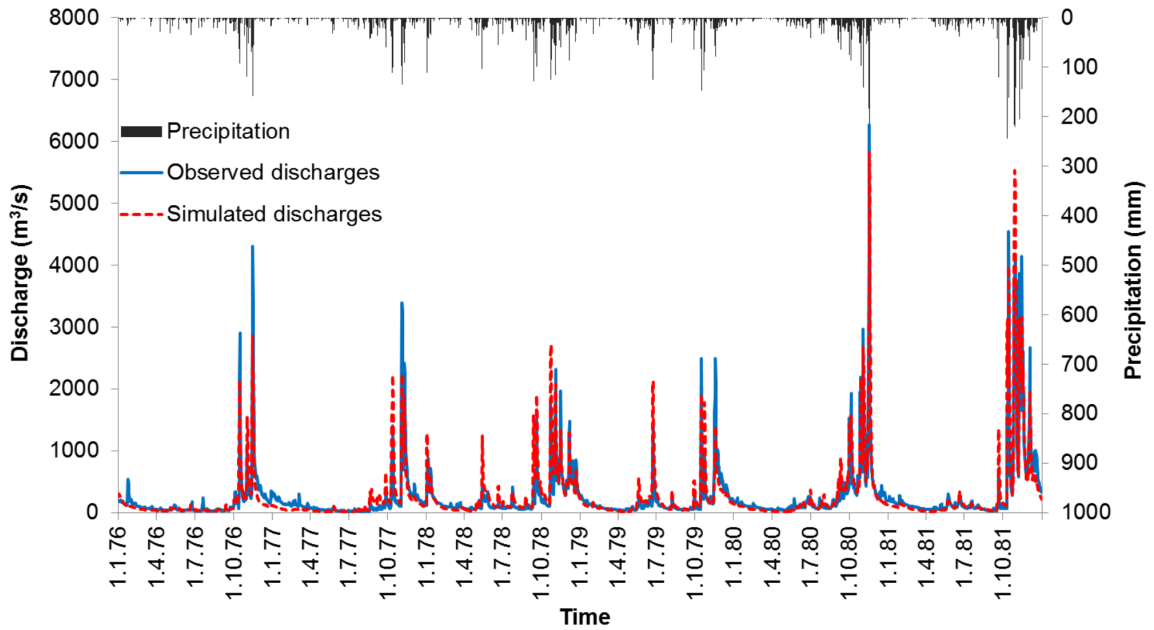
Figure 3.6: Runoff performance of the WaSiM at Nong Son station for the calibration period (1976-1981). Results are obtained using PEST.

3.3.2   Model validation

The quality of the model performance for the two independent validation periods (1982-1988 and 1995-2000) is shown in Table 3.5. It can be seen that values of NSE, R^2 are all positive and greater than 0.8 for both the manual (trial and error) and PEST approaches. The absolute values of PBIAS range between -5.6% and +1.7 %. Compared to the calibration period, the values of NSE and R^2 are in the same order of magnitude, but PBIAS is in general slightly larger.

Table 3.5: Values of performance criteria for the two validation periods 1982 - 1988 and 1995-2000 of the hydrological model WaSiM.

Criteria	NSE	R^2	PBIAS(%)	RMSE	NRMSE
Validation 1982 - 1988					
Manual	0.83	0.84	1.7	194	0.029
PEST	0.82	0.83	-1.3	191	0.028
Validation 1995 - 2000					
Manual	0.85	0.86	-5.6	317	0.036
PEST	0.86	0.86	-5.3	308	0.035

Figure 3.7 and Figure 3.8 show the simulated and observed hydrographs at Nong Son station for model validation (1982-1988) and (1995-2000). As shown, a slight underestimation of flows is observed. However, the general quality of fits are reasonable

and convincing for both validation periods.
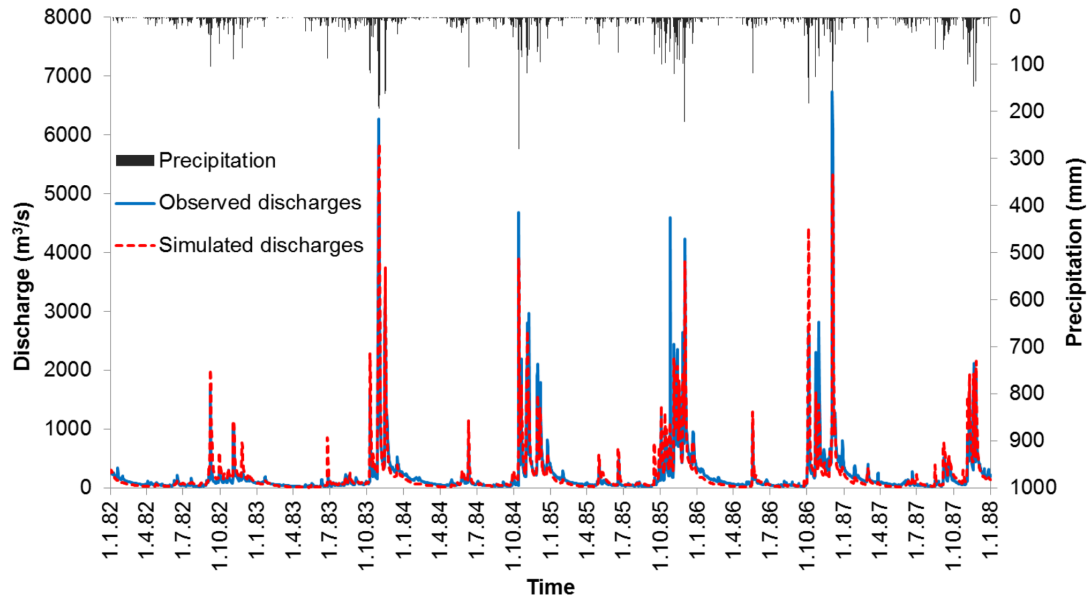
Figure 3.7: Runoff performance of the WaSiM at Nong Son station for the validation period (1982-1988). Results are obtained using PEST.
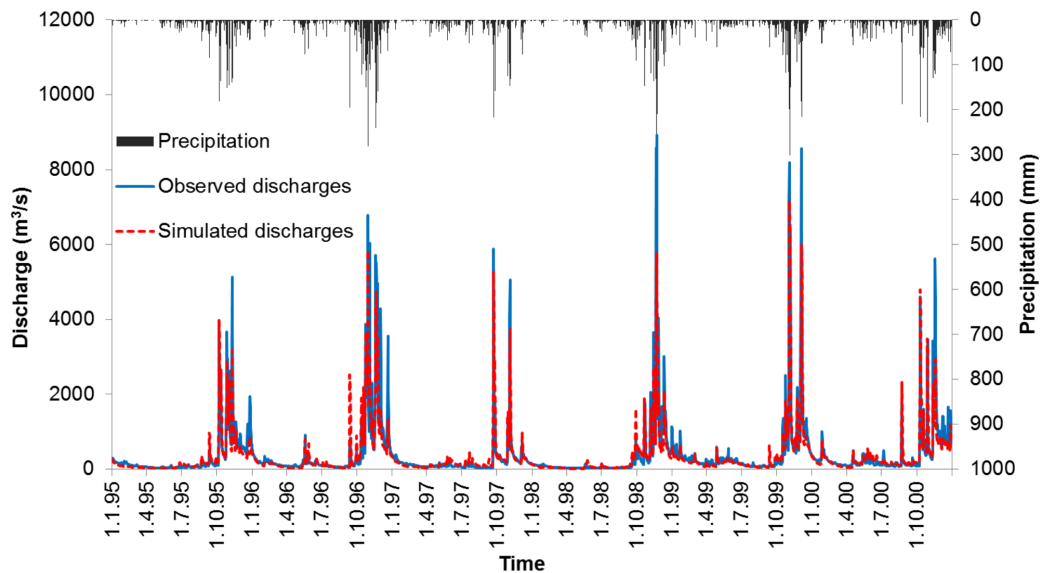
Figure 3.8: Runoff performance of the WaSiM at Nong Son station for the validation period (1995-2000). Results are obtained using PEST.

In addition to the temporal distribution, the WaSiM model also provides information on the full water balance in a spatially distributed manner such as actual evapotran-

spiration and total runoff as annual mean or sums. Figure 3.9 shows the spatial distribution of actual evapotranspiration and total runoff in the basin as an example. It can be seen that there is a high spatial variability of actual evapotranspiration and total runoff over the basin. This spatial distribution efficiently provides the physical basis required to support decision making processes in economically and ecologically sound water management in the VGTB basin.
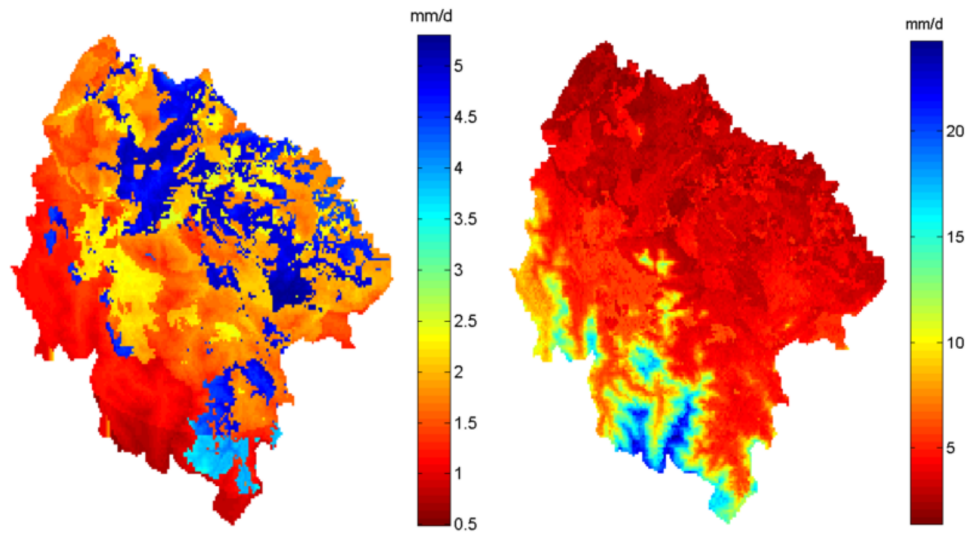
Figure 3.9: Daily mean actual evapotranspiration (left) and daily mean total discharge (right) in the Thu Bon basin (1982-1988).

3.3.3   Discussion

The NSE and R^2 values for the model calibration and validation obtained from the two approaches are in the same range and not lower than 0.82. NRMSE values are also at the same order of magnitude of about 0.03 for both calibration and validation periods. Negative values of PBIAS show underestimation of river flows at Nong Son station for both calibration and validation, however, the values are within acceptable ranges. The underestimation is also shown in the flow duration curve for the long-term simulation 1976-2000 (Figure 3.10), where simulated low flows show sightly lower values than observed values. Interpolation method applied in this complex orography conditions together with a small number of rainfall stations may result in this mismatch. The affect of different interpolation methods on precipitation input to hydrological models is also confirmed in a study by Wagner et al. (2012). Considering the complexity of the catchment and uncertainties introduced by meteorological input data, the calibrated WaSiM model shows a good agreement between the simulated and observed discharges. The calibrated WaSiM is found to be able to reproduce hydrographs for the VGTB basin, both for high and low flow situations. Similar performances of WaSiM are reported in literature for different study regions (Jasper et al., 2004; Kunstmann et al.,

2006; Ahrends et al., 2008; Cullmann et al., 2011). This indicates that the WaSiM model can be applied to tropical catchments. The results also show that PEST is a suitable tool for parameterizing the WaSiM model. This complements the findings of Kunstmann et al. (2006) and Cullmann et al. (2011). It is noted that the WaSiM model was calibrated using (local) station precipitation and reanalysis climate data. Under the assumption that the calibrated parameters of the WaSiM model will remain unchanged under future conditions, these parameters can be applied for hydrological simulations addressing future time slices.
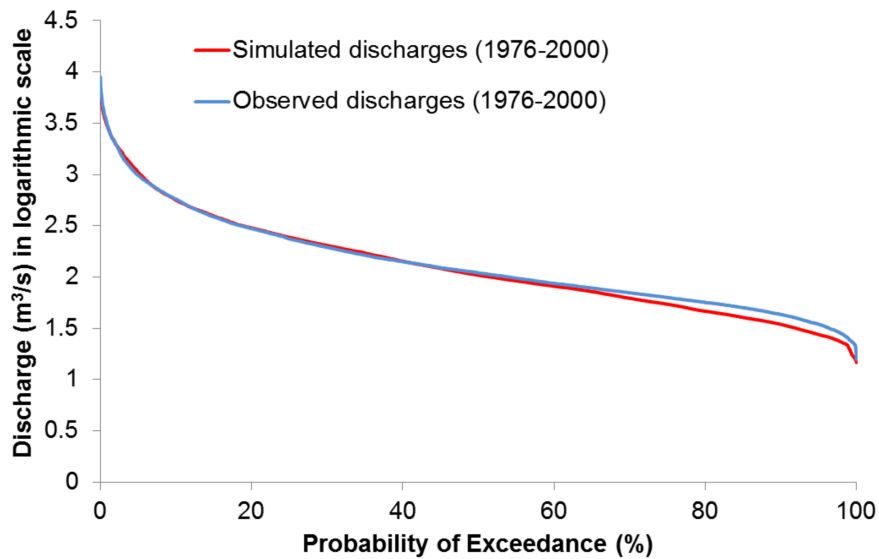
Figure 3.10: Flow duration curve at Nong Son station in the period (1976-2000).

Chapter 4

Integrated hydrological-irrigation optimization model

4.1 Introduction

In the Vu Gia - Thu Bon basin, agriculture is the primary economic sector in terms of labour. Over 50% of the population are employees working in agriculture. Total rice cultivation area for the entire Quang Nam province is about 87,396 ha for two rice crops winter-spring and summer-autumn. Irrigation in the VGTB basin relies on the availability of water in reservoirs prior to cropping seasons. In close consultation with stakeholders in the region, it is revealed that there is an increasing occurrence frequency of water shortages for irrigation during dry seasons. Particularly, water is often insufficient to irrigate the entire rice cropping areas during the summer-autumn rice season. In this PhD thesis, an irrigation optimization model is developed based on GAMS and combined with the hydrological model WaSiM to optimize the efficient-water irrigation technology and irrigation scheduling for a rice irrigation scheme in the VGTB basin.

4.2 Methodology

4.2.1 GAMS: Introduction

The General Algebraic Modelling System (GAMS) is a high-level language for solving mathematical and optimization problems (Rosenthal, 2016). This programming language is widely used in research studies on water resources and agriculture (Bharati et al., 2008). Although GAMS is designed for large mathematical optimization problems, it is not the optimizer itself but is combined with one optimization solver for optimization modeling (Ahrends et al., 2008). The optimization solvers include linear, non-linear, mixed integer, relaxed mathematical programs, mixed complementarity and extended mathematical programs. In this PhD thesis, the CPLEX - a solver that uses

branch and cut algorithms for solution search and is frequently used for mixed integer programming (MIP) is employed (GAMS, 2016). CPLEX contains a primal simplex algorithm, a dual simplex algorithm, a network optimizer, an interior point barrier algorithm, a mixed integer algorithm and a quadratic capability (Pedroso, 2013). The GAMS model defines the structures including model objects, data, variables, bounds and constraints of variables, objective function and equations. For more detailed information about GAMS, the reader is referred to https://www.gams.com.

4.2.2 Integration of the hydrological model WaSiM and the irrigation optimization model

A vast number of integrated hydrological and irrigation models have been developed for different spatial scales (e.g. Al-Juaidi et al., 2014; Ahrends et al., 2008; Bharati et al., 2008; Quinn et al., 2004; Rosegrant et al., 2000). The formulation of these integrated models can be done by either a compartment modelling approach or a holistic approach. Under the compartment modelling approach there is a loose connection between hydrologic and irrigation components and they are connected via outputs. Under the holistic approach, both the hydrologic and irrigation components are embedded in one single unit; this often requires a model interface (Cai et al., 2003).
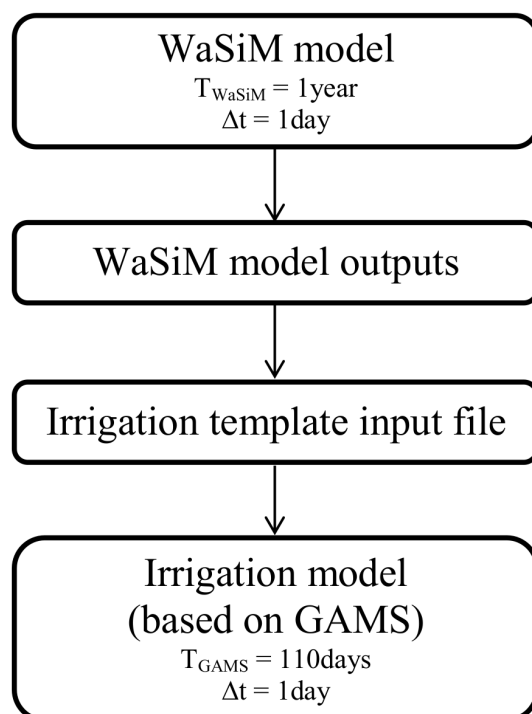
Figure 4.1: The connection between WaSiM and GAMS

In this PhD thesis, a simple one way coupled model system is used allowing the simulation of the connections between the hydrologic and irrigation for the water management via outputs. This modelling system consists of the hydrological model WaSiM and an irrigation optimization model written in GAMS. The hydrological model WaSiM simulates the hydrological response of the VGTB basin, which serves as input for the optimization model of agricultural management strategies in the Que Trung rice irrigation scheme. Figure 4.1 illustrates the connection between the hydrological model WaSiM and the irrigation optimization model GAMS.

The irrigation optimization model uses daily discharges at the Que Trung sub-catchment as reservoir inflow and reference evapotranspiration (ET_0) simulated by the WaSiM model (section 3.1) as input data. The crop evapotranspiration (ET_c) is calculated by the following equation.

$$ET_c = K_c \cdot ET_0 \tag{4.1}$$

where K_c is the crop coefficient for rice. K_c is dependent on rice development stage and is derived from (FAO, 1998). ET_0 is reference evapotranspiration simulated by the WaSiM model.

In this PhD thesis, two different rice irrigation technologies, i.e. Alternate Wetting and Drying (AWD) or Continuous Flooding (CF) are optimized in the irrigation optimization model. Details about these two irrigation technologies are described in the next section.

4.2.3 Alternate Wetting and Drying and Continuous Flooding technologies

Alternate Wetting and Drying is an eco-efficiency rice irrigation technology which is capable of saving irrigation water input by reducing the number of irrigation events required. In the AWD, the rice field is not kept continuously submerged during the rice growing stage. It is allowed to dry out intermittently for a certain number of days before being re-flooded (Lampayan et al., 2015a). In a specific form of AWD, the "safe" AWD, the water can be dropped to 15 cm below the soil surface before the next irrigation without yield reductions. The threshold of 15 cm will not cause any yield decline since the roots of the rice plants are still able to take up water from the perched ground water and the almost saturated soil above the water table. The period of non-flooded soil can vary from few days to more than 10 days in the absence of precipitation depending on soil type and weather/climate conditions (Bouman et al., 2007; Rejesus et al., 2011; Lampayan et al., 2015a).

In this PhD thesis, the "safe" AWD approach is applied for rice cropping. During

early growth stage, the water level is always maintained around 2-5 cm above soil surface for about two weeks to suppress weeds and control pests (Bouman et al., 2007; Lampayan et al., 2015a). After the early growth stage, the AWD irrigation is applied again until one week before the flowing period starts. From one week before to one week after the flowering period the field is again continuously flooded about 5 cm above the soil surface to avoid spikelet sterility and yield loss (Lampayan et al., 2015b). After this period the AWD is re-applied until maturity. In contrast to the AWD, *Continuous Flooding* (CF) technology water level is constantly kept above the soil surface during the growing season. It is usually kept at a certain level (5 cm above the soil surface) during the growing period from a few days after transplanting until few days before maturity. Figure 4.2 illustrates the AWD and CF technologies used.
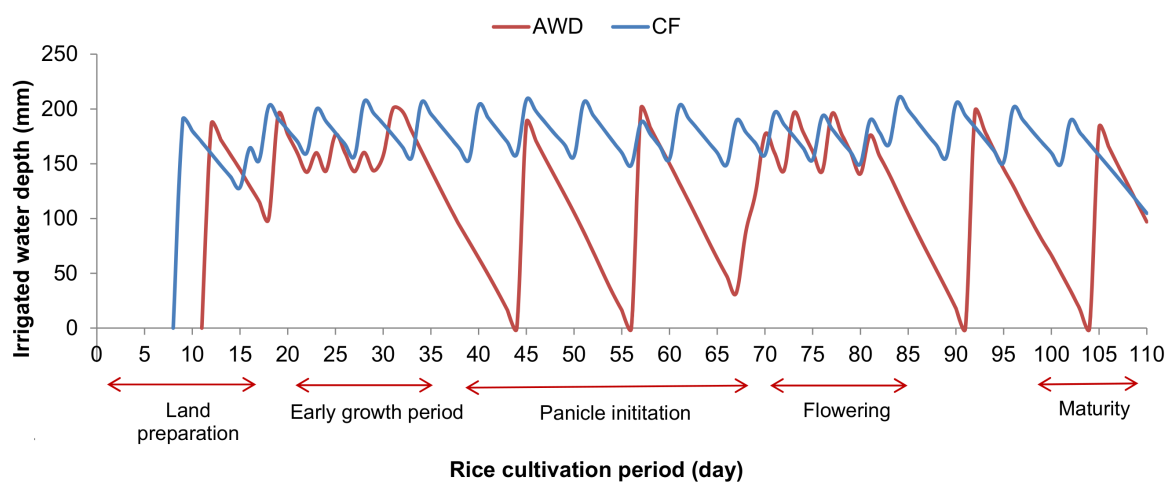
Figure 4.2: AWD and CF irrigation technologies

The application of the AWD practice in major rice cropping regions has been analyzed in several studies. The majority of these studies show that AWD can save irrigation water compared to CF without significant yield losses, as e.g. demonstrated for Bangladesh (Rahman and Bulbul, 2014), Southern China (Liang et al., 2016), and the Philippines (e.g. Rejesus et al., 2011; Zhang et al., 2012). Apart from similar yields obtained by AWD (compared to CF), a reduction in rice yield is revealed in (e.g. Tabbal et al., 2002; Belder et al., 2004) and, while an increase is found in (Li and Li, 2010).

In Vietnam, the AWD technology was introduced as a response to decreasing water availability for rice production and increasing greenhouse gas emissions. For instance, Lampayan et al. (2015a) conducted a research on adoption of AWD management for irrigated lowland rice in the Philippines, Bangladesh and Vietnam. The results showed that AWD can reduce necessary water input for irrigation up to 38% without

a yield reduction, if implemented correctly. Most of performance analyses of AWD are derived in small-scale field experiments.

The number of studies considering the adoption of water-saving technology for a complete rice irrigation system is limited for Southeast Asia. Hong et al. (2015) developed a water balance model to simulate water level changes in the rice field which accounts for interactions between the rice field and the irrigation system, and evaluated the effectiveness of different irrigation technologies for the Soc Trang province, Southern Vietnam. Results showed that AWD is the most effective irrigation technology in terms of water requirements and the number of irrigation events. The number of irrigation events (pumping times) are found to range between 11 and 32 among different considered irrigation technologies.

4.2.4   Development of the irrigation optimization model

The Que Trung rice irrigation system is shown in Figure 4.3. This irrigation scheme is selected during the field survey in 2015. This is a representative irrigation scheme for the VGTB basin.
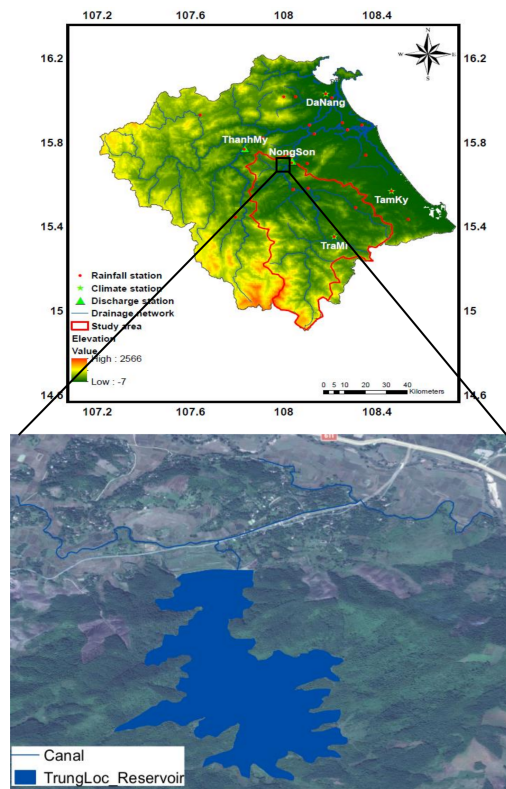
Figure 4.3: The VGTB basin (top). The red boundary dipicts the area used for hydrological modelling (WaSiM). The Que Trung rice irrigation system is shown in a small black squared box, the reservoir and canal system is shown below (bottom).

The irrigation optimization model developed for this irrigation system is written in GAMS. The model includes an irrigation network, a reservoir, irrigation technologies and schedules, and an objective function. The model maximizes the return of rice production for the whole irrigation scheme. There are three different irrigation areas (area 1, area 2 and area 3) accounting for 144 ha and each area can operate up to four irrigation blocks, tertiary level (Figure 4.4). Each block has a size of 12 ha. This leads to 12 tertiary irrigation units. Irrigation can be staggered on 15 different days and farmers can choose between AWD or CF. The allocation of land for irrigation (number of blocks), the irrigation technology, and the irrigation scheduling associated to each block are important decision variables to be optimized. Albeit the model design is closely related to the real situation in the Que Trung irrigation system, at the same time it is flexible enough to be applicable to similar irrigation schemes in the region.
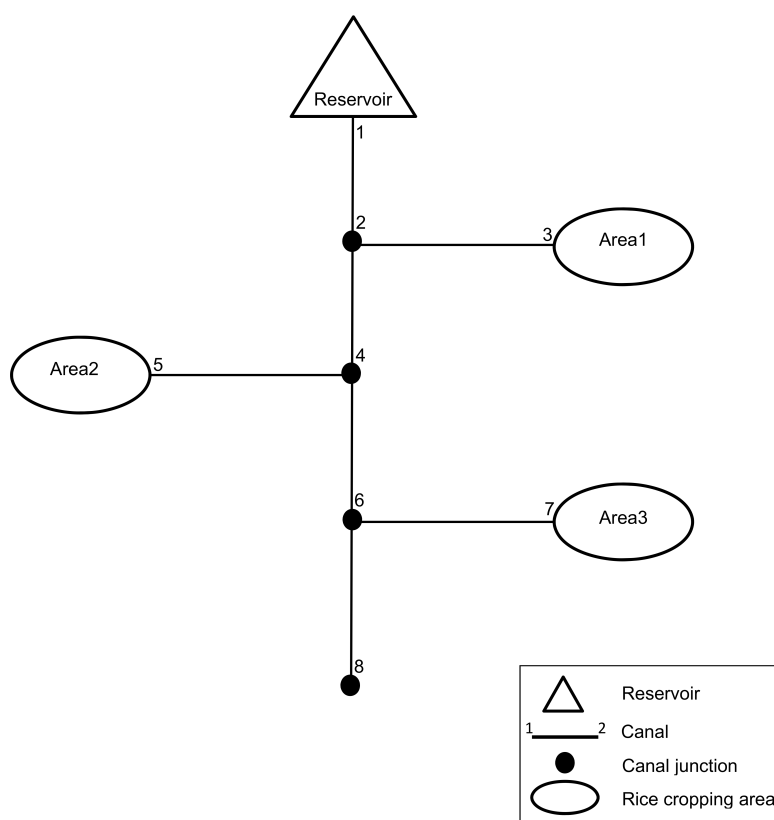
Figure 4.4: Schematic diagram of agricultural plot, consisting of 3 irrigated rice growing areas, each divided into 4 blocks. Water is taken from the Trung Loc reservoir for irrigation

The SA rice cultivation period covers a fixed period of 110 days starting from land preparation until maturity. The irrigation optimization model provides each block 200 mm water for land preparation. The model optimizes the date of the first irrigation for each block within the three irrigation areas during the land preparation stage (first 15 days). The following irrigation events depend on the crop evapotranspiration and the

percolation rate exclusively. Possible modeled irrigation options include AWD and CF. The choice of irrigation technology determines the irrigation water input for each block.

Objective function The objective function is to maximize the monetary profit under different scenarios. Economic variables include crop yield and rice price. Maximum profit will be obtained by maximizing cultivation area under different water availability scenarios. Based on previous studies (e.g. Rejesus et al., 2011; Rahman and Bulbul, 2014; Liang et al., 2016), it is assumed that rice yield is identical under AWD and CF.

$$\Phi_{Return} = Z = \sum_{ij=1}^{8} \sum_{b=1}^{4} \sum_{s=1}^{15} \sum_{tech=1}^{2} [price \cdot yield \cdot area_{tech} \cdot C_{(i,j,b,s,tech)}] \qquad (4.2)$$

where Z is the irrigated rice profit (VND), *yield* is the irrigated rice yield (kg/ha), *price* is the rice price (VND/kg). Rice price and rice yield are assumed to be 6000 VND (0.3 US$) and 5,000- kg/ha, respectively. Area (*area*) is the irrigated demand site (block), *i,j* is the primary $\{P\}$ and secondary canal $\{S\}$ respectively, *b* is the irrigated area of each site, *b* = 1,2,3,4, *s* is the order of irrigation event, and *tech* is the irrigation technology (AWD or CF) applied to each block. C is the binary variable indicating the chosen irrigation technology in the respective block and irrigation area.

The revenue is only obtained from the irrigated area (expressed by block in this study). Thus, the total profit is the sum of revenue from areas receiving irrigated water. The optimal value is obtained when limits set by the user is reached. One of the limits is the relative optimality criterion (OptCR) defined as below (following The Solvers Manuals, GAMS, 2016).

$$\frac{(|\, BP - BF\, |)}{(1.0e - 10 + |\, BF\, |)} < OptCR \qquad (4.3)$$

where BP is the best possible integer solution, BF is the objective function value of the current best integer solution. In this study, OptCr is set to 0. Another stopping criterion is the time limit. The solver will stop after a user-defined execution time (set to 100,000 second in the model), then the current solution is passed to the irrigation model.

Land constraints The binary variable C determines which block is in the optional solution, using either the AWD or the CF irrigation technology. There cannot be more than one starting time *s* and technology *tech* per irrigation single block *b* and area *i, j*. The maximum land to be irrigated must be smaller than or equals to the total available land.

$$\sum_{s=1}^{15} \sum_{tech=1}^{2} C_{(i,j,b,s,tech)} \leqslant 1 \qquad (4.4)$$

with i,j $\in \{S\}$

Reservoir balance The reservoir level in $t+1$ is equal to the level in t plus the water inflow (accounting rainfall) and the reservoir discharge for irrigation.

$$R_{(t+1)} = R_{(t)} + q_{in,t} - \overline{Q}_{(t)} \qquad (4.5)$$

where $q_{in,t}$ is the inflow coming to the reservoir at time t. $R(t=1) = \bar{r}$

Primary canals The discharge $\overline{Q}_{(t)}$ (water requirement for irrigation) at time t cannot exceed the reservoir released discharge $\bar{q}$:

$$\overline{Q}_{(t)} \leqslant \bar{q}, \forall t \qquad (4.6)$$

Secondary canals The mass balance at the secondary canals in the irrigation areas is

$$Q_{(ij,t)} = \sum_{b=1}^{4} \sum_{s=1}^{15} \sum_{tech=1}^{2} SQ_{(ij,b,s,tech,t)} \qquad (4.7)$$

with $i,j \in \{S\}$, t. SQ_t is the inflow to the block at time t (mm).

Paddy field water balance The paddy water balance for selected blocks and technologies is

$$WD_{(ij,b,s,tech,t)} = WD_{(ij,b,s,tech,t-1)} - [ETc_{(t,s)} + Perc_{(t,s)} - Prec_{(t,s)}] \cdot C_{i,j,b,s,tech} \qquad (4.8)$$

with $i,j \in \{S\}$, b, s, $tech$, t. WD_t is the irrigation water depth at time t (mm); $ETc_{t,s}$ is the crop evapotranspiration (mm/day); $Perc$ is the percolation (mm/day); $Prec$ is the daily rainfall (mm). Since the precipitation amount is very small during the dry summer autumn season in this region and no precipitation information in the vicinity of the irrigation scheme is available, precipitation here is assumed to be zero during the cropping period.

The WaSiM output of the year 2012 is employed as input data for the irrigation optimization model. The optimal irrigation is defined as the decision set, which maximizes the objective function in terms of irrigation technology, irrigation area and irrigation schedule under given water constraints, i.e. the reservoir outflows and the initial reservoir water levels.

4.3 Results and discussion

The irrigation optimization model is simulated with different scenarios of initial reservoir levels and various maximum water releases. The model is running on different computing environments including Windows, Mac and Linux and results presented here are mainly shown for the Windows personal computer. Altogether, four different scenarios are defined to demonstrate the interactions between irrigation needs under the AWD and CF technologies.

The initial reservoir water levels are assumed to be 100%, 90%, 80%, and 70% of the full reservoir storage ($1.85 \times 10^6 m^3$), which is defined as the water amount usable for irrigating SA rice cropping season. These assumptions are based on the results of focal group discussions with agricultural officials in this region in a field survey carried out in 2015. Maximum water rate released from the reservoir are set to range between 0.3 m^3/s and 1.0 m^3/s, with an increment of 0.1 m^3/s. This allows the model to investigate whether the design outlet is sufficient to apply the AWD irrigation technology for the entire cropping area and whether the initial reservoir levels play a role in the optimization results.

4.3.1 Optimized irrigation area and technology

The results for optimized irrigation area and its associated irrigation technology, i.e. AWD or CF for the Que Trung rice irrigation scheme under different scenarios of reservoir water levels are shown from Figure 4.5 to Figure 4.8. Each figure presents the optimized irrigated area (block) and the number of blocks irrigated by either AWD or CF under prescribed maximum water releases. The figure also shows the total irrigation water amount for one block (12ha) under different water releases. As shown in these figures, the irrigated area varies amongst scenarios and ranges from 8 to 12 blocks.

In scenario 1, under every case of reservoir releases, the entire rice cropping area of the QueTrung irrigation scheme (12 blocks) is irrigated. However, the difference in optimal fraction of the two irrigation technologies is found. The largest number of blocks, in which AWD is applied is 11, whereas the lowest number of blocks, in which CF is applied is 1. The number of blocks applying AWD and CF are equal (6 blocks each) at the water release of 0.7 m^3/s. The lowest number of AWD of 4 and the largest number of CF of 8 are found when water release equals 0.3 m^3/s and 0.4 m^3/s (Figure 4.5). For further increases of the reservoir release the number of blocks applying AWD are increasing and CF decreasing. Similar trends are also found for other scenarios.
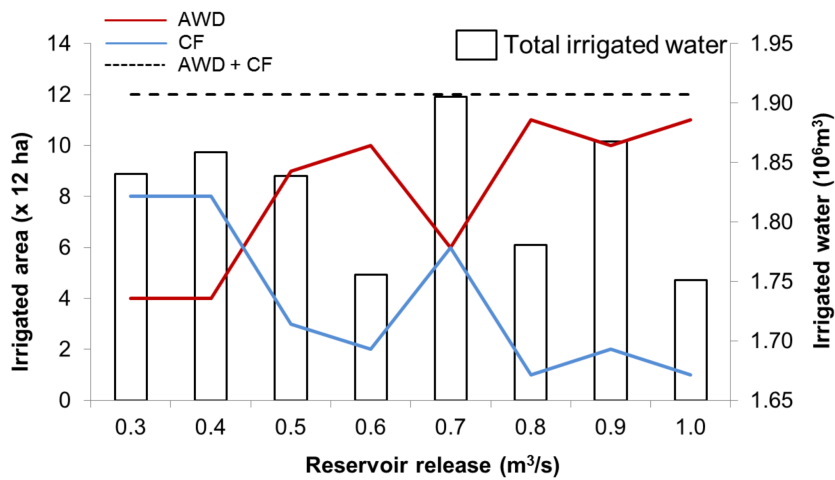
Figure 4.5: Optimized rice irrigation strategies under scenario 1 (initial reservoir storage of 100% at the beginning of the SA cropping season).

Under scenario 2 (Figure 4.6), maximum CF (applied to 12 blocks) and minimum AWD (no blocks), i.e. CF is applied for all blocks and no blocks of AWD are chosen, are found at the water release of 0.3 m^3/s while minimum CF (no blocks) and maximum AWD (12 blocks) are found at the water release of 1.0 m^3/s. In this scenario the number of AWD and CF are equal (6 blocks each) at water release of 0.5 m^3/s.
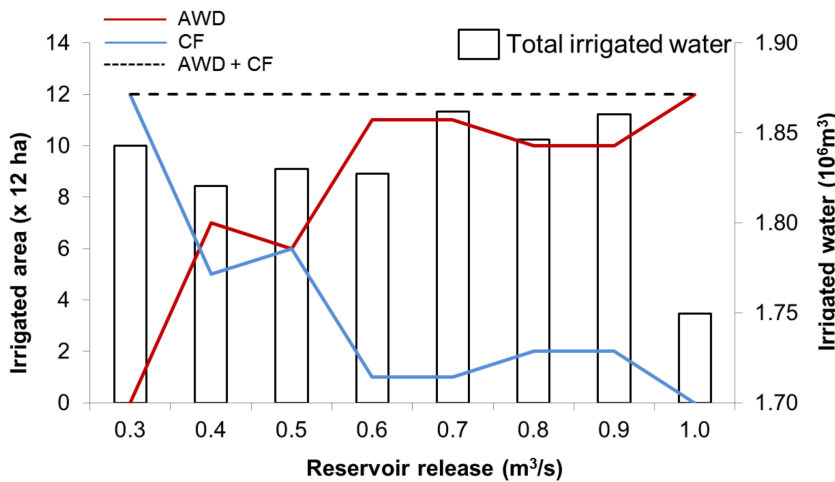
Figure 4.6: Optimized rice irrigation strategies under scenario 2 (initial reservoir storage of 90% at the beginning of the SA cropping season).

In scenario 3 (Figure 4.7), maximum AWD (applied to 11 blocks) and minimum CF (no blocks) are found when water release is larger than 0.6 m^3/s. Interestingly, the model identifies the maximum (minimum) number of blocks applying CF (AWD) for the smallest reservoir release of 0.3 m^3/s, the design water release of the TrungLoc reservoir. This also holds true for all other scenarios. This indicates that the current

reservoir outflow rate may not be optimal to facilitate the adoption of AWD in the Que Trung irrigation scheme, at least not for the entire irrigation scheme. Out of all simulated scenarios, the entire rice cropping area is irrigated under scenarios 1 and 2, under all considered water releases. While 11 blocks are irrigated in scenario 3, only 9 or 10 blocks are irrigated under scenario 4 (Figure 4.8) due to the smallest initial water level assumed in this scenario.
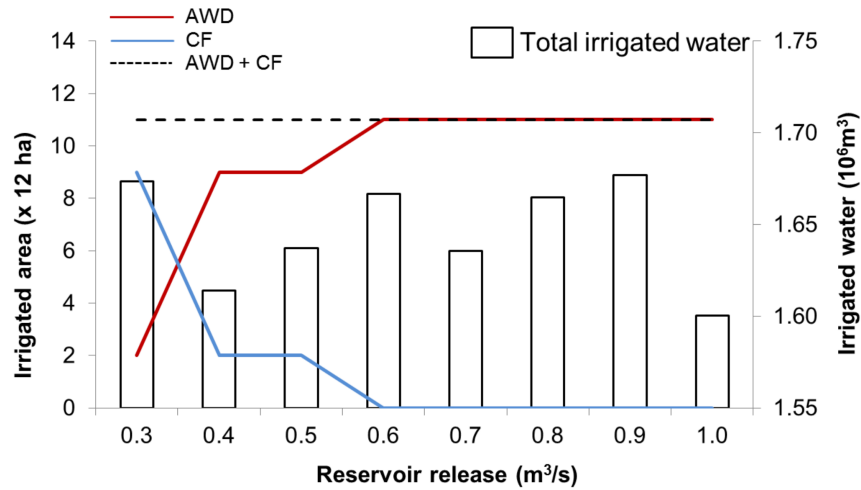
Figure 4.7: Optimized rice irrigation strategies under scenario 3 (initial reservoir storage of 80% at the beginning of the SA cropping season).
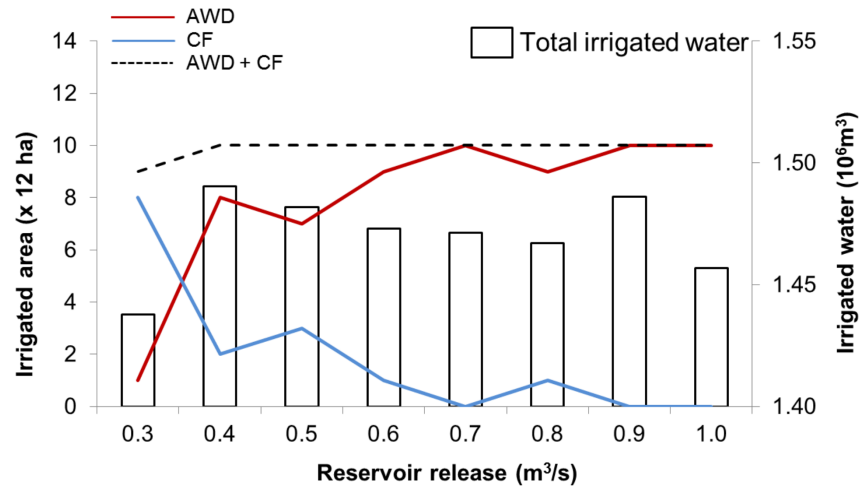
Figure 4.8: Optimized rice irrigation strategies under scenario 4 (initial reservoir storage of 70% at the beginning of the SA cropping season).

In terms of irrigation water requirement, there is a discrepancy of total irrigated water under different water releases in the four considered scenarios. It can be clearly seen from figure 4.5 that the total irrigated water is smallest (1.751 Mm^3) when the

release equals to 1.0 m^3/s, while it is largest (1.905 Mm^3) when the release is 0.7 m^3/s. It is found that comparatively more water can be saved when more AWD is applied. For instance under water release of 1.0 m^3/s approximately 7% of water can be saved (11 blocks applied AWD) compared to 5% under water release of 0.3 m^3/s (4 blocks applied AWD). In scenario 2, the smallest and largest water consumption is also under releases of 1.0 m^3/s and 0.7 m^3/s, respectively. The total irrigation water under release of 1.0 m^3/s in this scenario is smaller than that of scenario 1. However, the difference is insignificant. This could be attributed to the different in number of blocks applied AWD in these two scenarios (12 for scenario 2 and 11 for scenario 1). Total irrigation water is always smallest when water release is 1.0 m^3/s under three scenarios 1, 2 and 3. Under this water release, AWD is the predominant irrigation practice for all scenarios, leading to the lowest water demands for irrigation. It is noted that under scenario 4 shown in Figure 4.8, the total irrigation water is smallest when the release is 0.3 m^3/s, but in this case only 9 blocks are irrigated. This is also the smallest irrigated area associated the least initial water level in the reservoir amongst all scenarios.

4.3.2   Optimized irrigation schedule

Results of detailed irrigation schedule for 12 blocks under 4 scenarios are shown from Figure 4.9 to Figure 4.12. As shown, the optimization model provides the timetable (day) for staggered irrigation for every block and its associated irrigation technology (tech) under different water releases. The irrigation scheduling differs among the water release rates from 0.3 m^3/s to 1.0 m^3/s.

In scenario 1 (Figure 4.9), for example, with an outflow rate of 0.3 m^3/s, block 3 of area 2 starts the first irrigation on the first day using CF. After that, block 2 of area 3 is irrigated on day 2 while block 1 of area 1 is irrigated on day 4 and CF practice is also applied for these two blocks. Finally, block 2 of area 2 starts its first irrigation latest, on day 15 and irrigated with AWD.

When water release is 0.4 m^3/s, block 1 of area 1 starts its first irrigation on day 1, while block 2 of area 3 starts the first irrigation on day 15. CF technology is applied for both these blocks. Under water release of 1.0 m^3/s, two blocks (block 3, area 1 and block 1, area 2) start their first irrigation on day 5 and applied the same practice AWD and three blocks (blocks 1 and 2 of area 1 and block 2 of area 3) are irrigated on the day 11 applying AWD.

In this scenario, it is found that all blocks are irrigated on different days when water releases are equal to or less than 0.5 m^3/s. This finding is similar for other scenarios indicating maximum water release of more than 0.5 m^3/s are required to irrigate more than one block at the same time given different initial water levels in the reservoir.
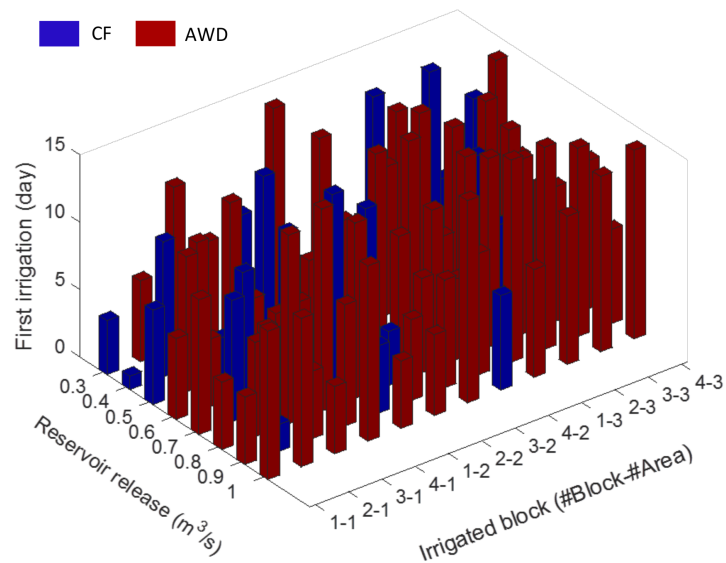
Figure 4.9: Optimized irrigation schedule for first irrigation and irrigation technology under initial reservoir storage of 100% at the beginning of the SA cropping season)

In scenario 2 (Figure 4.10) and scenario 3 (Figure 4.11), block 1 of area 1 starts its first irrigation on day 7 under water release of 0.3 m^3/s, while this block starts its first irrigation on day 3 under water release of 0.4 m^3/s. The CF technology is applied for this block.
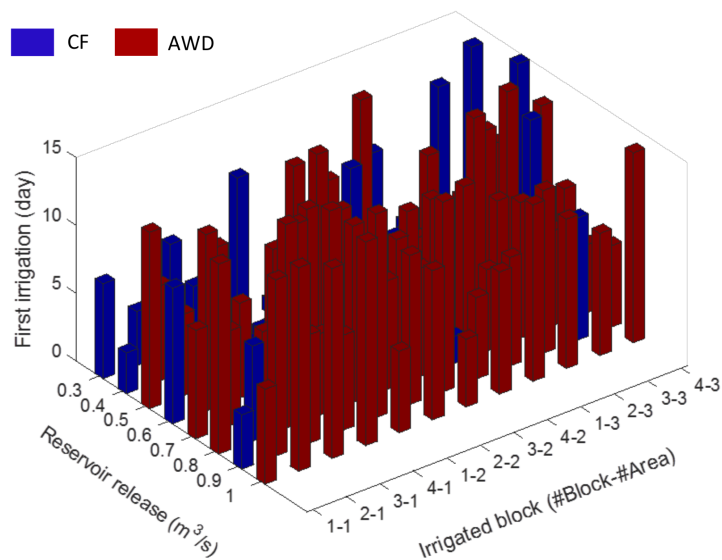
Figure 4.10: Optimized irrigation schedule for first irrigation and irrigation technology under initial reservoir storage of 90% at the beginning of the SA cropping season)
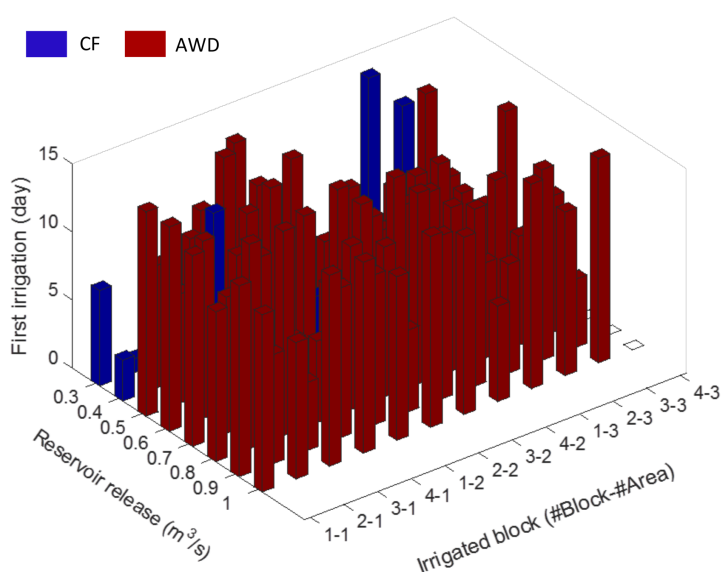
Figure 4.11: Optimized irrigation schedule for first irrigation and irrigation technology under initial reservoir storage of 80% at the beginning of the SA cropping season)

Figure 4.12 shows detailed irrigation schedule for blocks under scenario 4. Block 2 of area 2 starts its first irrigation on the day 1, block 4 of area 2 is on the day 2 and block 3 of area 1 is irrigated on the day 13 under water release of 0.3 m^3/s and CF technology is applied for all these blocks. In this scenario, it is found that under water releases of 0.9 m^3/s and 1.0 m^3/s, all irrigated blocks (10) are irrigated at the 4 last consecutive days of 15-day and the AWD technology is employed for all these blocks. This is probably because the initial water and inflow to the reservoir is insufficient to apply AWD practice before day 12. Likewise, as shown in Figure 4.5 to Figure 4.8, number of irrigated blocks decreases with decreasing initial reservoir level.

In terms of irrigation water input, table 4.1 exhibits the mean irrigation water required for one block by applying either AWD or CF under different scenarios. There is a slight difference in irrigation water input between AWD and CF. The range of total irrigation water for one block is between 0.145 M.m^3 to 0.147 M.m^3 for AWD and 0.151 M.m^3 to 0.159 M.m^3 for CF. On average, the irrigation water allocated for one block by AWD and CF is approximately 0.145 M.m^3 and 0.154 M.m^3 respectively. In general it is concluded here that AWD is more water-efficient than CF with water saving ranges from 4% to 10% depending on scenarios. On average, AWD saves about 6% of irrigation water input compared to CF.

Regarding irrigation events, AWD requires considerably less irrigation events than that of CF in all considered scenarios. The average number of irrigation events required by ADW and CF for one block during entire cropping season is 12 and 21, respectively
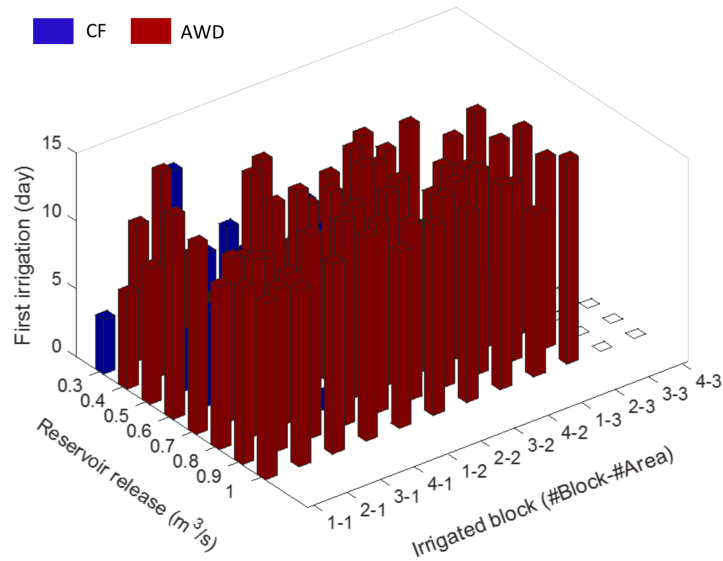
Figure 4.12: Optimized irrigation schedule for first irrigation and irrigation technology under initial reservoir storage of 70% at the beginning of the SA cropping season)

(Table 4.2). This is because the field surface under AWD is left to be dried longer than under CF, which leads to lower frequency of irrigation by AWD.

Table 4.2: Mean number of irrigation (events) for one block under different irrigation technologies.

Water release m^3/s	Scenario 1 No. of irrigations		Scenario 2 No. of irrigations		Scenario 3 No. of irrigations		Scenario 4 No. of irrigations	
	AWD	CF	AWD	CF	AWD	CF	AWD	CF
0.3	13	21	-	22	12	22	13	22
0.4	12	21	12	23	12	22	13	21
0.5	12	21	13	21	12	21	12	20
0.6	13	21	12	22	12	-	12	21
0.7	12	21	13	21	13	-	12	-
0.8	12	22	12	20	12	-	12	21
0.9	12	20	12	24	12	-	12	-
1.0	12	23	12	-	12	-	12	-

4.3.3   Optimization procedure

Figure 4.13 exemplarily shows the plot of objective function values of the Mixed Integer Programming (MIP) optimization problem against the number of iterations for scenario 1, with water release of 1.0 m^3/s. These values are obtained from equation 4.2. It can be seen that the values of the objective function (solid line) increase with increasing number of iterations. The stepwise increases in the function values indicate

Table 4.1: Mean water irrigation input (M.m³) for one block under different irrigation technologies. The results are obtained using the PC computer architecture.

Water release m³/s	Scenario 1			Scenario 2			Scenario 3			Scenario 4		
	Irrigation water input		Water saving (%)	Irrigation water input		Water saving (%)	Irrigation water input		Water saving (%)	Irrigation water input		Water saving (%)
	AWD	CF		AWD	CF		AWD	CF		AWD	CF	
0.3	0.145	0.152	5	-	0.152	-	0.145	0.152	5	0.147	0.157	7
0.4	0.145	0.153	5	0.145	0.155	7	0.145	0.155	7	0.145	0.153	6
0.5	0.146	0.152	4	0.146	0.152	4	0.145	0.155	7	0.146	0.152	4
0.6	0.145	0.151	4	0.146	0.155	6	0.145	-	-	0.145	0.159	10
0.7	0.145	0.153	6	0.145	0.154	6	0.146	-	-	0.146	-	-
0.8	0.146	0.154	6	0.145	0.151	4	0.145	-	-	0.146	0.153	5
0.9	0.145	0.152	5	0.145	0.155	7	0.145	-	-	0.146	-	-
1.0	0.145	0.155	7	0.145	-	-	0.146	-	-	0.146	-	-
Average	**0.145**	**0.153**	**5**	**0.145**	**0.153**	**6**	**0.145**	**0.154**	**6**	**0.146**	**0.155**	**6**

the iterations when a new solution is found. After a solution is found, the solver checks whether this solution is better than the currently best known integer solution. The dashed-line indicates the optimality gap (in %) between the possible best and current best known solutions. This line decreases as the gap becomes smaller. The gap obtains a smaller value after a solution is found and it becomes zero when the current best known solution is equal to the best possible solution.
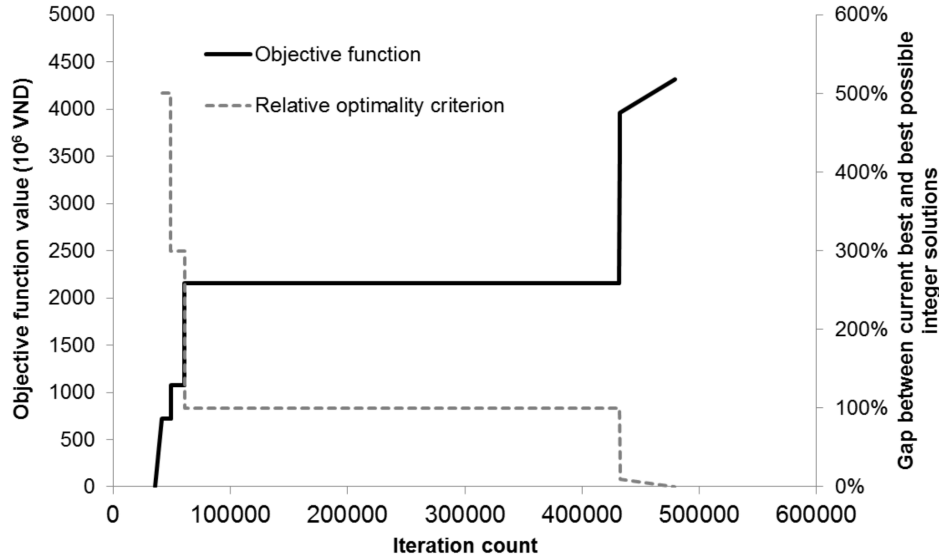
Figure 4.13: Optimized rice irrigation strategies under scenario 1 (100% of initial reservoir storage at the beginning of the SA cropping season). The results are obtained using the PC computer architecture.

4.3.4 Robustness of optimization results on different computer architectures

This study employs the latest GAMS version (24.7.3) with the latest Cplex solver (12.6.3.0) running on 64 bit mode on three different platforms to test the robustness of optimization results obtained from different computing environments. These platforms include a PC with Windows OS (i7 with 8 cores, x 2.6 GHz), a Mac (i7 with 2 cores, 2.8 GHz) and a Linux Cluster using a ivy CPU unit (Intel Xenon with 12 cores, 2.8 GHz). Two cores (threads) are used on each system in order to establish comparability.

Figure 4.14 presents the optimal results for scenario 1 performed on the three different platforms as an example. It can be seen that there is a slight difference in the total number of irrigated blocks. All 12 blocks are irrigated under the Windows PC and the Mac under all considered water releases, while 11 blocks are irrigated under the Linux Cluster for most water releases. It is also found that there are slight

differences in the maximum number of blocks applied AWD and CF. The largest
number of blocks irrigated by AWD is 11 on the Windows PC and the Mac, it is
only 10 on the Linux Cluster while the largest numbers of CF are 12, 9 and 8 for
Mac, Linux Cluster and Windows PC, respectively. Overall, the tendencies of the
optimization results between AWD and CF are similar for the different computer
architectures, i.e. increased AWD and decreased CF with increased reservoir releases.
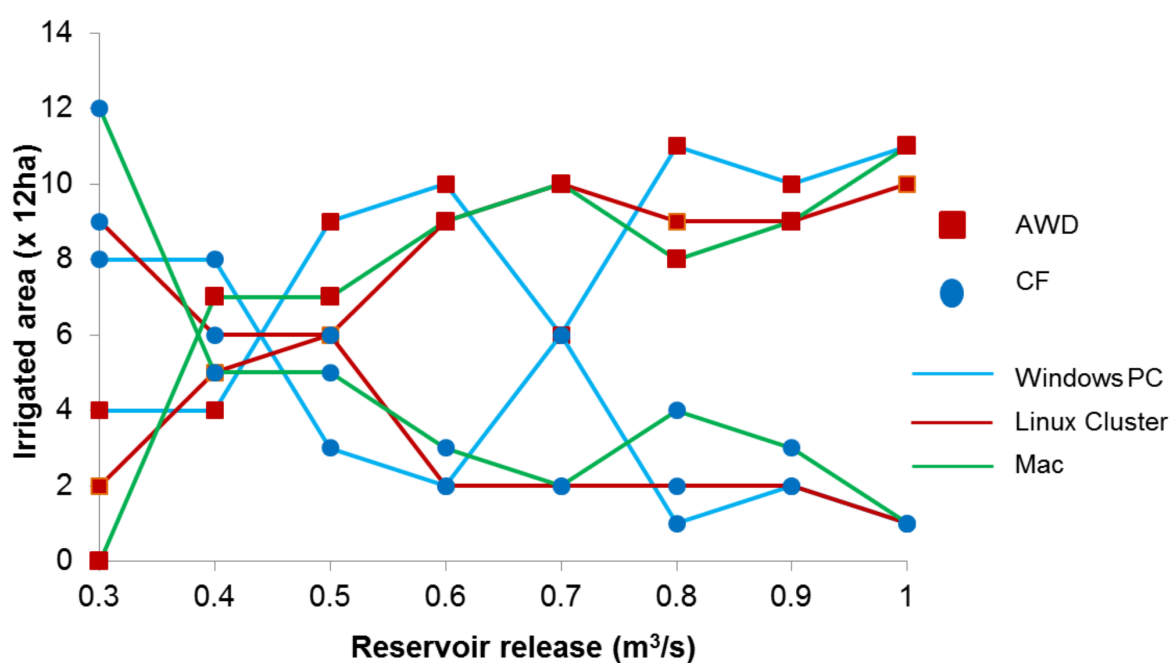
Figure 4.14: Optimization results for scenario 1 performed on different computer
architectures (Windows PC, Linux Cluster and Mac).

The only exception occurs for the selected reservoir release of 0.7 m^3/s, where
there is a significant difference between the Windows PC on the one hand, and the
Mac and Linux Cluster on the other hand (Figure 4.15). Despite of the same total
number of irrigated blocks (12) on three computer architectures, there are 6 blocks for
AWD and 6 for CF on the Windows PC, while the numbers are 10 AWD and 2 CF on
both, the Linux Cluster and the Mac.

Such a performance variability for MIP problems using the same model and the
same solver are well-known in computer engineering (e.g., Koch et al., 2011), but only
rarely considered and discussed in applications (Klotz and Newman, 2013). Potential
reasons comprise the imperfect tie-breaking when solving a MIP, i.e. the selections of
the best solution, which may be made arbitrarily based on the order, in which the best
solutions are considered or influenced by rounding errors. This shortcoming, in combi-
nation with e.g. different compiler options, depends on the platform (Koch et al., 2011).
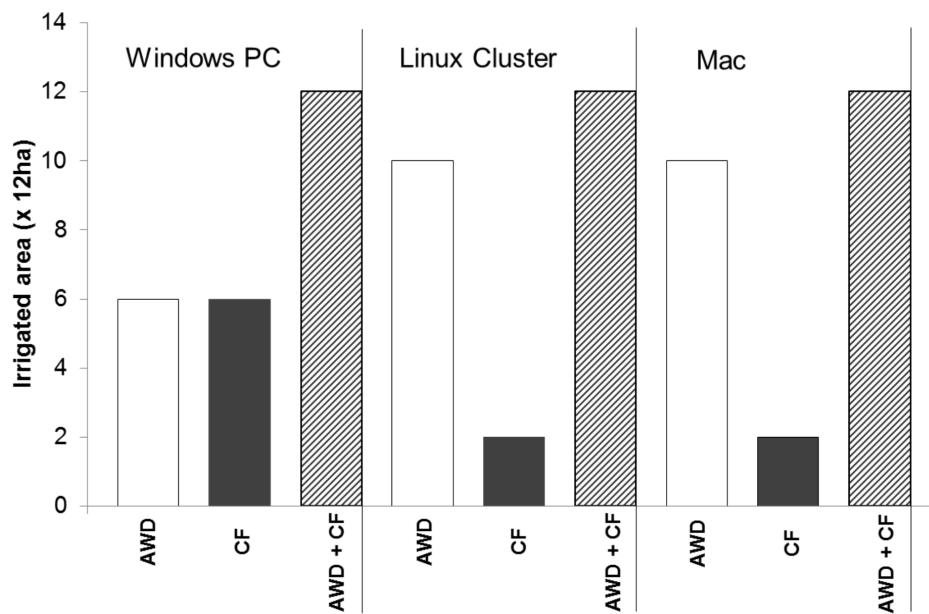
Figure 4.15: Optimization results for scenario 1 and a water release of 0.7 m^3/s, performed on three different computer architectures (Windows PC, Linux Cluster and Mac).

4.3.5   Discussion

Under different hypothesized initial water levels in the Trung Loc reservoir during the summer-autumn cropping season in 2012, the model results show that increasing the initial reservoir level would allow more irrigated area (more blocks), and increasing outflow rate leads to a shift of the irrigation technology towards AWD practice. The model results predominantly suggest the choice of AWD rather than CF. The findings, obtained for Central Vietnam, are consistent with other studies in Southeast Asia, in which AWD is found to be a technology, which can save more irrigation water compared to CF (e.g., Lampayan et al., 2015a,b; Rahman and Bulbul, 2014).

It is found that, when the discharge release from the reservoir is redesigned towards larger flow rates than the current one (0.3 m^3/s), the application of AWD potentially allows to irrigate more blocks in the Que Trung irrigation scheme. The irrigation optimization model indicates that reservoir outflows of >0.5 m^3/s are required to facilitate the adoption of AWD. The water use for irrigation is lower when more AWD is applied. This finally helps to save water for irrigation and to crop larger areas. The entire rice cropping area (12 blocks) can be irrigated only if the initial water levels of the reservoir are 100% and 90% of its capacity, thus the reservoir size is well designed for the size of this irrigation scheme.

Results also show that only 75% of the cropping area can be irrigated if the

initial water level in the reservoir is 70% and the maximum water release is 0.3 m^3/s. This finding is in agreement with statements from the local agricultural authorities (Nguyen, S., 2015, personal communication), it is assumed that the model reasonably represents the irrigation scheme. In addition, the model amount of irrigation water by CF for 1ha summer-autumn rice is comparable with the actual irrigation water running by local practices for Que Trung irrigation system, which ranges from 10,000 to 12,000 m^3/ha/crop. The total irrigation water requirement for 1ha of rice per summer-autumn cropping season by both the CF and AWD technologies is also in line with findings from a study of Nguyen and Ngo (2010), conducted for some areas in Quang Nam province, Central Vietnam. Results of this PhD thesis also reveal that total irrigation water for one block (12 ha) by AWD is less than that of CF, indicating that the AWD technology is more water-efficient (assuming the same rice yields based on CF and AWD). AWD saves about 6% of irrigation water input compared to CF, on average. By saving more irrigation water amount, the AWD practice could be a promising irrigation option in Central Vietnam, that can eliminate the increasing irrigation water stress as a small reduction of water use for rice can free up large volumes of this vital resource for increasing rice production and other uses (Lampayan et al., 2015a).

Since there is no other actual irrigation data available for the Que Trung irrigation scheme to validate the modelling results, in the following the model results in this PhD thesis are compared with similar studies across Southeast Asia. The modeled water saving by AWD compared to CF is less than the one obtained from a field study of Lampayan et al. (2015a) for Bangladesh and the Philippines. In this study the differences in total water input for rice irrigation between AWD and CF range between 13% and 38%. It is noted that such discrepancies are possible due to difference in soil properties, climate conditions, cultivation practices and cropping seasons.

In terms of number of irrigation events, the average number of irrigation events by AWD is 12 and by CF is 21, respectively. This suggests that AWD reduces the number of irrigation events approximately 43% as compared to CF. Thus, costs induced by irrigation operation can be reduced if AWD is applied properly in the region. Field studies and also modelling results have reported similar results when applying AWD and CF for rice growing areas in the region, such as Liang et al. (2016) for Southern China, Lampayan et al. (2015a) for Bangladesh, the Philippines and Vietnam, and Rahman and Bulbul (2014) for Bangladesh. The model results of irrigation events are also in line with findings from Hong et al. (2015) conducted for the Soc Trang province in Southern Vietnam.

Besides the suggested optimal irrigation technology, this coupled hydrological and irrigation optimization model further provides information about the optimal area

for cropping as well as irrigation schedules associated to each block. The staggered irrigation scheduling modeled by the irrigation optimization model suggests the irrigation time for blocks irrigated by either AWD or CF to maximize the benefit of limited water availability. This could be of crucial importance for agricultural managers to better plan their cropping preparations.

Moreover, the optimization results for performance variability from different computer architectures are analyzed. This has been done since a performance variability for MIP problems using the same model and the same solver are well-known in computer engineering (Koch et al., 2011), which may lead to non-robust solutions and difficulties for decision support. The test simulations showed similar tendencies and varied only slightly on the 3 computing environments. This consolidates the confidence in the robustness of the model for decision support.

It is noted that only the hydrological model has been validated, a quantitative validation of the irrigation model was not possible. However, the modelling results in terms of water requirement for irrigation, number and interval of irrigation events, and irrigated area are compared with studies and data as well as practical information from Central Vietnam, in particular and studies done for the Southeast Asia.

Although hydrological extremes under a changing climate are of great relevance for water management and climate change adaptation (Hoang et al., 2016), only few insights on how climate change will impact the future high and low flows in the VGTB region have been obtained so far. Notably, there were earlier studies focusing on the changes in annual and monthly flows in Vietnam in general and in the VGTB region in particular, but they are not widely available. The impact of climate change on high and low flows in the VGTB basin is analysed in the next chapter.

Chapter 5

Impact of climate change on high and low flows

5.1 Introduction

Vietnam is ranked amongst countries suffering the most from severe climate change impacts, and is likely to have an increased exposure to extreme events (IPCC, 2007, 2013). Possible changes in hydrological extremes are consequently expected under projected changes of monsoon rainfalls. Therefore, insights about future high flows and low flows due to climate change for the VGTB basin are of paramount importance, especially for water resources management and water-related risk mitigation. Based on projected information about future high and low flows, decisions on climate change response activities and adaptation measures can be made.

Although a relatively large number of studies exist on the impact of climate change on river flows, the changes on high flows and low flows in Southeast Asia are not widely documented in the literature. Most studies are conducted for Europe and other regions for which a large amount of climate projections are available (e.g. Kay et al., 2006; van Pelt et al., 2009; Hurkmans et al., 2010; Dobler et al., 2012a; Gu et al., 2015). Readily available information of climate data facilitates the application of multi-model ensembles, which is often used in hydrological impact studies.

In Central Vietnam, only a small number of studies on the impact of climate change on river flows have been carried out. Souvignet et al. (2014) investigated the linkages between discharge changes and trends in rainfall and temperature in the VGTB basin. They found that the maximum discharge responds significantly to precipitation changes which result in a prolonged wet season and an increase in extreme rainfall events. Most research studies in the region rely on climate data derived from one emission scenario (e.g. Vu et al., 2017) and/or one single GCM and one statistical downscaling method exclusively due to limitations of regional cli-

mate projections from different global and regional climate models for Central Vietnam.

The dynamic downscaled data under the new RCP scenarios has been available recently. For instance, CORDEX simulations are being conducted for various parts of the globe, and few are readily available nowadays such as for the European and the African domain. For the CORDEX East Asia domain (CORDEX-EA), there is only 1 GCM-RCM combination available for the historical period, i.e. the HadGEM2-AO – HadGEM3-RA combination. For projected (future) time slices, only 1 GCM in combination with 4 RCMs (RegCM_v4, SNU_MM5, SNU_WRF_v3, YSU-RSM_v3) and two scenarios are available. There is no regional climate data available for download for the Southeast Asia domain (CORDEX-SEA).

5.2 Methodology

Modelling chain approach is often used in hydrological impact analysis. Many impact studies have relied on the robustness of full modelling chains. Most studies are conducted for European countries (e.g. Dobler et al., 2012a; Hurkmans et al., 2010; van Pelt et al., 2009; Kay et al., 2006) while little is known about changes on hydrological extremes in Southeast Asia in particular. These studies are often still based on a single or limited number of GCMs/RCMs due to computational constraints. Results obtained from studies based on a single global and/or regional climate model that could not adequately represent the range of future flood frequencies and magnitudes, therefore, should be interpreted with care (e.g. Gu et al., 2015; Delgado et al., 2014; Rasmussen et al., 2012; Minville et al., 2008; Prudhomme et al., 2003).

In this PhD thesis a modelling chain is employed to study the possible impact of climate change on future extreme high and low flows in the VGTB river basin. The modelling chain consists of climate emission scenarios, a multi-model ensemble of GCM/RCMs, various bias correction (BC) approaches, a fully distributed hydrological model and flow frequency analyses. The modelling chain applied for the analysis of future high and low flows in the VGTB basin is presented in Figure 5.1.

GCM/RCMs were described in chapter 2 while the fully distributed hydrological WaSiM was presented in chapter 3, the followings sections focus on the descriptions of bias correction and flow frequency analysis.

5.2.1 Bias correction methods

It is well known that outputs from RCMs are usually systematically biased compared to observation stations (Kleinn et al., 2005). Reasons for this mismatch are diverse but mainly include the imperfect conceptualization, incorrect initialization, climate
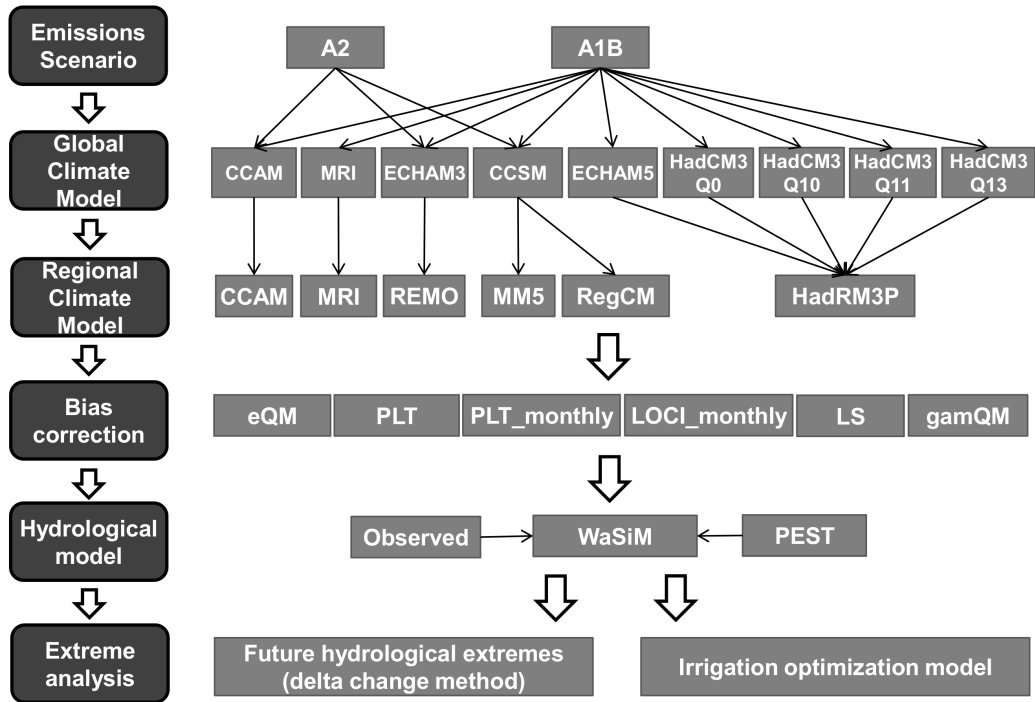
Figure 5.1: Flow chat of the applied hydrometeorological modeling chain

variability, discretization and spatial averaging within grid cells (Teutschbein and Seibert, 2012). Therefore, further post-processing methods correcting for the biases of RCMs data are recommended in the literature for hydrological applications (Driessen et al., 2010; Dobler et al., 2012b; Vormoor et al., 2015). A correction is mainly required for variables that inhibit a high spatial and temporal variability such as precipitation (e.g., Di Luca et al., 2012; Tselioudis et al., 2012), since variability of rainfall is a central driver of many processes in nature (Fiener and Auerswald, 2009).

There is a number of different methodologies in the literature to correct for biases in RCMs outputs. The complexities of the methods are different, but most of the methods employ a transfer function between modeled RCM and observed data. The BC methods can range from simple linear methods (e.g. Hay et al., 2000; Lenderink et al., 2007; Leander and Buishand, 2007) or non-linear power transformation (Shabalova et al., 2003; Lenderink et al., 2007) and statistical distribution-based algorithms (e.g., Themeßl et al., 2011; Piani et al., 2010) towards more complex transfer functions using Copulas (Laux et al., 2011; Vogl et al., 2012; Mao et al., 2015). Table 5.1 provides an overview of the applied bias correction methods.

Of all bias correction methods considered, the power law transform e.g. (Shabalova et al., 2003) adjusts both the variance and the mean of precipitation time series (Teutschbein and Seibert, 2012), while the linear scaling (e.g. Lenderink et al., 2007)

only corrects for biases in the monthly mean.

Table 5.1: Applied bias correction methods for precipitation (P) and temperature (T)

Name	Abbreviation	Variable
Power law transform (monthly)	PLT_monthly	P
Local intensity scaling (monthly)	LOCI_monthly	P
Empirical Quantile Mapping	eQM	P, T
Linear Scaling	LS	P, T
Gamma distribution Quantile Mapping	gamQM	P
Power law transform	PLT	P

The local intensity scaling (e.g. Schmidli et al., 2006) accounts for the monthly mean as well as both wet-day frequencies and wet-day intensities separately. For the LOCI method, a specific RCM precipitation threshold is determined first, then a linear scaling factor is estimated based on the long-term monthly mean wet-day intensities (Teutschbein and Seibert, 2012). The Quantile Mapping method corrects most of the statistical characteristics, such as the mean value, the standard deviation and the percentiles by matching the distribution function of raw RCM outputs to that of the observations. This is done by creating a transfer function to shift the probability distributions of precipitation and/or temperature (Sennikovs et al., 2009; Teutschbein et al., 2012). In this PhD thesis, both the Quantile Mapping based on the Gamma distribution and on the empirical distribution (e.g. Fang et al., 2015) are employed. The Gamma distribution is often assumed to be suitable for precipitation (e.g. Teutschbein and Seibert, 2012; Fang et al., 2015), whereas the empirical Quantile Mapping can be used for both precipitation and temperature (Fang et al., 2015). A comprehensive review of these bias correction methods is given in Teutschbein and Seibert (2012) or Fang et al. (2015).

5.2.2 Performance measures of extreme discharge based on applied BC methods

A performance indicator is introduced in this PhD thesis to assess the overall performance of both the GCM/RCM model combinations and the six BC methods, for both the high river flows and the low river flows. The performance is evaluated based on the simulated extreme high and low flow distributions for the baseline (1980-1999), obtained by the hydrological model WaSiM. The indicators are obtained by calculating the *Percent Error* (PE), i.e. the absolute change between the observed and BC simulated discharge values, divided by the observed discharge, between: i) the medians, ii) the interquartile ranges, and iii) the 0.95 and 0.05 percentiles of observed and bias corrected data. For each criterion an indicator is derived, i.e. '+' for PE < 20% indicating good performance, '*' for 20% < PE < 40%, indicating fair performance, and '-' for PE > 40%, indicating poor performance. The final indicator is chosen based on the

majority of indicator occurrence. In case of equal occurrence, the '*' indicator symbol
is selected.

5.2.3   Delta change method

Apart from the applied methods for bias correction of regional climate model inputs
for WaSiM, i.e. precipitation and temperature, the delta change method (Prudhomme
et al., 2003; Minville et al., 2008; Dobler et al., 2012b; Teutschbein and Seibert, 2012) is
employed to adjust the modeled discharges. Particularly, the delta change is applied to
values for the high and low flows of Nong Son station, separately for the three different
time slices. First, the ratio Δx between the projected high/low flow for the future time
slices x_{fut} and the corresponding baseline values x_{bse} is calculated:

$$\Delta x_{ij} = \frac{x_{fut,ij}}{x_{bse,ij}}, \tag{5.1}$$

where i is the return period (in years), and j is the specific GCM/RCM model combi-
nation. Second, the adjusted high or low flow for the future time slices Q_{adj}^{fut} is obtained
by multiplying the observed discharges Q_{obs} with the discharge ratio Δx:

$$Q_{adj,ij}^{fut} = Q_{i,obs} \cdot \Delta x_{ij}. \tag{5.2}$$

The adjusted high and low flows are calculated for return periods from 1 to 50 years.
Note that the underlying data is 20 years only, thus the uncertainties of the results
may increase with increasing return periods. The main limitation of the delta change
method is that only the first-order statistics (changes in the mean between future and
baseline scenarios) are considered, while other statistical properties remain unchanged
(Fowler et al., 2007; Sunyer et al., 2012; Kidmose et al., 2013; Camici et al., 2013).

5.2.4   Extreme frequency analysis

The calibrated WaSiM model is applied to reproduce river flows at Nong Son station
under future climate conditions using different climate scenarios. The annual maxima
values for different GCM/RCM combinations and time slices are selected for high flow
frequency analysis. The N-day minima approach is employed for low flow frequency
analysis. The minimum values are averaged over different durations to produce annual
minimum (n-day) series (WMO, 2008). In this PhD thesis, the minimum 1-day, 7-
day and 15-day moving average series derived from daily data are considered. The
Generalized Extreme Value (GEV) probability distribution is applied for the high and
low flows frequency analysis. The GEV allows the combination of the description of
three extreme distributions, i.e. Gumbel (type I), Fréchet (type II), and Weibull (type

III), into one single form (Towler et al., 2010). The cumulative distribution function of the GEV is defined by the following equation:

$$F(x;\theta) = exp\left\{ -\left[1 + \beta \cdot \left(\frac{x - \lambda}{\sigma} \right) \right]^{\frac{-1}{\beta}} \right\} \tag{5.3}$$

where $\theta = [\lambda, \sigma, \beta]$, λ is the location parameter which describes the position of the distribution indicating where it is centered, σ is the scale parameter which indicates the spread of the distribution, and β is the shape parameter defining the type of the distribution. If $\beta = 0$, the GEV corresponds to the type I, if $\beta > 0$, the GEV is equivalent to the type II, and if $\beta < 0$, the GEV is equivalent to the type III. In this study, the GEV distribution based on the Maximum Likelihood Estimator (MLE) was fitted to simulated annual maximum and annual minimum discharges to estimate high and low flows with return periods going beyond the length of the available data. For the MLE, the unknown parameters θ is estimated by numerically maximizing the likelihood function which is of the following form (Towler et al., 2010):

$$llh(\theta) = \sum_{i=1}^{N} log f(x_i; \theta), \tag{5.4}$$

where $f(x;\theta)$ is the derivative of $F(x;\theta)$ with respect to x. N is the sample size. Equation 5.4 can be expanded as

$$llh(\theta) = -N \cdot log\sigma - \left(1 + \frac{1}{\beta} \right) \cdot \sum_{i=1}^{N} log\left[1 + \beta \cdot \left(\frac{x_i - \lambda}{\sigma} \right) \right] - \sum_{i=1}^{N} \left[1 + \beta \cdot \left(\frac{x_i - \lambda}{\sigma} \right) \right]^{\frac{-1}{\beta}} \tag{5.5}$$

where $[1 + \beta \cdot (\frac{x_i - \lambda}{\sigma})] \geq 0$. For computational convenience, -llh(θ) is usually minimized instead of directly maximizing llh(θ). For more details on the MLE, the reader is referred to Towler et al. (2010) and Myung (2003).

The sample size may impact the fit of the GEV distributions, i.e. the maximum likelihood estimator might be unstable for sample sizes of n < 50 (e.g., Hosking and Wallis, 1997; Coles and Dixon, 1999; Martins and Stedinger, 2000). To quantify the uncertainties related to a reduced sample size n (20-year period in this PhD thesis), a permutation test i.e. bootstrapping test was developed and applied to check whether the parameters (shape, location, and scale parameter) from the fitted distribution based on a sample size of n = 20 come from the same distribution based on a larger sample size of 50 (the sample size that indicates as a sample size to obtain robust estimations). The bootstrap sampling with replacement i.e. one or more data points may be absent and one or more may be repeated more than once in any resampled data set (Hall et al.,

2004), was applied based on the observed discharge series (1980-1999) at Nong Son station to artificially increase the sample size for the maximum likelihood estimation.

5.3 Results and discussion

5.3.1 Performance of different bias correction methods

Baseline period

In this section, the hydrological WaSiM model is forced with different bias-corrected GCM/RCM outputs to reproduce daily discharges at Nong Son station for the baseline (1980-1999). These discharges are then compared with simulated discharges without bias correction as well as the observed discharges. Results of the observed and simulated long-term mean monthly discharges (1980-1999) at Nong Son station based on the different BC methods for the MRI-MRI combination are shown in Figure 5.2 as an example. It can be seen that the raw GCM/RCM and most of the BC methods lead to a significantly (41% on average) underestimated discharge during the rainy season (September to December). Of all the considered BC methods, the PLT_monthly performs fair for the rainy season, however, it leads to a considerable overestimation during the period from June to August. This overestimation mainly occurs when the discharge based on the raw GCM/RCM data is considerably higher than the observed discharge. It is thus not able to reproduce the seasonality of the discharge hydrograph. The same holds true for all other GCM/RCM combinations.
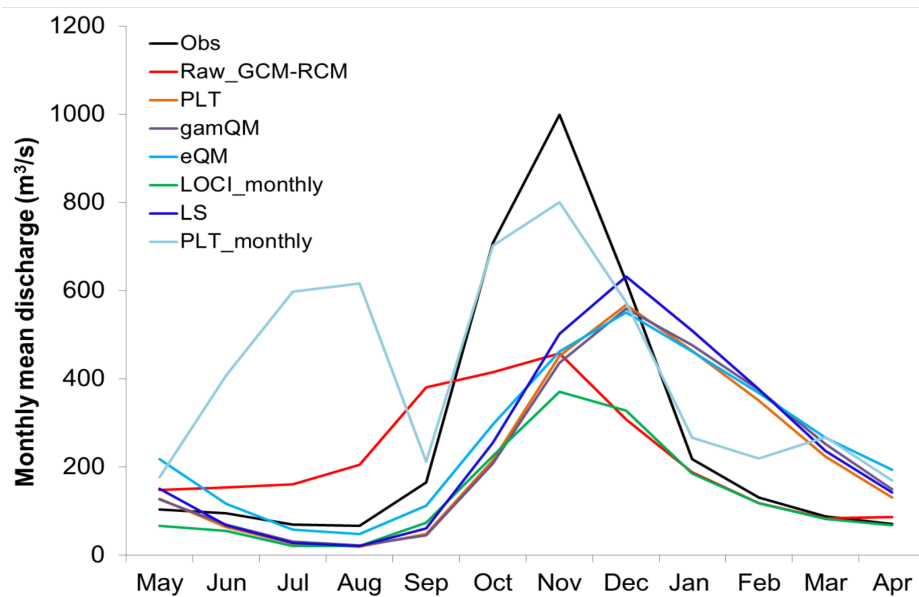
Figure 5.2: Observed and modeled long-term mean monthly discharge (1980-1999) at Nong Son station based on 6 different BC methods, for the MRI-MRI combination

Figure 5.3 shows the spread of the high flows and low flows simulated with the WaSiM hydrological model, forced with HadCM3Q10-HadRM3P combination as an example. For the high flows derived from the raw climate data, one can observe a large underestimation leading to a reduced variance compared to the observed flows. Similar findings can be found for all other model combinations. While CCAM-CCAM shows the smallest range of the high flows, HadCM3Q11-HadRM3P presents the largest range amongst all GCM/RCM combinations (Figure 5.4). Considering the low flows, the majority of GCM/RCM combinations leads to underestimations, except for the CCAM-CCAM, CCSM-RegCM, ECHAM3-REMO and MRI-MRI. Generally, tendencies of underestimations using the raw GCM/RCM combinations are observed for both high and low flows.
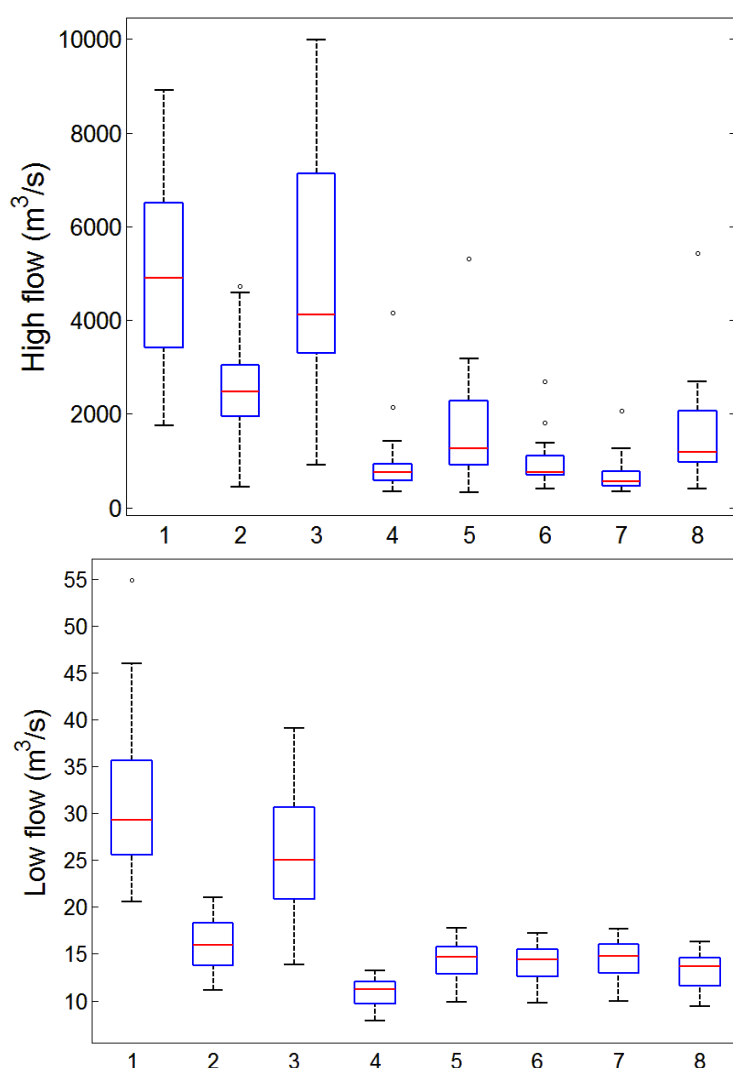
Figure 5.3: High flows (top) and low flows (bottom) for the baseline period (1980-1999) simulated with WaSiM, forced with HadCM3Q10-HadRM3P using different bias corrected methods (1- Obs, 2- no BC, 3- PLT_monthly, 4- LOCI_monthly, 5- eQM, 6- LS, 7- gamQM, 8- PLT).
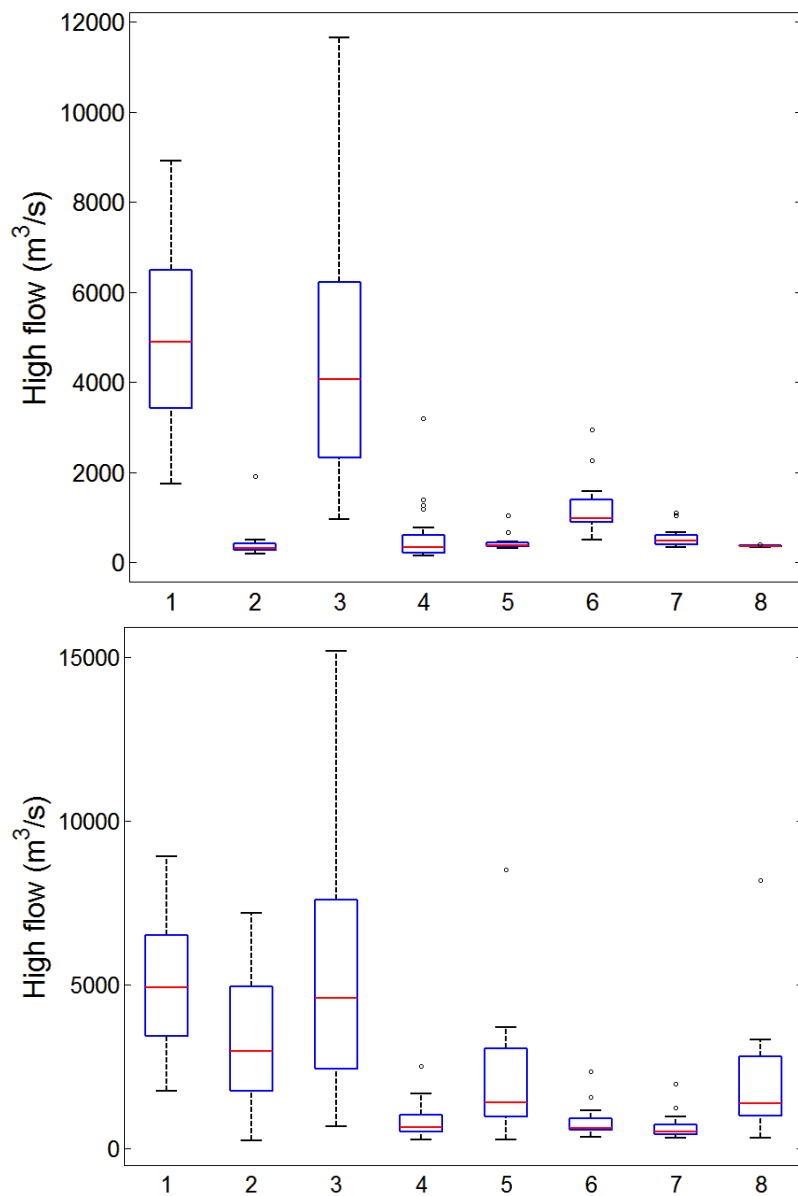
Figure 5.4: High flows for the baseline period (1980-1999) simulated with WaSiM, forced with CCAM-CCAM (top) and HadCM3Q11-HadRM3P (bottom) using different bias corrected methods (1- Obs, 2- no BC, 3- PLT_monthly, 4- LOCI_monthly, 5- eQM, 6- LS, 7- gamQM, 8- PLT).

When forcing the WaSiM model with the bias-corrected GCM/RCM data, the impact of the different BC methods on the resulting flow distributions varies largely. Table 5.2 shows the median and the interquartile range, which is the differences between 75 percentile and 25 percentile, of simulated high flows for the different BC methods and different GCM/RCM combinations. It can be seen from the table that the interquartile range varies between 19 m^3/s (CCAM-CCAM & PLT) and 5371 m^3/s (CCSM-MM5 & PLT_monthly) while the median values range between 341 m^3/s (CCAM-CCAM & LOCI_monthly) and 6498 m^3/s (ECHAM5-HadRM3P & PLT_monthly).

Table 5.2: Median and interquartile range (iqr) of simulated high flows (m^3/s) at Nong Son station using raw (uncorrected) and BC data. The applied BC methods are: 1- PLT_monthly, 2- LOCI_monthly, 3- eQM, 4- LS, 5- gamQM, 6- PLT.

GCM/RCM combination		Raw	BC method					
			1	2	3	4	5	6
CCAM-CCAM	median	327	4062	341	383	984	486	361
	iqr	109	3437	304	77	433	177	19
CCSM-MM5	median	2395	5786	1830	1674	1579	1419	1733
	iqr	1513	5371	911	968	597	600	775
CCSM-RegCM	median	1895	3604	1539	1500	1931	1021	1337
	iqr	1021	4706	796	546	667	350	369
ECHAM3-REMO	median	2574	5250	1731	1998	2080	1509	1938
	iqr	1493	5018	918	942	719	519	660
ECHAM5-HadRM3P	median	2848	6498	863	1628	1029	812	1571
	iqr	2637	3419	367	1861	479	439	1387
HadCM3Q0-HadRM3P	median	2657	4431	1018	1648	988	767	1660
	iqr	2723	2390	324	1774	466	401	1509
HadCM3Q10-HadRM3P	median	2468	4115	758	1258	748	566	1186
	iqr	848	3419	313	1308	393	315	1086
HadCM3Q11-HadRM3P	median	2951	4574	652	1406	626	506	1382
	iqr	3131	4516	508	1998	365	284	1773
HadCM3Q13-HadRM3P	median	2550	5898	752	1351	634	503	1303
	iqr	3070	3512	350	1577	368	282	1557
MRI-MRI	median	2785	5391	1070	1646	1759	1097	1647
	iqr	778	4076	533	1175	633	391	605

Although the annual high flows generated from most bias correction methods are smaller than observed discharges as well as smaller than discharges simulated by uncorrected GCM/RCM outputs, the high flows derived from PLT_monthly are larger than discharges simulated by uncorrected GCM/RCM outputs in most model combinations. Considering annual low flows, a similar impact of the BC methods on the resulting low flow distributions is found. In most model combinations, the low flows derived from PLT_monthly are larger than discharges simulated by uncorrected GCM/RCM outputs, whereas the low flows derived from other BC methods are smaller. While the interquartile ranges from 2 m^3/s to 14.5 m^3/s, the median is between 11 m^3/s to 58 m^3/s. Results for all GCM/RCM combinations and BC methods for low flows are shown in Table 5.3.

Table 5.4 and Table 5.5 show the overall performance of both the GCM/RCM model combinations and the 6 BC methods, for the high river flows and the low river flows. It can be seen that, for most model combinations and the BC methods the "-" sign is dominant for both high and low flows. It is an indication that none of the BC methods applied to RCM outputs can lead to reasonable high and low flows for the

control period.

Table 5.3: Median and interquartile range (iqr) of simulated low flows (m^3/s) at Nong Son station using raw (uncorrected) and BC data. The applied BC methods are: 1- PLT_monthly, 2- LOCI_monthly, 3- eQM, 4- LS, 5- gamQM, 6- PLT.

GCM/RCM combination		Raw	BC method					
			1	2	3	4	5	6
CCAM-CCAM	median	46.2	42.1	10.9	57.9	15.1	15.8	17.5
	iqr	23.6	11.2	2.7	7	2.9	3.5	2.9
CCSM-MM5	median	15.8	23.8	14.6	18.2	17.1	17.6	16.8
	iqr	5.4	6.6	3	5	4.4	4.3	4.3
CCSM-RegCM	median	42.5	36	14.8	45.7	18.1	19.9	19.2
	iqr	7	14.5	3.1	7.5	4.3	4.5	4.9
ECHAM3-REMO	median	47.8	38.5	16.2	23	17.9	19	18.1
	iqr	19.7	10.5	4.6	5.9	4.3	4.5	4.4
ECHAM5-HadRM3P	median	24.6	29.3	12.3	16.2	15.6	16.1	14.9
	iqr	6.7	11.1	2.4	3.7	3.4	3.6	2.9
HadCM3Q0-HadRM3P	median	16.9	32.7	12.3	15.7	15.4	15.8	14.4
	iqr	6.5	9.9	2.3	3.5	3.2	3.5	2.8
HadCM3Q10-HadRM3P	median	16	25.1	11.3	14.7	14.5	14.8	13.7
	iqr	4.4	8.7	2.3	2.9	2.8	2.9	2.8
HadCM3Q11-HadRM3P	median	12.8	18.2	10.9	12.9	13.7	13.8	12.2
	iqr	3.2	7.1	2.2	2.4	2.5	2.6	2.6
HadCM3Q13-HadRM3P	median	13.4	26.6	10.6	13.1	13.8	14	12.5
	iqr	4.1	10.2	2	2.5	2.6	2.7	2.7
MRI-MRI	median	53.3	39.9	13.6	44.7	17.5	18.7	17.6
	iqr	23.7	12.2	2.9	7.1	4.3	4.4	4.3

Table 5.4: Performance of different models and bias correction methods for the high flow (baseline period). The applied BC methods are: 1- PLT_monthly, 2- LOCI_monthly, 3- eQM, 4- LS, 5- gamQM, 6- PLT. '+' indicates good, '*' fair, and '-' poor performance.

GCM/RCM combination	BC method					
	1	2	3	4	5	6
CCAM-CCAM	*	-	-	-	-	-
CCSM-MM5	*	-	-	-	-	-
CCSM-RegCM	-	-	-	-	-	-
ECHAM3-REMO	-	-	-	-	-	-
ECHAM5-HadRM3P	*	-	*	-	-	-
HadCM3Q0-HadRM3P	*	-	*	-	-	-
HadCM3Q10-HadRM3P	+	-	-	-	-	-
HadCM3Q11-HadRM3P	-	-	*	-	-	*
HadCM3Q13-HadRM3P	*	-	-	-	-	-
MRI-MRI	*	-	-	-	-	-

Table 5.5: Performance of different models and bias correction methods for low flow (baseline period). The applied BC methods are: 1- PLT_monthly, 2- LOCI_monthly, 3- eQM, 4- LS, 5- gamQM, 6- PLT. '+' indicates good, '*' fair, and '-' poor performance.

GCM/RCM combination	BC method					
	1	2	3	4	5	6
CCAM-CCAM	*	-	*	-	-	-
CCSM-MM5	*	-	-	-	-	-
CCSM-RegCM	*	-	*	-	-	-
ECHAM3-REMO	*	-	*	-	-	-
ECHAM5-HadRM3P	*	-	-	-	-	-
HadCM3Q0-HadRM3P	*	-	-	-	-	-
HadCM3Q10-HadRM3P	*	-	-	-	-	-
HadCM3Q11-HadRM3P	*	-	-	-	-	-
HadCM3Q13-HadRM3P	*	-	-	-	-	-
MRI-MRI	*	-	-	-	-	-

Future period

In this section, the WaSiM model is forced with different bias-corrected GCM/RCM outputs to reproduce series of daily flows at Nong Son station for future periods 2011-2030, 2031-2050 and 2080-2099 under the two emission scenarios A1B and A2. Subsequently, annual maxima and minima flows are calculated accordingly. The expected changes in the mean of high and low flows are calculated for future periods by comparing them with that of the baseline period (1980-1999). Figure 5.5 shows the expected range of changes in the mean of high flow for the A1B scenario from 6 different BC

methods.
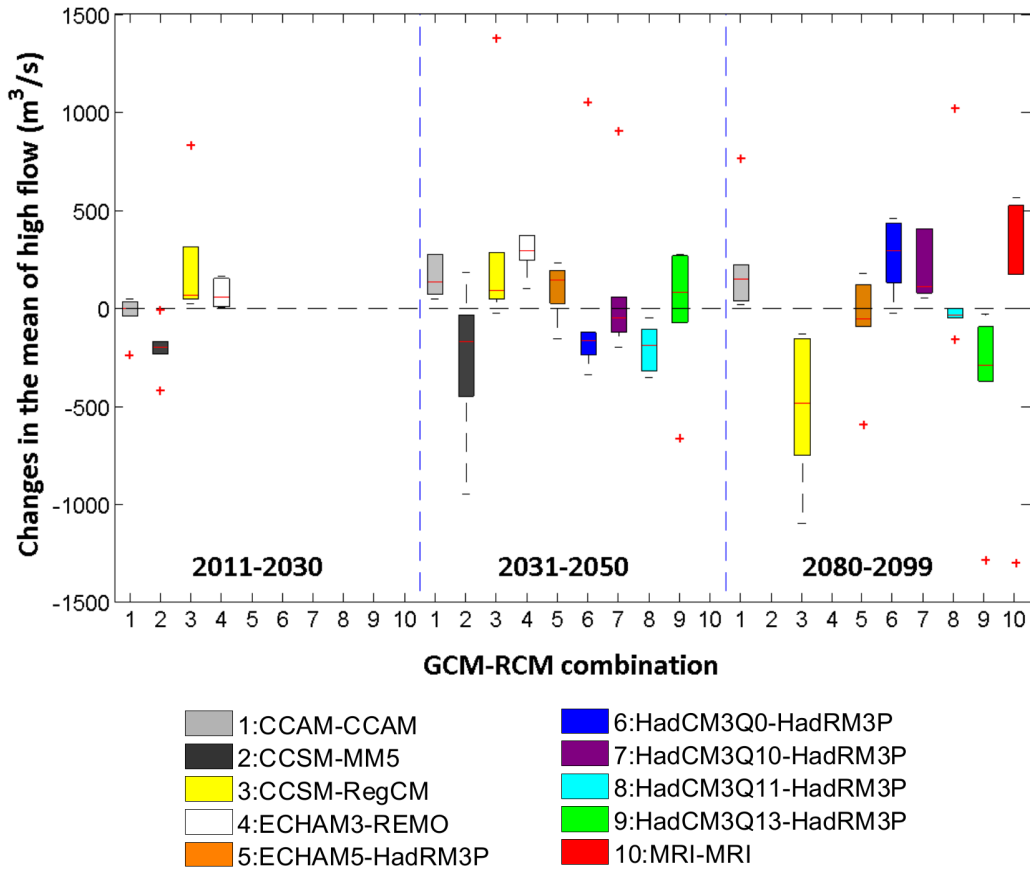
Figure 5.5: Range of the mean simulated high flows at Nong Son station using different GCM/RCM combinations and 6 different bias correction methods, represented by the boxes. The absolute changes of the mean values between future and baseline (future minus baseline) are shown for the A1B scenario.

In general, large differences between the different combinations can be observed. For each time slice, the projected changes of the mean of high flows are positive for the majority of the GCM/RCM combinations. In other words, the high flows tend to increase in general. CCSM-MM5 provides one exception, showing a negative signal, while ECHAM3-REMO exhibits a positive change in all time slices. For the period 2031-2050, four models (CCAM-CCAM, CCSM-RegCM, ECHAM3-REMO and ECHAM5-HadRM3P) project an increase of the mean of the high flows whereas three models (CCSM-MM5, HadCM3Q0-HadRM3P and HadCM3Q11-HadRM3P) show a negative change. Meanwhile HadCM3Q10-HadRM3P and HadCM3Q13-HadRM3P indicate an inconsistent tendency.

For the time slice 2080-2099, CCAM-CCAM, HadCM3Q0-HadRM3P, HadCM3Q10-HadRM3P, and MRI-MRI shows a positive increase while CCSM-RegCM,

HadCM3Q11-HadRM3P, and HadCM3Q13-HadRM3P present a decreasing signal. For all model combinations, the largest spread in the change of median values for all time slices is between -450 m^3/s (CCSM-RegCM, 2080-2099, A1B) and +300 m^3/s (MRI-MRI, 2080-2099, A1B). For the A2 scenario, a similar finding can be observed. While CCAM-CCAM and ECHAM3-REMO show a positive change for both time slices 2011-2030 and 2031-2050, the CCSM-MM5 shows a negative change (Figure 5.6). The largest spread in the change of median values for all time slices is between -440 m^3/s (CCSM-RegCM, 2080-2099, A2) and +400 m^3/s (ECHAM3-REMO, 2031-2050, A2).
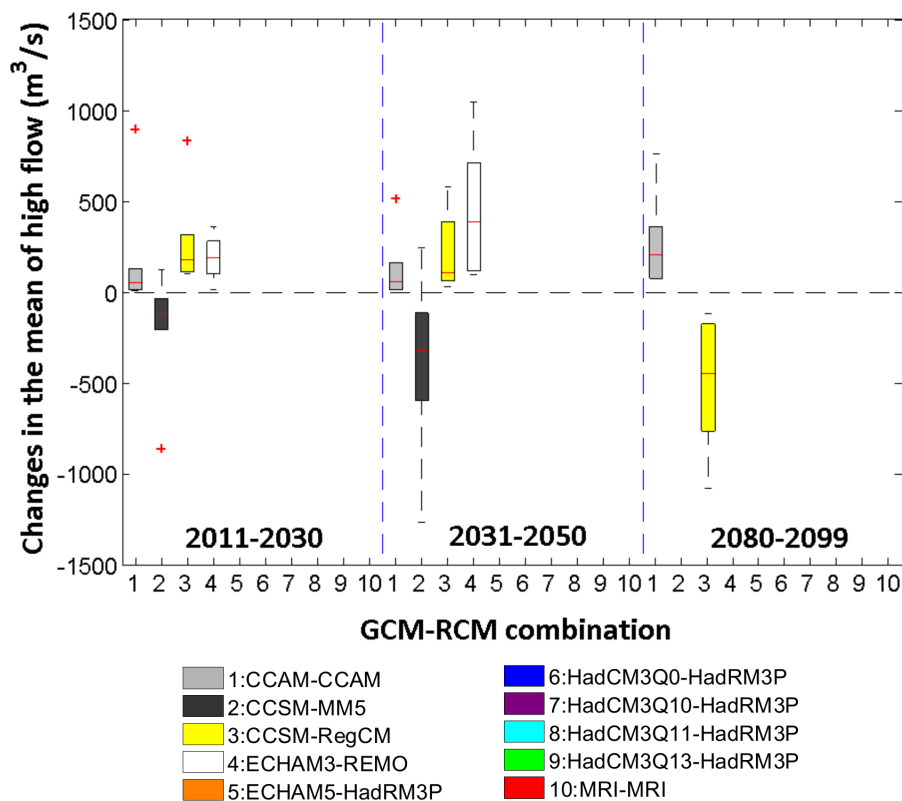
Figure 5.6: Range of the mean simulated high flows at Nong Son station using different GCM/RCM combinations and 6 different bias correction methods, represented by the boxes. The absolute changes of the mean values between future and baseline (future minus baseline) are shown for the A2 scenario.

Similarly, there is a large variation in the low flows between model combinations for the two scenarios. For scenario A1B, most models exhibit a negative projected change, except for the CCAM-CCAM, which points towards positive changes for all time slices (Figure 5.7). The same holds true for scenario A2 (Figure 5.8). Among all combinations, the CCSM-RegCM shows the largest negative change of the median value (about -5 m^3/s in 2080-2099, A2) while CCAM-CCAM shows the largest positive value (about +1.5 m^3/s in 2080-2099, A2).
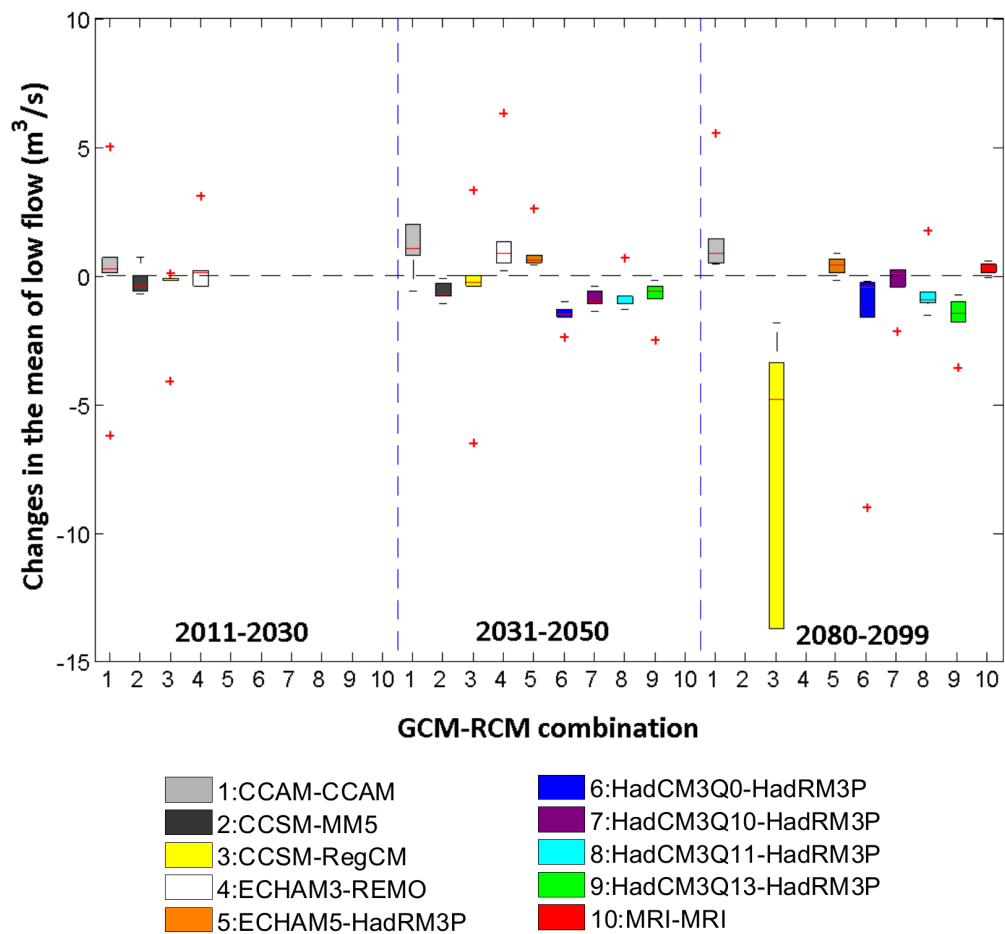
Figure 5.7: Range of the mean simulated low flows at Nong Son station using different GCM/RCM combinations and 6 different bias correction methods, represented by the boxes. The absolute changes of the mean values between future and baseline (future minus baseline) are shown for the A1B scenario.
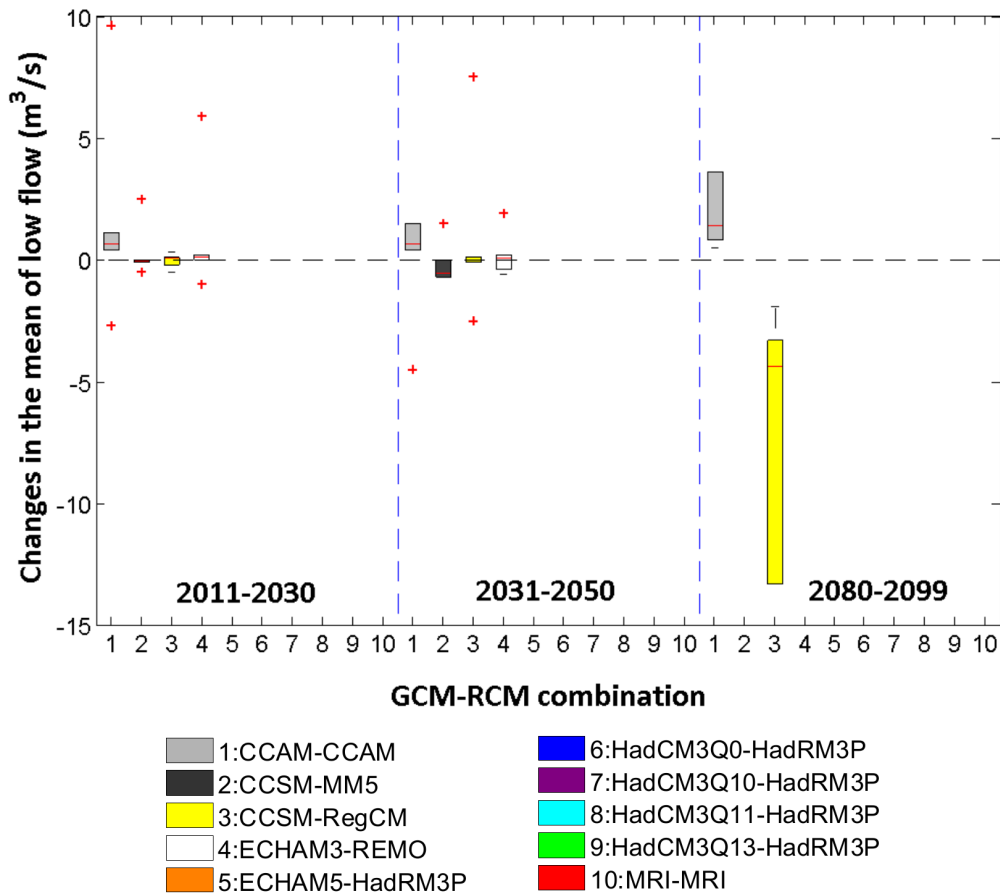
Figure 5.8: Range of the mean simulated low flows at Nong Son station using different GCM/RCM combinations and 6 different bias correction methods, represented by the boxes. The absolute changes of the mean values between future and baseline (future minus baseline) are shown for the A2 scenario.

5.3.2   Extreme value analysis: expected future high flow

The results of the high flow analysis are shown in Table 5.6 and Table 5.7 for the A1B scenario and the A2 scenario, respectively.

The high flow analysis is performed based on the observations at Nong Son station due to the limited skills of the applied BC methods in reproducing the extreme high flows for the baseline period. The observations are adjusted by the delta change approach instead (section 3.1.9), i.e. climate change induced discharge signals, simulated by WaSiM and forced by the raw GCM/RCM data are transferred to the observations according to equation 5.2.

Adjusted discharges for different return periods ranging from 2 to 50 years are based on yearly maxima. It can be seen that there is a high discrepancy among GCM/RCM

model ensemble members on whether the adjusted peak discharges will increase or decrease for the different time slices. Some models always show a positive signal in high flows for all time slices and scenarios (e.g. ECHAM3-REMO, HadCM3Q10-HadRM3P, HadCM3Q13-HadRM3P and MRI-MRI). The A2 scenario yields stronger positive changes of the high flows than the A1B scenario for ECHAM3-REMO (from +6% to +56%, depending on return periods and time slices).

Table 5.6: Adjusted high flows (m^3/s) for different return periods, A1B scenario, obtained from different GCM/RCM outputs (values of negative changes in italic).

Scenario/	A1B				
Return period (year)	2	5	10	20	50
2011-2030					
CCAM-CCAM	*3450*	*3475*	*3519*	*3615*	*3995*
CCSM-MM5	*3654*	*3678*	*3719*	*3809*	*4167*
CCSM-RegCM	5545	7178	7726	*7809*	*7896*
ECHAM3-REMO	6306	7410	8288	9186	10393
2031-2050					
CCAM-CCAM	5440	7646	9896	13145	19698
CCSM-MM5	*4242*	*4267*	*4311*	*4407*	*4782*
CCSM-RegCM	5903	*5921*	*5952*	6012	6269
ECHAM3-REMO	7657	9293	10510	11674	13116
ECHAM5-HadRM3P	6149	8005	9566	11245	13640
HadCM3Q0-HadRM3P	*4808*	*4846*	*4912*	*5057*	*5651*
HadCM3Q10-HadRM3P	*4675*	8194	12430	18716	31821
HadCM3Q11-HadRM3P	5782	*6284*	*6350*	*6368*	*6427*
HadCM3Q13-HadRM3P	*4901*	8636	13421	20927	37672
2080-2099					
CCAM-CCAM	6032	*6060*	*6100*	*6205*	*6605*
CCSM-RegCM	*3121*	*4413*	*5295*	*6188*	*7443*
ECHAM5-HadRM3P	*4710*	*5649*	*6462*	*7352*	*8642*
HadCM3Q0-HadRM3P	6907	8734	8773	8856	9139
HadCM3Q10-HadRM3P	7413	8718	9439	9966	10438
HadCM3Q11-HadRM3P	*4655*	7632	11238	16626	27997
HadCM3Q13-HadRM3P	6532	7618	8205	8629	*9008*
MRI-MRI	7117	11337	16178	23043	36585
Observed flow	**4947**	**6667**	**7574**	**8302**	**9076**

Table 5.7: Adjusted high flows (m^3/s) for different return periods, A2 scenario, obtained from different GCM/RCM outputs (values of negative changes in italic).

Scenario/ Return period (year)	2	5	A2 10	20	50
2011-2030					
CCAM-CCAM	*4744*	*6411*	7977	10148	14362
CCSM-MM5	5458	7137	*7209*	*7273*	*7475*
CCSM-RegCM	6869	8094	8128	*8201*	*8454*
ECHAM3-REMO	7243	9272	11077	13116	16194
2031-2050					
CCAM-CCAM	5240	*6613*	*7300*	*7873*	*8535*
CCSM-MM5	*4371*	*4466*	*4538*	*4703*	*5264*
CCSM-RegCM	6191	8296	9251	9900	10416
ECHAM3-REMO	8144	10244	12171	14414	17840
2080-2099					
CCAM-CCAM	6868	8874	9635	10014	10117
CCSM-RegCM	*3465*	*4384*	*4789*	*5060*	*5278*
Observed flow	**4947**	**6667**	**7574**	**8302**	**9076**

On the other hand CCAM-CCAM, CCSM-MM5, CCSM-RegCM, ECHAM5-HadRM3P, HadCM3Q0-HadRM3P and HadCM3Q11-HadRM3P show different signals in the change of the high flows for different time slices. For example CCAM-CCAM projects a positive signal for the A1B scenario in 2031-2050 and for the A2 scenario in 2080-2099, while it shows a negative signal for the A1B scenario in 2011-2030 and 2080-2099. CCSM-MM5 shows a negative signal of high flows in 2011-2030 and 2031-2050 for the A1B scenario and for the A2 scenario in 2031-2050, but it shows a positive signal for high flows with the frequency less than 10-year return period and a negative signal with higher return periods for the A2 scenario in 2011-2030. ECHAM5-HadRM3P shows a positive signal in 2031-2050, but a negative signal in 2080-2099 for the A1B scenario. In contrast, HadCM3Q0-HadRM3P shows a negative change for high flows in 2031-2050, but it exhibits positive signal for A1B in 2080-2099. HadCM3Q10-HadRM3P shows a positive signal for A1B in 2080-2099 but it shows a negative change for high flow with frequency less than 5-year return period and a very high positive change in the high flows with frequency larger than 20-year return period are simulated in the period 2031-2050 for A1B scenario.

In the period 2031-2050, very high changes in the high flows are simulated for

the A1B scenario. The HadCM3Q13-HadRM3P shows the largest positive change
(+315%) among others followed by HadCM3Q10-HadRM3P (+250%) and CCAM-
CCAM (+117%) for 50-year return period. Largest extremely high flow with return
period of 50 year is about four times higher than that of the observation in baseline
period. Interestingly, other realizations of the HadCM3-HadRM3, e.g. the Q11 and
Q13 runs even show negative changes for high flow at some return periods. There is
no individual model showing a continuous decrease of peak flows for all time slices.

Figure 5.9 exemplarily show results for the high flows, in combination with return
periods for period 2031-2050, A1B scenario. It can be clearly seen in the figure that
five curves (HadCM3Q10-HadRM3P, HadCM3Q13-HadRM3P, ECHAM3-REMO,
CCAM-CCAM and ECHAM5-HAdRM3P) are higher than that of observation whereas
other four curves (HadCM3Q0-HadRM3P, HadCM3Q11-HadRM3P, CCSM-MM5 and
CCSM-RegCM) are lower.
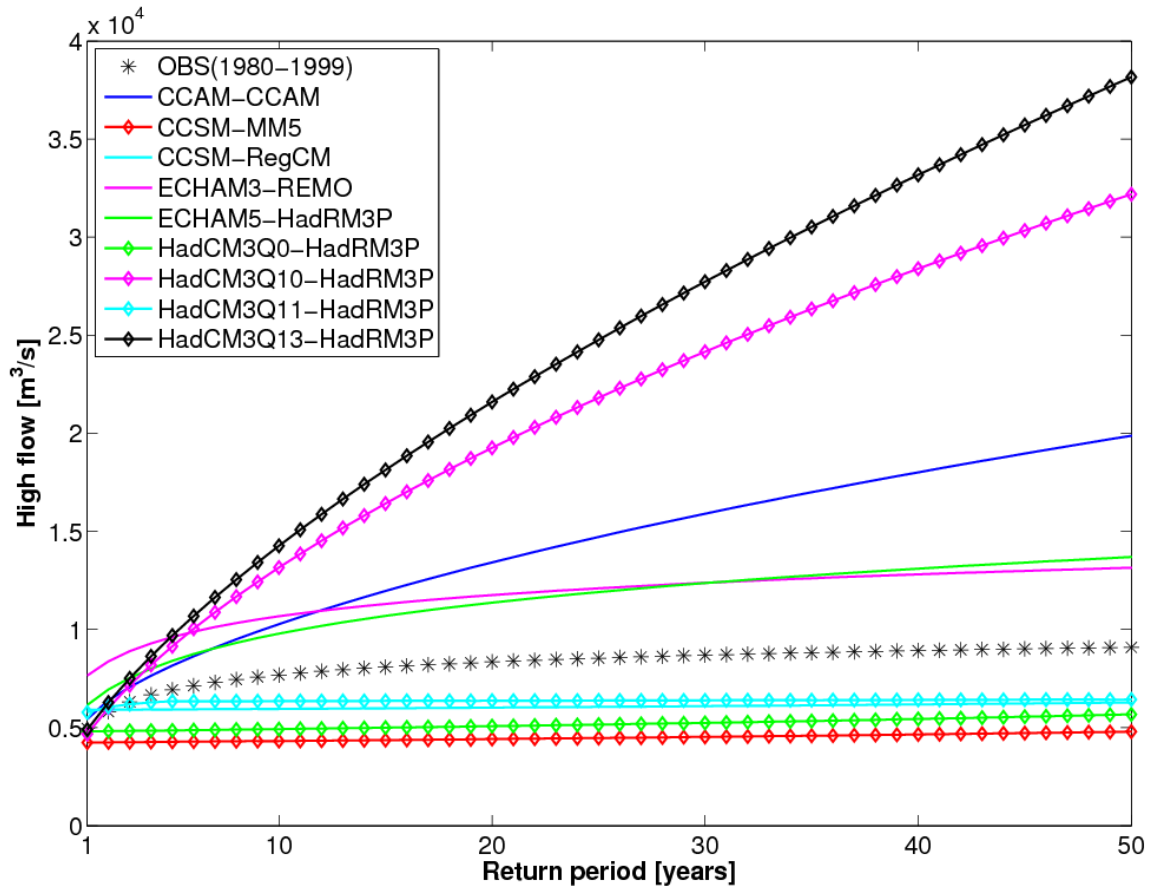
Figure 5.9: Maximum high flow for return periods ranging from 1 to 50 years, for
different GCM/RCM combinations and the time slice 2031-2050 (A1B scenario).

Of all considered GCM/RCM combinations, a return period of 50 years results

in the largest spread in the adjusted high flows, ranging between -56 % and +315 %, compared to observed flows. Although individual GCM/RCM combinations show contrasting directional changes, on average, the number as well as the magnitude of the positive signals is larger than that of the negative ones.

The statistical bootstrap test is applied to analyze the robustness of the results as a consequence of the reduced sample (n = 20). It is found that for all three parameters of the GEV, the H_o hypothesis, i.e. the values of the GEV parameters from n = 20 from same distribution with the values from n = 50 has to be accepted at $\alpha = 0.01$, giving a strong indication that the GEV fits (based on a 20-year period) are robust. This is critical, in particular for the shape parameter β, since a negative β value and $\beta = 0$ would indicate a Type III or a Type I extreme value distribution, respectively, whereas $\beta > 0$ indicates a Type II distribution. Based on the statistical tests, the chances to erroneously apply a Type II distribution instead of a Type III distribution are very low.

Figure 5.10 illustrates the probability distribution function (PDF) of scale parameter σ, location parameter λ and shape parameter β for n = 20 and n = 50. The vertical line at each figure illustrates the empirical corresponding value (σ, λ and β, respectively) from the observations (n = 20). It can be seen that this value is close to the mean value of the bootstrap PDF of both, the n = 20 and the n = 50 sample size. This finding holds true for three parameters.

Apart from the statistical bootstrap test, the impact of the sample size on the mean values and the standard deviations of the three GEV parameters is analyzed (Figure 5.11). It can be seen that the mean values are relatively robust for sample sizes of n = 20. The standard deviations of the location parameters are always larger than those of the scale parameters, the values decreases with increased sample sizes.

The impact of the sample size of the maximum likelihood estimator on the derived flow situation is also quantified. Figure 5.12 illustrates how the estimation of the GEV parameters based on different sample sizes propagate into the estimated high flows calculated for the observations (1980-1999). As shown in the figure, small sample sizes of n = 10 and n = 20 lead to non-robust estimations while sample sizes higher than n = 50 are converging (e.g. Hosking and Wallis, 1997; Coles and Dixon, 1999; Martins and Stedinger, 2000). The exact value of the relative differences related to a sample size of n = 50 for several selected return periods can be obtained from Table 5.8. Compared to a sample size of n = 50, the highest deviation is found for n = 20, resulting in a relative difference of 2.6% for a return period of 100 years. Overall, the estimated error of the limited sample size is expected to be small. In the same way, similar errors are assumed for the future time slices of 20 years (2020s, 2040s, and 2090s).
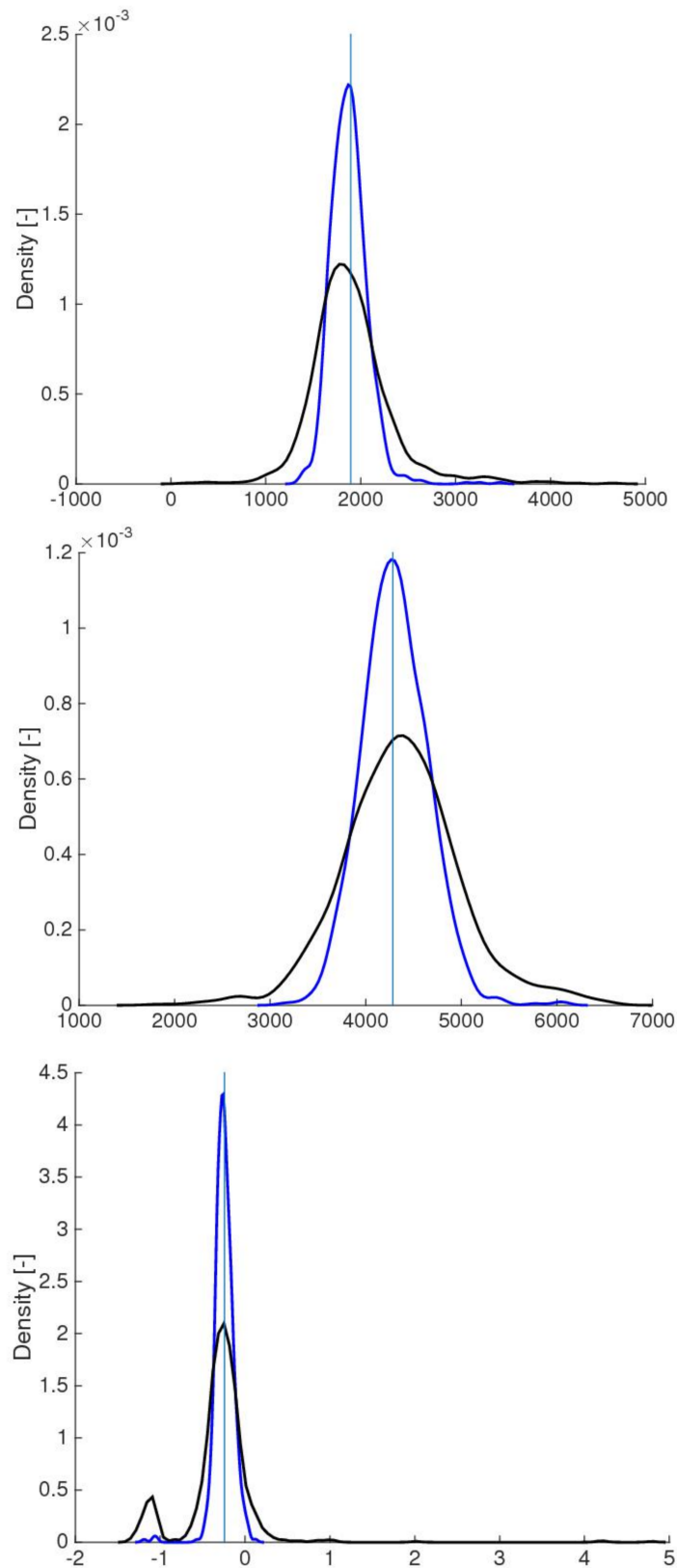
Figure 5.10: Probability Density Functions of fitted scale parameter σ (top), location parameter λ (middle) and shape parameter β (bottom), obtained from 1000 bootstrap samples from the observed high flow population for the period 1980-1999, based on a sample size of n = 20 (black line) and n = 50 (blue line).
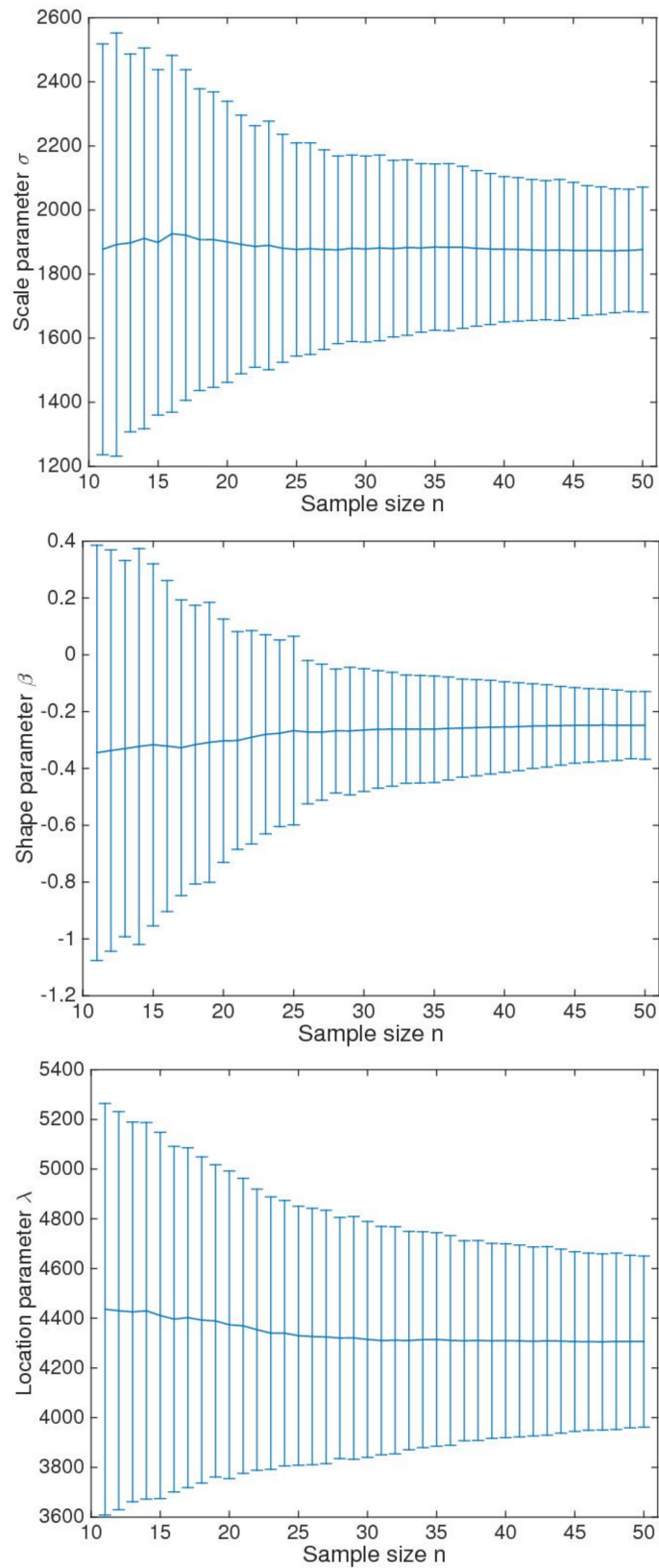
Figure 5.11: Fitted parameter of the GEV distribution based on the sample size (top: scale, middle: shape, bottom: location), ranging from 11-50. The horizontal line indicates the mean of the 1000 permutations, whereas the vertical whiskers represent the standard errors (+/- 1 standard deviation).
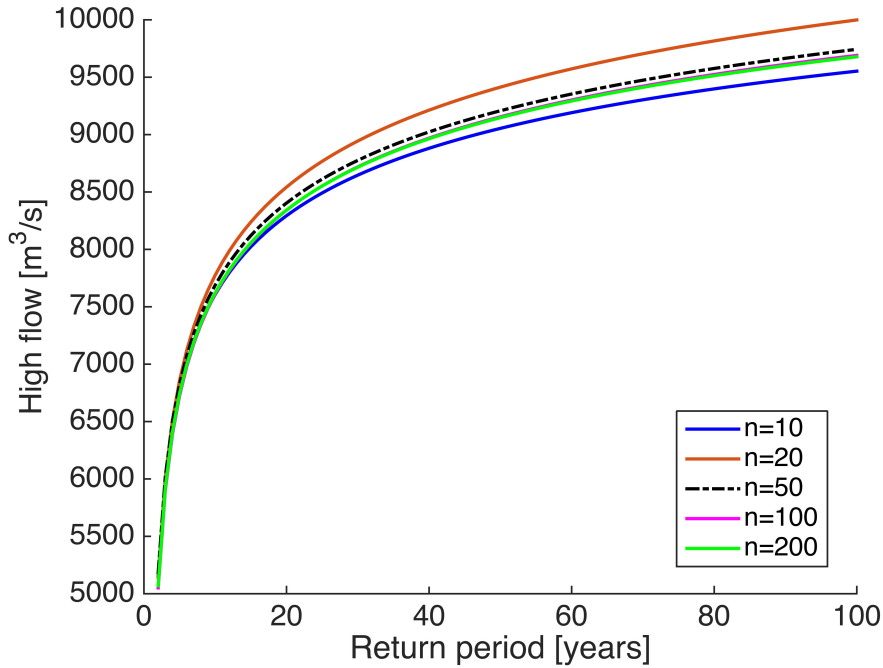
Figure 5.12: Impact of the sample size on the simulated high flows for different return periods.

Table 5.8: Relative difference [%] of small sample sizes on estimated high flows for different return periods. A sample size of n = 50 is taken as a reference.

Number of sample	Return period (years)					
	2	5	10	25	50	100
10	0.44	0.79	1.05	1.4	1.67	1.95
20	0.79	0.49	1.13	1.8	2.23	2.63
30	0.69	0.6	0.5	0.42	0.4	0.42
40	0.65	0.58	0.28	0.15	0.28	0.31

5.3.3   Extreme value analysis: expected future low flow

This section subsequently presents results of low flow analysis with different durations (1-, 7-, and 15-day moving average) rather than the annual minimum value since the information on mid long-term low flows is relatively important for the VGTB region.

The low flow analysis is performed based on the observations at Nong Son station due to the limited skills of the applied BC methods in reproducing the extreme low flows for the baseline period. The observations are adjusted by the delta change approach, i.e. climate change induced discharge signals, simulated by WaSiM and forced by the raw GCM/RCM data are transferred to the observations according to equation 5.2.

Table 5.9 to Table 5.11 shows results for the low flow frequency analysis for both the A1B and the A2 scenario under different time slices 2011-2030, 2031-2050 and 2080-2099. The results are obtained in the same way as high flow but now for 1-, 7- and 15-d annual minimum flow. As shown, there is a large variation in 1-day, 7-day and 15-day minimum flows between the different models. However, under both scenarios, for most considered models and for all time slices, low flows of different durations show a negative change compared to observed low flow frequency. Notably, realizations of HadCM3-HadRM3, CCSM-RegCM and MRI always show a negative signal for all time slices under both scenarios.

There is only the CCAM-CCAM model that shows positive signals for the A2 scenario in 2080-2099 for 1-day, 7-day and 15-day minimum flows and it shows contrasting directional changes for other time slices. ECHAM3-REMO often shows a positive signal for low flows with a return period larger than 10 years for both scenarios A1B and A2. Overall, the changes of low flows range between -68% and +39% across all considered scenarios and the negative changes are dominant. The 15-day low flow shows the largest negative signal (-68%), followed by 7-day low flow (-67%) and 1-day low flow (-65%). This implies less water availability in dry conditions, in which mid long-term duration (the 15-day) low flow is likely more severe in the future.

Table 5.9: Adjusted low flows (m^3/s) for different return periods, A1B scenario, obtained from different GCM/RCM outputs (values of negative changes in italic).

Scenario/ Return period (years)	Moving average	A1B 2	5	10	20	50
2011-2030						
CCAM-CCAM	1-day	*25.7*	*24.0*	*23.9*	*23.6*	22.9
	7-day	*28.8*	*24.1*	*23.3*	*23.2*	22.9
	15-day	*31.6*	*26.2*	*24.8*	*24.4*	24.3
CCSM-MM5	1-day	*28.1*	*24.6*	*22.5*	*20.4*	*17.6*
	7-day	*31.3*	*26.7*	*24.0*	*21.5*	*18.1*
	15-day	*34.8*	29.6	26.5	*23.6*	*19.9*
CCSM-RegCM	1-day	*25.9*	*22.1*	*20.2*	*18.6*	*16.8*
	7-day	*28.5*	*23.9*	*21.6*	*19.9*	*18.0*
	15-day	*31.1*	*26.0*	*23.5*	*21.5*	*19.4*
ECHAM3-REMO	1-day	*23.7*	*23.5*	23.2	22.8	21.3
	7-day	*26.2*	*26.0*	*25.7*	*25.0*	*23.1*
	15-day	*28.5*	*24.4*	*24.1*	*23.4*	*22.1*
2031-2050						
CCAM-CCAM	1-day	31.7	25.6	*22.6*	*20.0*	*16.7*
	7-day	35.8	28.1	*24.2*	*20.7*	*16.3*
	15-day	39.7	30.9	*26.1*	*22.0*	*16.7*
CCSM-MM5	1-day	*27.4*	*23.5*	*22.1*	*21.1*	*20.2*
	7-day	*30.5*	*25.6*	*23.7*	*22.5*	*21.2*
	15-day	*33.7*	*28.0*	*25.8*	*24.2*	*22.6*
CCSM-RegCM	1-day	*24.5*	*22.3*	*21.6*	*21.2*	*20.9*
	7-day	*27.0*	*24.1*	*23.1*	*22.4*	*21.8*
	15-day	*29.4*	*26.2*	*25.1*	*24.4*	*23.6*
ECHAM3-REMO	1-day	29.9	29.7	29.4	28.7	26.5
	7-day	33.2	32.9	32.4	31.5	28.8
	15-day	*34.8*	30.3	29.8	29.0	27.2
ECHAM5-HadRM3P	1-day	32.3	24.8	*21.4*	*18.9*	*16.1*
	7-day	36.1	27.1	*23.2*	*20.2*	*17.0*
	15-day	39.8	29.8	*25.4*	*22.0*	*18.4*
HadCM3Q0-HadRM3P	1-day	21.4	20.5	20.4	20.3	19.9
	7-day	23.9	21.0	20.9	20.9	20.6
	15-day	26.2	22.7	21.9	21.6	21.5
HadCM3Q10-HadRM3P	1-day	*24.0*	*20.7*	*19.8*	*19.5*	*19.4*
	7-day	*26.6*	*22.5*	*21.4*	*20.8*	*20.7*
	15-day	*29.3*	*24.8*	*23.3*	*22.5*	*22.1*
HadCM3Q11-HadRM3P	1-day	*23.2*	*18.8*	*17.3*	*16.4*	*15.6*
	7-day	*25.8*	*20.5*	*18.7*	*17.5*	*16.5*
	15-day	*28.2*	*22.3*	*20.3*	*19.0*	*17.8*
HadCM3Q13-HadRM3P	1-day	*26.3*	*22.3*	*20.6*	*19.3*	*18.0*
	7-day	*29.3*	*24.4*	*22.2*	*20.6*	*19.0*
	15-day	*32.4*	*26.9*	*24.3*	*22.3*	*20.3*

Table 5.10: Adjusted low flows (m³/s) for different return periods, A1B scenario, obtained from different GCM/RCM outputs (values of negative changes in italic).

Scenario/ Return period (years)	Moving average	A1B				
		2	5	10	20	50
2080-2099						
CCAM-CCAM	1-day	*26.9*	*22.9*	22.8	22.6	22.1
	7-day	*30.2*	*24.6*	*23.1*	*22.4*	22.2
	15-day	*33.0*	*27.0*	*25.4*	24.7	24.5
CCSM-RegCM	1-day	*9.7*	*8.5*	*7.9*	*7.4*	*6.9*
	7-day	*10.6*	*9.1*	*8.4*	*7.8*	*7.1*
	15-day	*11.4*	*9.8*	*8.9*	*8.2*	*7.5*
ECHAM5-HadRM3P	1-day	*26.4*	*21.6*	*20*	*19.1*	*18.3*
	7-day	*29.4*	*23.6*	*21.7*	*20.6*	*19.6*
	15-day	*32.3*	*25.9*	*23.8*	*22.5*	*21.5*
HadCM3Q0-HadRM3P	1-day	*21.6*	*19.6*	*19.6*	*19.5*	*19.3*
	7-day	*24.1*	*21.1*	*20.3*	*20.1*	*20.0*
	15-day	*26.6*	*23.0*	*22.0*	*21.4*	*21.0*
HadCM3Q10-HadRM3P	1-day	*18.1*	*15.4*	*15.4*	*15.3*	*15.0*
	7-day	*20.1*	*16.6*	*16.4*	*16.3*	*16.0*
	15-day	*22.0*	*18.2*	*17.3*	*17.2*	*17.1*
HadCM3Q11-HadRM3P	1-day	*22.8*	*18.5*	*17.2*	*16.4*	*15.6*
	7-day	*25.4*	*20.1*	*18.4*	*17.3*	*16.3*
	15-day	*27.7*	*22.0*	*20.1*	*18.8*	*17.7*
HadCM3Q13-HadRM3P	1-day	*23.7*	*19.2*	*17.3*	*15.8*	*14.3*
	7-day	*26.4*	*20.9*	*18.6*	*16.8*	*15.0*
	15-day	*29.2*	*23.0*	*20.2*	*18.1*	*16.1*
MRI-MRI	1-day	*24.6*	*20.8*	*20.3*	*20.2*	*20.0*
	7-day	*27.4*	*22.6*	*21.5*	*21.3*	*21.1*
	15-day	*30.4*	*24.7*	*23.1*	*22.4*	*22.0*
Observed flow	1-day	**28.9**	**24.2**	**22.5**	**21.3**	**20.1**
	7-day	**32.3**	**26.4**	**24.2**	**22.6**	**21.1**
	15-day	**35.6**	**29.0**	**26.3**	**24.4**	**22.5**

Table 5.11: Adjusted low flows (m³/s) for different return periods, A2 scenario, obtained from different GCM/RCM outputs (values of negative changes in italic).

Scenario/ Return period (years)	Moving average	A2				
		2	5	10	20	50
2011-2030						
CCAM-CCAM	1-day	*27.2*	*22.4*	*21.2*	*21.1*	20.8
	7-day	*30.6*	*24.5*	*22.6*	*21.5*	*20.7*
	15-day	*33.4*	*26.5*	*24.3*	*23.0*	*22.1*
CCSM-MM5	1-day	29.1	24.4	22.2	20.5	18.5
	7-day	*31.3*	*26.7*	*24.0*	*21.5*	*18.1*
	15-day	35.7	29.1	26.0	23.5	20.9
CCSM-RegCM	1-day	*26.9*	*22.1*	*20.3*	*19.1*	*17.8*
	7-day	*28.5*	*23.9*	*21.6*	*19.9*	*18.0*
	15-day	*32.3*	*25.8*	*23.3*	*21.5*	*19.7*
ECHAM3-REMO	1-day	29.6	29.3	29.0	28.2	25.8
	7-day	*26.2*	*26.0*	25.7	25.0	23.1
	15-day	*29.5*	*29.2*	28.7	27.6	24.9
2031-2050						
CCAM-CCAM	1-day	*26.5*	*22.9*	*22.5*	22.3	22.0
	7-day	*29.9*	*25.0*	*23.6*	22.9	22.6
	15-day	*32.8*	*27.4*	*25.7*	24.9	24.6
CCSM-MM5	1-day	*27.3*	*23.6*	*22.2*	*21.2*	20.2
	7-day	*30.5*	*25.7*	*23.8*	*22.5*	21.1
	15-day	*33.7*	*28.2*	*25.9*	*24.3*	22.6
CCSM-RegCM	1-day	*27.3*	*22.4*	*19.9*	*17.8*	*15.4*
	7-day	*30.1*	*24.1*	*21.0*	*18.6*	*15.8*
	15-day	*32.5*	*25.8*	*22.5*	*19.8*	*17.0*
ECHAM3-REMO	1-day	*26.2*	25.9	25.5	24.6	21.9
	7-day	*28.1*	27.9	27.4	26.2	23.6
	15-day	*30.7*	29.8	29.2	28.1	25.5
2080-2099						
CCAM-CCAM	1-day	29.7	24.5	23.3	23.1	22.9
	7-day	33.5	26.9	25.0	23.9	23.3
	15-day	37.2	29.7	27.4	26.1	25.3
CCSM-RegCM	1-day	*9.9*	*8.6*	*8.0*	*7.4*	*6.8*
	7-day	*10.8*	*9.3*	*8.5*	*7.8*	*7.1*
	15-day	*11.7*	*9.9*	*9.0*	*8.3*	*7.5*
Observed flow	1-day	**28.9**	**24.2**	**22.5**	**21.3**	**20.1**
	7-day	**32.3**	**26.4**	**24.2**	**22.6**	**21.1**
	15-day	**35.6**	**29.0**	**26.3**	**24.4**	**22.5**

Figure 5.13 shows 7-day low flows for different GCM/RCM combinations and the time slice 2080-2099 under the A1B scenario. The figure is constructed in the same way as for high flows, but with a 7-day moving-average low flow. The baseline's non-exceedance curve is higher than most of those from GCM/RCM combinations, indicating decreased low flows for all return periods. This holds true for the other time slices and scenarios.
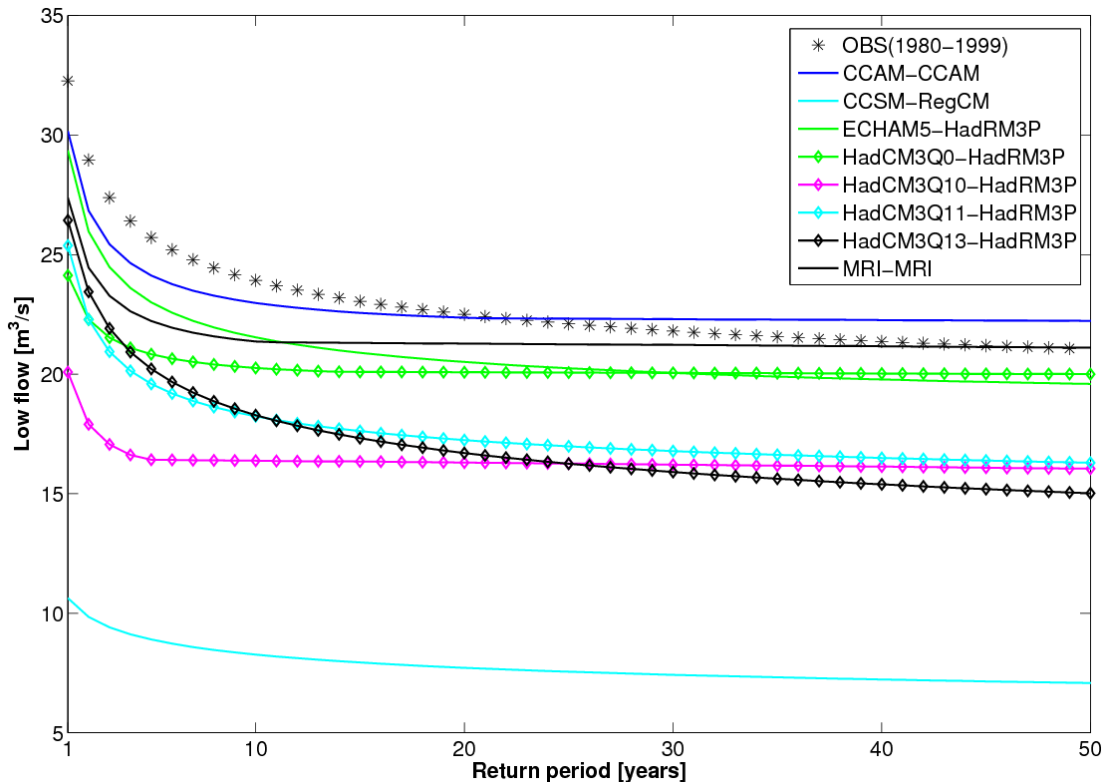
Figure 5.13: 7-day low flow for return periods ranging from 1 to 50 years, for different GCM/RCM combinations and the time slice 2080-2099 (A1B scenario).

Similar to the high flows, the bootstrap tests are done for the low flows, the fitted GEV distribution based on a limited sample size of n = 20 is found to be robust. The H_o hypothesis where values of the GEV parameters from n = 20 from the same distribution with the values from n = 50 has to be accepted at $\alpha = 0.01$ (Figure 5.14). The vertical line illustrates the empirical corresponding values from the observations (n = 20). This value is relatively close to the mean value of the bootstrap PDF of both, the n = 20 and the n = 50 sample size.

Similar to the high flows, the mean values for sample sizes of n = 20 is found to be robust, while the standard errors decrease with increasing sample size (Figure 5.15).
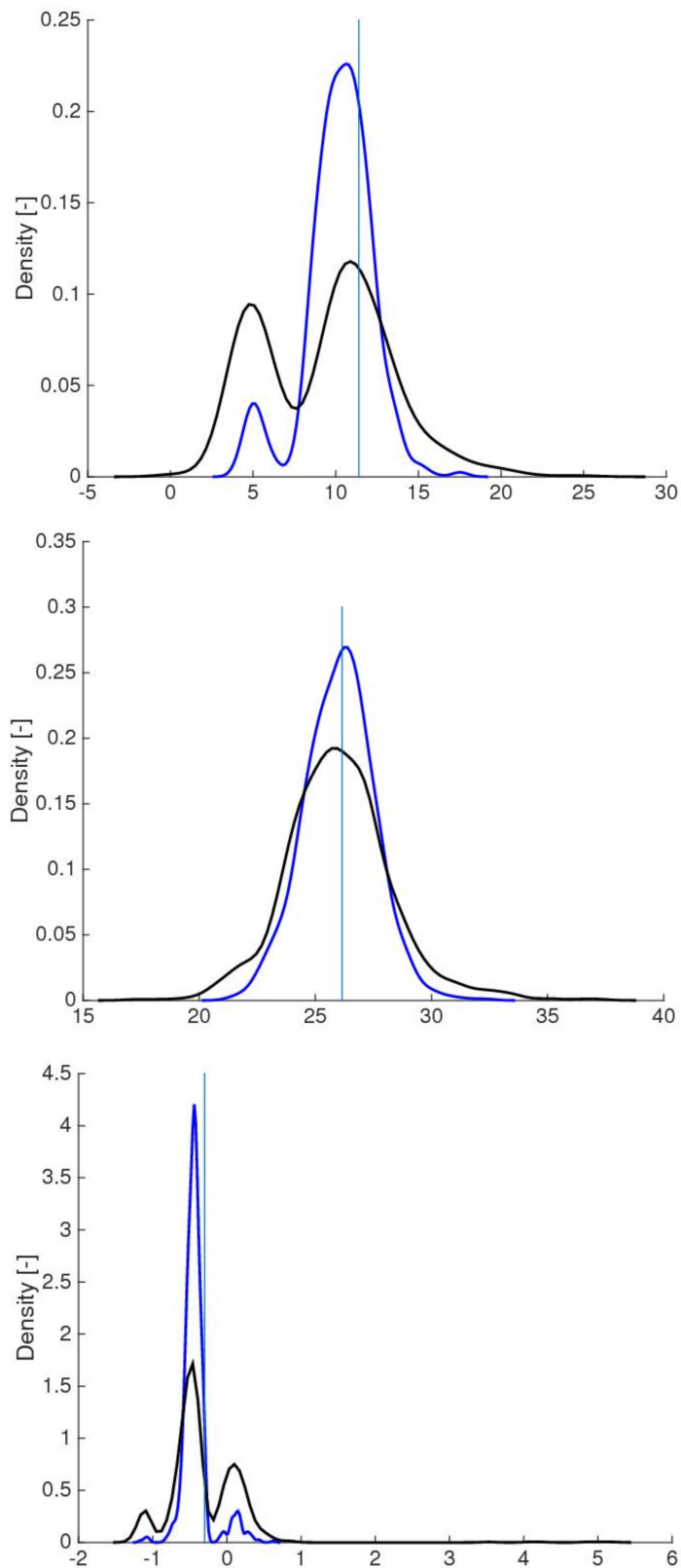
Figure 5.14: Probability Density Functions (PDF) of fitted scale parameter σ (top), location parameter λ (middle) and shape parameter β (bottom), obtained from 1000 bootstrap samples from the observed low flow population for the period 1980-1999, based on a sample size of n = 20 (black line) and n = 50 (blue line).
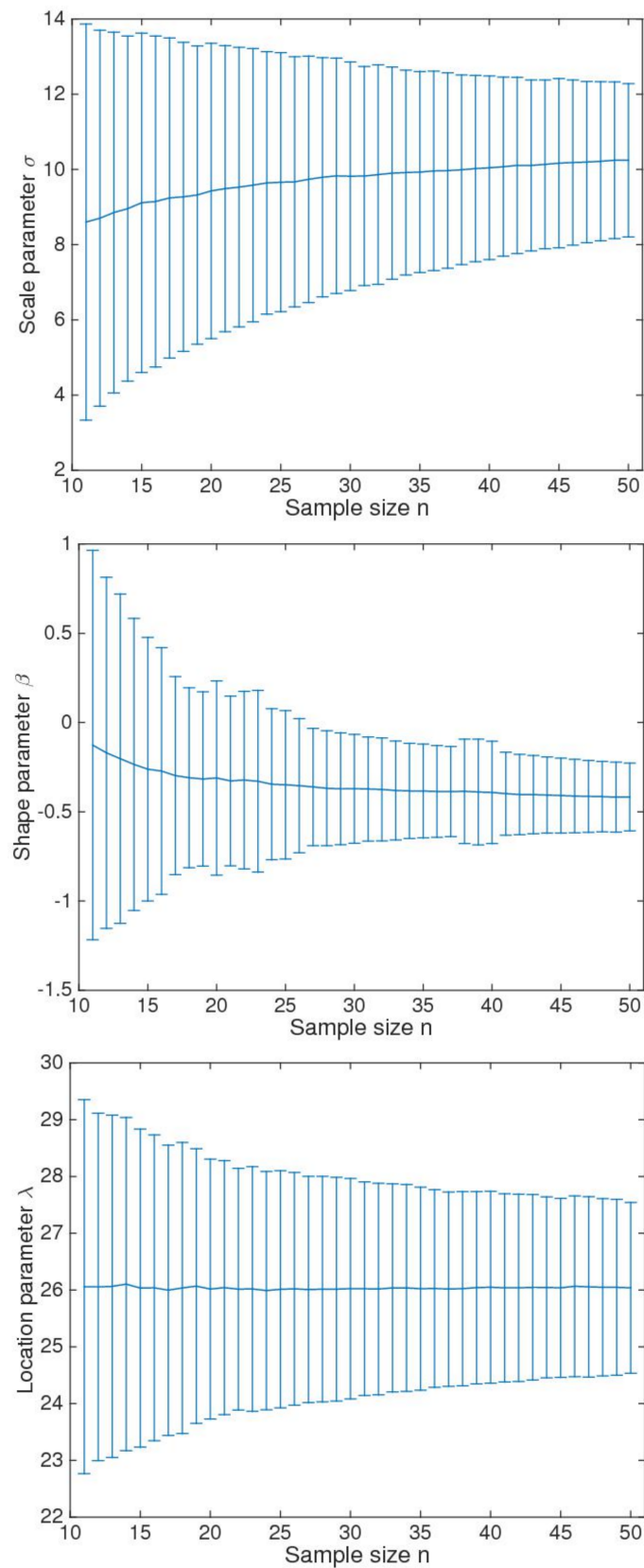
Figure 5.15: Fitted parameter of the GEV distribution based on the sample size (top: scale, middle: shape, bottom: location), ranging from 11-50. The horizontal line indicates the mean of the 1000 permutations, whereas the vertical whiskers represent the standard errors (+/- 1 standard deviation).

However, the impact of the small sample sizes, given as relative differences compared to a n = 50 sample size, on the estimated low flows is much higher (Figure 5.16).
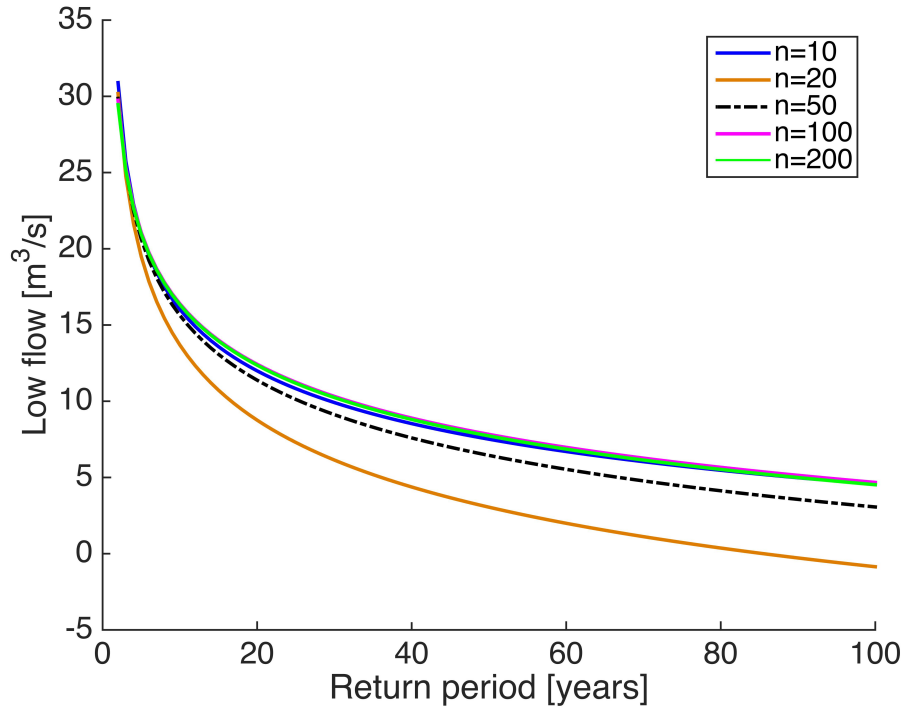
Figure 5.16: Impact of the sample size on the simulated low flows for different return periods.

Table 5.12 presents estimates of the relative errors for all resamples, 1000 Bootstrap resamples and for several different sample sizes.

Table 5.12: Relative difference [%] of small sample sizes on estimated low flows for different return periods. A sample size of n = 50 is taken as a reference.

Number of samples	Return period (years)					
	2	5	10	25	50	100
10	3.5	1.8	2.5	7	16.5	48.6
20	1.1	5.5	12.4	27.9	52.7	127.9
30	0.4	2.8	5.6	11.9	22.1	53.4
40	0.1	0.4	0.5	0.7	0.9	1.4

Of all considered sample sizes, the relative errors for n = 40 are smallest for all return periods. Compared to a sample size of n = 50, the highest deviation is found for n = 20, resulting in a relative difference of 128% for a return period of 100 years. This implies the interpretation of the derived low flows for the future is not robust, since the results are affected by high uncertainties.

5.3.4 Discussion

All considered GCM/RCMs model combinations underestimate the high flows and the majority of model combinations underestimate the low flows when using the raw RCM outputs. This is in line with e.g. Fowler et al. (2007); van Pelt et al. (2009); Fang et al. (2015). The possible reason for this underestimation may be attributed to the underestimation of extreme precipitation in the GCMs due to improper physical parameterizations (Delgado et al., 2014). The difficulty of GCMs in simulating monsoon characteristics and the associated precipitation frequencies and amounts for complex climatic regions across Asia is mentioned in various studies (e.g. Yang et al., 2008; Gain et al., 2011; Hoang et al., 2016). Another possible reason, but rather of minor importance, may originate from the underestimation of the discharges simulated with WaSiM, as mentioned earlier in the model calibration section (section 4.1.1).

Most of the considered bias correction methods applied to precipitation and temperature as input for WaSiM merely adjust extreme events. When forcing WaSiM with bias-corrected GCM/RCMs, discharges remain underestimated, particularly if LS, eQM, LOCI_monthly, PLT, and gamQM are used. This finding is consistent with the results of Fang et al. (2015), who stated that the LS and LOCI method underestimate extreme precipitation, and are therefore less suitable for hydrological impact assessment. In contrast to all other BC methods, simulations derived from the PLT_monthly method overestimate the projected discharges considerably. Similar deficiencies can also be found in previous studies (e.g. van Pelt et al., 2009; te Linde et al., 2010). Potentially, BC methods can also remove much of the spread in the driving variables, which could disrupt signals of climate change. There is no guarantee that the corrected statistics of the driving variables will remain unchanged for the future, especially if the physical processes are expected to change (Cloke et al., 2013). Thus, the application of BC methods may even add more uncertainties to climate change impact studies than using the raw climate projections (Teutschbein and Seibert, 2012).

These limitations require improved BC methods, especially for extreme hydrological flows. More sophisticated GCM/RCM output BC methods that also target extreme values, such as Copula-based approaches, are proposed (e.g. Laux et al., 2011; Mao et al., 2015). However, these BC methods are not applied here due to high computation demands. Considering the urgent need of information on expected future hydrological extremes for hydrological decision support, the delta change approach was used. It possibly provides another feasible option to adjust the observed extreme flows directly by the climate change signal, rather than correcting the WaSiM input data is suggested. Based on results adjusted by the delta change method, the projected hydrological extreme flows better transfer the GCM/RCM spread to the extreme high and low flows than any of the six considered BC methods. This spread,

i.e. differences in the magnitude of the projected extreme high and low flows, can be primarily associated to the selection (and the parameterization) of the GCM/RCM combinations as well as the emission scenarios (e.g. Xu et al., 2011; Jung et al., 2011), providing possible realizations of the expected future.

In this study, the extreme value analyses are based on relatively short time series of 20 years for the baseline as well as the scenario periods, similarly to other studies (e.g. Gain et al., 2011; Taye et al., 2011; Kidmose et al., 2013). Since larger periods are suggested to derive future high and low flows (e.g., Martins and Stedinger, 2000), further uncertainties can be expected due to potential non-robust estimates of the GEV distributions using the maximum likelihood method. By following a statistical bootstrap sampling strategy, these uncertainties can be roughly estimated (Coles and Dixon, 1999). It is found that the GEV parameter uncertainties have a stronger impact on the derived low flows, while only small impacts are identified for the high flows.

Considering the modeling chain applied in climate impact studies, GCMs are found to exhibit the largest uncertainties (e.g. Minville et al., 2008; Dobler et al., 2012b; Aich et al., 2014). But, considering a relatively large GCM/RCM ensemble, as done in this study, still remains the best option to quantify the potential spread of future hydrological extremes using impact models.[1]

---

[1]This chapter was published as Dang et al. (2017)

Chapter 6

Summary, conclusions and perspective

6.1 Overall summary

The first central objective of this study was to investigate the performance of a fully spatially distributed hydrological model for a weak infrastructure basin in Central Vietnam. The hydrological model WaSiM was set up and adapted to the upper part of the VGTB basin. The model was calibrated (1976-1981) and validated (1982-1988 and 1995-2000) using station rainfall and climatic reanalysis data. Both, the manual approach and the automate parameter estimation tool PEST (Doherty, 2002) were applied for the model calibration. A quantification of hydrological model parameter uncertainty was done for the region using a covariance analysis approach.

Second, an irrigation optimization model was developed and integrated with WaSiM to identify the optimal water-efficient irrigation technology, irrigation area and irrigation scheduling under limited water availabilities for a typical irrigation scheme which was elaborated jointly with focal groups of local stakeholders in the VGTB basin. The irrigation optimization model was designed to account for water shortages, often occurring during the summer-autumn season in this region. Irrigation strategies are derived based on different initial reservoir water levels at the beginning of the rice cropping season as well as different maximum water releases.

Third, the impact of climate change on extreme high and low river flows has been investigated using a complex modelling chain. The modelling chain consisted of six GCMs and six RCMs making up to ten combinations, six BC approaches, the fully distributed hydrological model WaSiM running in a continuous mode, the delta change method to adjust observed discharge, and the extreme frequency analysis to derive high and low flows for the future based on GEV distribution. In addition, a bootstrapping test was applied using observed discharges to quantify the uncertainties from the limited

95

availability data for fitting the GEV distribution. The possible effects on high and low flows were analysized and discussed.

6.2 Conclusions

The PhD thesis presented the first climate change impact assessment on hydrological extremes and is amongst the first modelling studies considering different irrigation technologies in the VGTB basin, Central Vietnam, under limited data availability. It has been analyzed how climate change could potentially impact on high and low flows and to identify a suitable irrigation management for the VGTB basin under limited water availability and thereby contributing to the hydrological and agricultural decision support in the region.

6.2.1 Hydrological modelling for the VuGia-ThuBon basin

The calibrated hydrological model WaSiM showed a good performance in the reproduction of the historical river flows of the VGTB basin, and was thus found suitable to study the hydrological dynamics in the tropical monsoon climate of Central Vietnam. Compared to lumped and semi-distributed hydrological models in operation, it provides another alternative to address additional, more physically-based research questions in the future.

The nonlinear parameter estimation tool PEST is a robust tool for automatic parameter estimation applied for the Vu Gia - Thu Bon basin, central Vietnam. Both model calibration approaches (manual approach and PEST tool) show a good agreement between modeled and observed discharges. The analysis of the confidence ellipses revealed small uncertainties for most of the estimated model parameters obtained using PEST tool.

6.2.2 Integrated hydrological-irrigation optimization model

An integrated hydrological and irrigation optimization model was developed to identify optimal agricultural management strategies in a typical rice irrigation scheme in Central Vietnam. Under different hypothesized initial water levels in the reservoir during the summer-autumn cropping season in 2012, the results predominantly suggest the usage of AWD rather than CF. The irrigation water input by AWD is less than that by CF, indicating that the AWD technology is more water-efficient. In addition, the model provides staggered irrigation schedules for AWD and CF for a typical rice irrigation system.

The AWD practice could be a promising irrigation option that can eliminate the increasing irrigation water stress in the Central Vietnam. The results also suggest that the AWD technology reduce the number of irrigation events significantly compared to CF. Thus costs induced in irrigation can be reduced if AWD is applied properly in the region.

The integrated hydrological-irrigation optimization model is found to be robust on different computing environments. The results demonstrate that this coupled modeling system may provide a useful tool for water and agricultural managers in the region to support crucial decisions such as suitable irrigation technologies, the irrigation scheduling as well as the irrigation area under given water constraints. Despite the aforementioned limitations, this study is intended to lay a foundation for further studies aiming at the improvement of existing or the design of new irrigation systems in the region. In the long run, the model can potentially be transferred to similar irrigation schemes in the region. However, actual experiments need to be set up in the region to validate the model results under different environmental conditions.

6.2.3 Impact of climate change on high and low flows

Due to limitations of the considered BC methods (applied to precipitation and temperature as input correction for WaSiM) for the assessment of the extreme flows, this PhD thesis concludes on the usage of the delta change approach (applied directly to the WaSiM output) to facilitate hydrological decision support.

In the VGTB basin, substantial changes in hydrological extremes concerning both high and low flows in the VGTB basin have been found. On the one hand, the future high flows are likely to increase, while low flows show a systematical reduction for all considered durations: 1-, 7- and 15-days moving average, indicating that low flow problems become more severe in the future and are probably more important than the increase in flood risk.

Conclusions about future changes of low flow and high flows are affected with high uncertainties, resulting from the different compartments of the modelling chain. In general, this limits the applicability in decision making in water management. Special care has to be taken if design numbers for flood protection and irrigation systems are derived, which are based on long return periods.

Large spreads of the magnitude (even with different signs) in the projected future flows are found. This highlights a challenge in quantifying future hydrological extreme changes. Therefore, the emphasize should be on the need for combined climate and hydrological ensemble simulations rather than single realizations in hydrological

impact analysis and caution should be taken when implementing any actions against climate change. The issue of impact of climate change on high and low flows should be considered and integrated into policy and development plan rather than merely focusing on evaluation the magnitude of effect of climate change on the high and low flows.

The applied SRES scenarios cover a RCP-equivalent range of 6-8 W/m^2, and still provide the only source of climate projections for hydrological decision support in the Vu Gia - Thu Bon basin due to the limited climate simulations based on different RCP scenarios.

6.3   Perspective

This PhD thesis made clear that climate change impact assessment on hydrological extremes remains a complex issue associated with uncertainties in climate change projections, model parameterization and structures, bias correction methods and extreme value analysis. Even though more recent climate simulations based on different RCP scenarios would be favorable, the applied SRES scenarios still provide the only source of climate projections for hydrological decision support in this region. The available data employed in this dissertation study cover a RCP-equivalent range of 6-8 W/m^2 only. Special care has to be taken if design numbers for flood protection and irrigation systems are derived, which are based on long return periods. Thus, encouraging more research on this topic is important in order to increase awareness and to help improve further investigations and predictions. Future research should take into consideration the following:

Hydrological changes of a basin are not solely dependent upon climate inputs but simultaneously driven by multiple factors such as land use/land cover (Laux et al., 2017), urbanization and irrigation works. Projected simulations were conducted with current land use and land cover conditions. This could lead to inaccuracies. Thus, possible changes in future land use and land cover, hydropower dam constructions and water transfer project from Thu Bon river to Vu Gia river resulted from a rapid development of the basin's socio-economy should be included in future studies so as to yield more comprehensive insights on hydrological regimes and water resources in the VGTB river basin.

The validation of the hydrological model was restricted to observed discharges only. Therefore, the validation should be extended to other variables e.g. estimated evapotranspiration, if observations become available. Moreover, the distributed hydrological model WaSiM should be applied for further regions having similar conditions to investigate the model performance.

Application of a wider range of RCP scenarios (if applicable i.e. more CORDEX data are available for East Asia domain) instead of SRES emission scenarios to account for improvements of GCMs' technical development as well as the emission scenarios.

Additional monetary (e.g. labor and reservoir operation costs) and environmental factors (different global warming potentials of the cropping technologies) are not included in the optimization model, thus a more detailed cost-benefit analysis is still missing and should be included in future studies.

The integrated hydrological and irrigation optimization model was developed and tested for one cropping cycle (2012) only. Applicability with long-term climate projections or seasonal climate forecasts will be more beneficial for decision making, i.e. for designing new irrigation schemes and for seasonal reservoir management. For this purpose, however, further modelling as well as actual field experiments in Central Vietnam is necessary to validate the strength and the benefit of the model system.

Bibliography

ADB (2011). Greater mekong subregion - environment operations center. review of macroeconomic data for quang nam province – vietnam. 67p.

Ahrends, A., Mast, M., Rodgers, C., and Kunstmann, H. (2008). Coupled hydrological-economic modelling for optimised irrigated cultivation in a semi-arid catchment of west africa. *Environmental Modelling & Software*, 23:385–395.

Aich, V., Liersch, S., Vetter, T., Huang, S., Tecklenburg, J., Hoffmann, P., Koch, H., Fournet, S., Krysanova, V., Müller, E. N., and Hattermann, F. F. (2014). Comparing impacts of climate change on streamflow in four large african river basins. *Hydrol. Earth Syst. Sci.*, 18(4):1305–1321.

Al-Juaidi, A. E., Kaluarachchi, J. J., and Mousa, A. I. (2014). Hydrologic-economic model for sustainable water resources management in a coastal aquifer. *Journal of Hydrologic Engineering*, 19(11):04014020.

Belder, P., Bouman, B., Cabangon, R., Guoan, L., Quilang, E., Yuanhua, L., Spiertz, J., and Tuong, T. (2004). Effect of water-saving irrigation on rice yield and water use in typical lowland conditions in asia. *Agricultural Water Management*, 65(3):193 – 210.

Bharati, L., Rodgers, C., Erdenberger, T., Plotnikova, M., Shumilov, S., Vlek, P., and Martin, N. (2008). Integration of economic and hydrologic models: Exploring conjunctive irrigation water use strategies in the volta basin. *Agricultural Water Management*, 95(8):925–936.

Bordoy, R. and Burlando, P. (2013). Bias correction of regional climate model simulations in a region of complex orography. *Journal of Applied Meteorology and Climatology*, 52(1):82–101.

Bouman, B., Lampayan, R., and Tuong, T. (2007). *Water Management in irrigated rice: coping with water scarcity.* Number 54 p in 1. International Rice Research Institute, Los Banos, Philippines.

Breuer, L., Huisman, J. A., Willems, P., Bormann, H., Bronstert, A., Croke, B. F. W., Frede, H. G., Graft, T., Hubrechts, L., Jakeman, A. J., Kite, G., Lanini, J., Leavesley, G., Lettenmaier, D. P., Lindstrom, G., Seibert, J., Sivapalan, M., and Viney, N. R. (2009). Assessing the impact of land use change on hydrology by ensemble modeling (luchem). i: Model intercomparison with current land use. *Advances in Water Resources*, 32(2):129–146.

Cai, X., McKinney, D., and Lasdon, L. S. (2003). Integrated hydrologic-agronomic-economic model for river basin management. *Journal of Water Resources Planning and Management*, 129(1):4–17.

Camici, S., Brocca, L., Melone, F., and Moramarco, T. (2013). Impact of climate change on flood frequency using different climate models and downscaling approaches. *J. Hydrol. Eng.*, 19(8):1–15.

Chai, T. and Draxler, R. R. (2014). Root mean square error (rmse) or mean absolute error (mae)? – arguments against avoiding rmse in the literature. *Geoscientific Model Development*, 7(3):1247–1250.

Chen, H., Xu, C.-Y., and Guo, S. (2012). Comparison and evaluation of multiple gcms, statistical downscaling and hydrological models in the study of climate change impacts on runoff. *Journal of Hydrology*, 434-435(0):36–45.

Chiew, F. H. S., Kirono, D. G. C., Kent, D. M., Frost, A. J., Charles, S. P., Timbal, B., Nguyen, K. C., and Fu, G. (2010). Comparison of runoff modelled using rainfall from different downscaling methods for historical and future climates. *Journal of Hydrology*, 387:10–23.

Cloke, H. L., Wetterhall, F., He, Y., Freer, J. E., and Pappenberger, F. (2013). Modelling climate impact on floods with ensemble climate projections. *Quarterly Journal of the Royal Meteorological Society*, 139(671):282–297.

Coles, S. G. and Dixon, M. J. (1999). Likelihood-based inference for extreme value models. *Extremes*, 2(1):5–23.

Cullmann, J., Krausse, T., and Saile, P. (2011). Parameterising hydrological models - comparing optimisation and robust parameter estimation. *Journal of Hydrology*, 404:323–331.

Cullmann, J., Mishra, V., and Peters, R. (2006). Flow analysis with wasim-eth - model parameter sensitivity at different scales. *Adv. Geosci.*, 9:73–77.

Dang, Q. T., Laux, P., and Kunstmann, H. (2017). Future high- and low-flow estimations for central vietnam: a hydro-meteorological modelling chain approach. *Hydrological Sciences Journal*, 62(11):1867–1889.

Delgado, J. M., Merz, B., and Apel, H. (2014). Projecting flood hazard under climate
  change: an alternative approach to model chains. *Nat. Hazards Earth Syst. Sci.*,
  14(6):1579–1589.

Di Luca, A., de Castro, M.Elía, R., and Laprise, R. (2012). Potential for added value
  in precipitation simulated by high-resolution nested regional climate models and
  observations. *Climate Dynamics*, 38(5-6):1229–1247.

Dobler, C., Bürger, G., and Stötter, J. (2012a). Assessment of climate change impacts
  on flood hazard potential in the alpine lech watershed. *Journal of Hydrology*, 460-
  461(0):29–39.

Dobler, C., Hagemann, S., Wilby, R. L., and Stötter, J. (2012b). Quantifying different
  sources of uncertainty in hydrological projections in an alpine watershed. *Hydrol.
  Earth Syst. Sci.*, 16(11):4343–4360.

Doherty, J. (2002). *PEST Model-Independent Parameter Estimation*. Number 336p in
  1. Watermark Numerical Computing, Australia.

Driessen, T. L. A., Hurkmans, R. T. W. L., Terink, W., Hazenberg, P., Torfs, P. J.
  J. F., and Uijlenhoet, R. (2010). The hydrological response of the ourthe catchment
  to climate change as modelled by the hbv model. *Hydrol. Earth Syst. Sci.*, 14(4):651–
  665.

Fang, G. H., Yang, J., Chen, Y. N., and Zammit, C. (2015). Comparing bias correction
  methods in downscaling meteorological variables for a hydrologic impact study in an
  arid area in china. *Hydrol. Earth Syst. Sci.*, 19(6):2547–2559.

FAO (1998). Crop evapotranspiration - guidelines for computing crop water require-
  ments. *FAO Irrigation and Drainage Paper 56*, M-56.

FAO (2012). *Harmonized World Soil Database (version 1.2)*. FAO, Rome, Italy and
  IIASA, Laxenburg, Austria.

Fiener, P. and Auerswald, K. (2009). Spatial variability of rainfall on a sub-kilometre
  scale. *Earth Surface Processes and Landforms*, 34(6):848–859.

Fiener, P., Neuhaus, P., and Botschek, J. (2013). Long-term trends in rainfall erosivity-
  analysis of high resolution precipitation time series (1937-2007) from western ger-
  many. *Agricultural and Forest Meteorology*, (171-172):115 – 123.

Fink, M., Fischer, C., Führer, N., Firoz, A. M. B., Viet, T. Q., Laux, P., and Flügel,
  W. A. (2013). Distributed hydrological modeling of a monsoon dominated river sys-
  tem in central vietnam. In *20th International Congress on Modelling and Simulation,
  Adelaide, Australia*. http://www.mssanz.org.au/modsim2013/.

Fowler, H. J., Blenkinsop, S., and Tebaldi, C. (2007). Linking climate change modelling to impacts studies: recent advances in downscaling techniques for hydrological modelling. *International Journal of Climatology*, 27(12):1547–1578.

Gain, A. K., Immerzeel, W. W., Sperna Weiland, F. C., and Bierkens, M. F. P. (2011). Impact of climate change on the stream flow of the lower brahmaputra: trends in high and low flows based on discharge-weighted ensemble modelling. *Hydrol. Earth Syst. Sci.*, 15(5):1537–1545.

GAMS (2016). *GAMS - The Solver Manuals.* Number 818p in 2. GAMS Development Corporation, Washington, DC, USA.

Gu, H., Yu, Z., Wang, G., Wang, J., Ju, Q., Yang, C., and Fan, C. (2015). Impact of climate change on hydrological extremes in the yangtze river basin, china. *Stochastic Environmental Research and Risk Assessment*, 29(3):693–707.

Gupta, H. V., Sorooshian, S., and Yapo, P. O. (1999). Status of automatic calibration for hydrologic models: Comparison with multilevel expert calibration. *Journal of Hydrologic Engineering*, 4(2):135–143.

Hall, M. J., van den Boogaard, H. F. P., Fernando, R. C., and Mynett, A. E. (2004). The construction of confidence intervals for frequency analysis using resampling techniques. *Hydrol. Earth Syst. Sci.*, 8(2):235–246.

Hay, L. E., Wilby, R. L., and Leavesley, G. H. (2000). A comparison of delta change and downscaled gcm scenarios for three mountainous basins in the united states1. *JAWRA Journal of the American Water Resources Association*, 36(2):387–397.

Ho, H. T. M., Phan, V. T., Le, N. Q., and Nguyen, Q. T. (2011). Extreme climatic events over vietnam from observational data and regcm3 projections. *Clim Res*, 49(2):87–100.

Hoang, P., Lauri, H., Kummu, M., Koponen, J., van Vliet, M., Supit, I., Leemans, R., Kabat, P., and Ludwig, F. (2016). Mekong river flow and hydrological extremes under climate change. *Hydrol. Earth Syst. Sci.*, 20:3027–3041.

Hong, M. H., Van, P. D. T., and Nguyen, H. T. (2015). So sanh luong nuoc va so lan tuoi cua cac ky thuat tuoi nuoc cho cay lua: Ap dung mo hinh he thong stella (in english: Comparing the amount of water and pumping times of irrigation techniques for rice: Appying model system stella). *Tap chi Khoa hoc Truong Dai hoc Can Tho (Journal of Sciences, Can Tho University)*, 40(2015):50–61.

Hosking, J. and Wallis, J. (1997). *Regional frequency analysis: An approach based on L-Moment.* Cambridge University Press, London, UK.

Hurkmans, R., Terink, W., Uijlenhoet, R., Torfs, P., Jacob, D., and Troch, P. A. (2010).
    Changes in streamflow dynamics in the rhine basin under three high-resolution re-
    gional climate scenarios. *J. Climate*, 23(3):679–699.

ICEM (2008). Strategic environmental assessment of the quang nam province hy-
    dropower plan for the vu gia-thu bon river basin, prepared for the adb, monre, moitt
    & evn, hanoi, viet nam. Technical Assistance Consultant's Report 204p, Interna-
    tional Centre for Environmental Management, Brisbane, Queensland, Australia.

IMHEN (2010). Impacts of climate change on water resources and adaptation measures.
    Technical report, Vietnam Institute of Meteorology, Hydrology and Climate Change
    IMHEN.

IMHEN and UNDP (2015). Viet nam special report on managing the risks of extreme
    events and disaster to advance climate change adaptation. Technical report ISBN
    978-604-904-623-0, [Tran, T., Neefjes, K., Ta, T. T. H., Nguyen, V. T., Mai, T. N.,
    Le, Q. T., Le, D. T., Huynh, T. L. H., Vo, T. S., Nguyen, T. H. T and Le, N. T].
    Vietnam Publishing House of Natural Resources, Environment and Cartography, Ha
    Noi, Vietnam.

IPCC (2007). Climate change 2007: Impacts, adaptation and vulnerability, contribu-
    tion of working group ii to the fourth assessment report of the intergovernmental
    panel on climate change. Technical Report 976 pp, [Parry, M., Canziani, O., Pa-
    lutikof, J., van der Linden, P and Hanson, C]. Cambridge University Press, United
    Kingdom.

IPCC (2013). Climate change 2013: The physical science basis. contribution of working
    group i to the fifth assessment report of the intergovernmental panel on climate
    change,. Technical Report 1535 pp, [Stocker, T.F., D. Qin, G.-K. Plattner, M. Tignor,
    S.K. Allen, J. Boschung, A. Nauels, Y. Xia, V. Bex and P.M. Midgley]. Cambridge
    University Press, Cambridge, United Kingdom and New York, NY, USA.

Jasper, K., Pierluigi, C., Dimitrios, G., and Fuhrer, J. (2004). Differential impacts of
    climate change on the hydrology of two alpine river basins. *Clim Res*, 26(2):113–129.

Jung, G. (2006). *Regional Climate Change and the Impact on Hydrology in the Volta
    Basin of West Africa*. PhD thesis, Forschungszentrum Karlsruhe and University of
    Augsburg.

Jung, I.-W., Chang, H., and Moradkhani, H. (2011). Quantifying uncertainty in ur-
    ban flooding analysis considering hydro-climatic projection and urban development
    effects. *Hydrol. Earth Syst. Sci.*, 15(2):617–633.

Kasei (2009). *Modelling impacts of climate change on water resources in the Volta
    Basin, West Africa*. PhD thesis, Mathematisch-Naturwissenschaftlichen Faculty,
    Rheinischen Friedrich-Wilhelms-University of Bonn.

Kay, A. L., Jones, R. G., and Reynard, N. S. (2006). Rcm rainfall for uk flood frequency estimation. ii. climate change results. *Journal of Hydrology*, 318:163–172.

Khazaei, M. R., Zahabiyoun, B., and Saghafian, B. (2012). Assessment of climate change impact on floods using weather generator and continuous rainfall-runoff model. *Int. J. Climatol.*, 32(13):1997–2006.

Kidmose, J., Refsgaard, J. C., Troldborg, L., Seaby, L. P., and Escrivà , M. M. (2013). Climate change impact on groundwater levels: ensemble modelling of extreme values. *Hydrol. Earth Syst. Sci.*, 17(4):1619–1634.

Kleinn, J., Frei, C., Gurtz, J., Lüthi, D. t. D., Vidale, P. L., and Schär, C. (2005). Hydrologic simulations in the rhine basin driven by a regional climate model. *J. Geophys. Res.*, 110(D4):n/a–n/a.

Klok, E. J., Jasper, K., Roelofsma, P., Gurtz, J., and Badoux, A. (2001). Distributed hydrological modelling of a heavily glaciated alpine river basin. *Hydrological Sciences Journal*, 46(4):553–570.

Klotz, E. and Newman, A. M. (2013). Practical guidelines for solving difficult mixed integer linear programs. surveys in operations research and management science.

Koch, T., Achterberg, T., Andersen, E., Bastert, O., Berthold, T., Bixby, R. E., Danna, E., Gamrath, G., Gleixner, A. M., Heinz, S., Lodi, A., Mittelmann, H., Ralphs, T., Salvagnin, D., Steffy, D. E., and Wolter, K. (2011). Miplib 2010 mixed integer programming library version 5. *Mathematical Programming Computation*, 3(2):103–163.

Kunstmann, H., Krause, J., and Mayr, S. (2006). Inverse distributed hydrological modelling of alpine catchments. *Hydrol. Earth Syst. Sci.*, 10(3):395–412.

Lampayan, R. M., Rejesus, R. M., Singleton, G. R., and Bouman, B. A. (2015a). Adoption and economics of alternate wetting and drying water management for irrigated lowland rice. *Field Crops Research*, 170:95 – 108.

Lampayan, R. M., Samoy-Pascual, K. C., Sibayan, E. B., Ella, V. B., Jayag, O. P., Cabangon, R. J., and Bouman, B. A. M. (2015b). Effects of alternate wetting and drying (awd) threshold level and plant seedling age on crop performance, water input, and water productivity of transplanted rice in central luzon, philippines. *Paddy and Water Environment*, 13(3):215–227.

Laux, P., Nguyen, P. N. B., Cullmann, J., Van, T. P., and Kunstmann, H. (2017). How many rcm ensemble members provide confidence in the impact of land-use land cover change? *International Journal of Climatology*, 37(4):2080–2100.

Laux, P., Phan, V. T., Lorenz, C., Tran, T., Ribbe, L., and Kunstmann, H. (2013). *High Performance Computing in Science and Engineering '12: Transactions of the High Performance Computing Center, Stuttgart (HLRS) 2012*, chapter Setting Up Regional Climate Simulations for Southeast Asia, pages 391–406. Springer Berlin Heidelberg.

Laux, P., Vogl, S., Qiu, W., Knoche, H. R., and Kunstmann, H. (2011). Copula-based statistical refinement of precipitation in rcm simulations over complex terrain. *Hydrol. Earth Syst. Sci.*, 15(7):2401–2419.

Leander, R. and Buishand, T. A. (2007). Resampling of regional climate model output for the simulation of extreme river flows. *Journal of Hydrology*, 332(3–4):487 – 496.

Lenderink, G., Buishand, A., and van Deursen, W. (2007). Estimates of future discharges of the river rhine using two scenario methodologies: direct versus delta approach. *Hydrol. Earth Syst. Sci.*, 11(3):1145–1159.

Levenberg, K. (1944). A method for the solution of certain non-linear problems in least squares. *Quarterly of Applied Mathematics*, 2(2):164–168.

Li, H. and Li, M. (2010). Sub-group formation and the adoption of the alternate wetting and drying irrigation method for rice in china. *Agricultural Water Management*, 97(5):700–706.

Liang, K., Zhong, X., Huang, N., Lampayan, R. M., Pan, J., Tian, K., and Liu, Y. (2016). Grain yield, water productivity and ch4 emission of irrigated rice in response to water management in south china. *Agricultural Water Management*, 163:319 – 331.

Mao, G., Vogl, S., Laux, P., Wagner, S., and Kunstmann, H. (2015). Stochastic bias correction of dynamically downscaled precipitation fields for germany through copula-based integration of gridded observation data. *Hydrol. Earth Syst. Sci.*, 19(4):1787–1806.

Marquardt, D. (1963). An algorithm for least-squares exstimation of nonlinear parameters. *J. Soc. Indust. Mathematics*, 11:431–441.

Martins, E. S. and Stedinger, J. R. (2000). Generalized maximum-likelihood generalized extreme-value quantile estimators for hydrologic data. *Water Resour. Res.*, 36(3):737–744.

Minville, M., Brissette, F., and Leconte, R. (2008). Uncertainty of the impact of climate change on the hydrology of a nordic watershed. *Journal of Hydrology*, 358:70–83.

MONRE (2012). Climate change, sea level rise scenarios for vietnam. Technical report, Ministry of Natural Resources and Environment of Vietnam.

Myung, I. J. (2003). Tutorial on maximum likelihood estimation. *Journal of Mathematical Psychology*, 47(1):90 – 100.

Nakicenovic, N., Alcamo, J., Davis, G., de Vries, B., Fenhann, J., Gaffin, S., Gregory, K., Griibler, A., Jung, T. Y., Kram, T., La Rovere, T., Michaelis, L., Mori, S., Morita, T., Pepper, W., Pitcher, H., Price, L., Riahi, K., Roehrl, A., Rogner, H. H., Sankovski, A., Schlesinger, M., Shukla, P., Smith, S., Swart, R., van Rooijen, S., Victor, N., and Dadi, Z. (2000). *Emissions Scenarios in: A Special Report of Working Group III of tiie Intergovernmental Panel on Climate Change.* Cambridge University Express.

Nash, J. and Sutcliffe, J. (1970). River flow forecasting through conceptual models part i - a discussion of principles. *Journal of Hydrology*, 10(3):282 – 290.

Nelson, A., Wassmann, R., Sander, B. O., and Palao, L. K. (2015). Climate-determined suitability of the water saving technology "alternate wetting and drying" in rice systems: A scalable methodology demonstrated for a province in the philippines. *PLoS ONE*, 10(12):1–19.

Ngo, D. T., Kieu, C., Thatcher, M., Nguyen, L. D., and Phan, V. T. (2014). Climate projections for vietnam based on regional climate models. *Clim Res*, 60(3):199–213.

Nguyen, D. C. and Ngo, V. H. (2010). Co so ly luan nghien cuu moi quan he giua luong mua thuc te va luong mua hieu qua cua cac vung thuoc cac he thong thuy nong tinh quang nam (in english: Research of relationship between actual rainfall and the effective rainfall in areas belong to quang nam irigation system). *Tap chi Khoa hoc ky thuat Thuy loi va Moi truong (Journal of Water resources and Environmental Enginerring)*, 29:104–110. ISSN: 1859-3941.

Nguyen, H. H., Vo, T. Q. N., Brown, P. R., Nguyen, T. M. P., and Singleton, G. R. (2010). *Rodent out breaks: Ecology and Impacts. Rodent impacts in lowland irrigated intensive rice systems in Vietnam.* International Rice Research Institute, Los Banos, Philippines, 289p.

Oke, T. R. (1987). *Boundary Layer Climates.* Psychology Press.

Pedroso, R. M. C. (2013). *Dimensioning Branched Water Distribution Networks for Agriculture.* PhD thesis, Rheinischen Friedrich-Wilhelms-University of Bonn.

Penman, H. L. (1978). Vegetation and the atmosphere. ed. monteithj. l.. london: Academic press. Vol. 1; principles:298.

Piani, C., Haerter, J. O., and Coppola, E. (2010). Statistical bias correction for daily precipitation in regional climate models over europe. *Theoretical and Applied Climatology*, 99(1):187–192.

Press, W. H., , Teukolsky, S. A., Vetterling, W. T., and Flannery, B. P. (1992). *Numerical recipes in C. The Art of Scientific Computing*. Cambridge University Press., second edition.

Prudhomme, C., Jakob, D., and Svensson, C. (2003). Uncertainty and climate change impact on the flood regime of small uk catchments. *Journal of Hydrology*, 277:1 – 23.

Quinn, N., Brekke, L., Miller, N., Heinzer, T., Hidalgo, H., and Dracup, J. (2004). Model integration for assessing future hydroclimate impacts on water resources, agricultural production and environmental quality in the san joaquin basin, california. *Environmental Modelling & Software*, 19(3):305 – 316. Concepts, Methods and Applications in Environmental Model Integration.

Rahman, M. R. and Bulbul, S. H. (2014). Effect of alternate wetting and drying irrigation for boro rice cultivation in bangladesh. *Agriculture, Forestry and Fisheries*, 3(2):86–92.

Rasmussen, J., Sonnenborg, T. O., Stisen, S., Seaby, L. P., Christensen, B. S. B., and Hinsby, K. (2012). Climate change effects on irrigation demands and minimum stream discharge: impact of bias-correction method. *Hydrol. Earth Syst. Sci.*, 16(12):4675–4691.

Raymond, A, K. (2009). *Modelling impacts of climate chchange water resources in the Volta basin, West Africa*. PhD thesis.

Rejesus, R. M., Palis, F. G., Rodriguez, D. G. P., Lampayan, R. M., and Bouman, B. A. (2011). Impact of the alternate wetting and drying (awd) water-saving irrigation technique: Evidence from rice producers in the philippines. *Food Policy*, 36(2):280 – 288.

Riahi, K., Rao, S., Krey, V., Cho, C., Chirkov, V., Fischer, G., Kindermann, G., Nakicenovic, N., and Rafaj, P. (2011). Rcp 8.5—a scenario of comparatively high greenhouse gas emissions. *Climatic Change*, 109(1):33.

Rosegrant, M., Ringler, C., McKinney, D., Cai, X., Keller, A., and Donoso, G. (2000). Integrated economic–hydrologic water modeling at the basin scale: the maipo river basin. *Agricultural Economics*, 24(1):33 – 46.

Rosenthal, R. (2016). *GAMS - A User's Guide*. GAMS Development Corporation, Washington, DC, USA. Tutorial.

Schmidli, J., Frei, C., and Vidale, P. L. (2006). Downscaling from gcm precipitation: a benchmark for dynamical and statistical downscaling methods. *International Journal of Climatology*, 26(5):679–689.

Schulla, J. (1997). *Hydrologische Modellierung von Fliessgebieten zur Abschatzung der Folgen van Klimaandenmgen.* PhD thesis, Verlag Geographisches Institut ETH Zurich. ETH 12018.

Schulla, J. (2012). *Model Description WaSiM (Water balance Simulation Model).* Hydrology Software Consulting J. Schulla, CH 8049 Zurich. Technical report 305p.

Schulla, J. and Jasper, K. (2000). Model description wasim-eth. Technical report, ETH Zurich.

Shabalova, M. V., van Deursen, W. P. A., and Buishand, T. A. (2003). Assessing future discharge of the river rhine using regional climate model integrations and a hydrological model. *Climate Research*, 23(3):233–246.

Sheffield, J. and Wood, E. F. (2008). Projected changes in drought occurrence under future global warming from multi-model, multi-scenario, ipcc ar4 simulations. *Climate Dynamics*, 31(1):79–105.

Smiatek, G. and Kunstmann, H. (2016). Expected future runoff of the upper jordan river simulated with a cordex climate data ensemble. *Journal of Hydrometeorology*, 17(3):865–879.

Souvignet, M., Laux, P., Freer, J. E., Cloke, H., Dang, T., Tran, T., Cullmann, J., Nauditt, A., Flügel, W.-A., Kunstmann, H., and Ribbe, L. (2014). Recent climatic trends and linkages to river discharge in central vietnam. *Hydrological Processes*, 28(4):1587–1601.

Sunyer, M., Madsen, H., and Ang, P. (2012). A comparison of different regional climate models and statistical downscaling methods for extreme rainfall estimation under climate change. *Atmospheric Research*, 103(0):119–128.

Tabbal, D., Bouman, B., Bhuiyan, S., Sibayan, E., and Sattar, M. (2002). On-farm strategies for reducing water input in irrigated rice; case studies in the philippines. *Agricultural Water Management*, 56(2):93 – 112.

Taye, M. T., Ntegeka, V., Ogiramoi, N. P., and Willems, P. (2011). Assessment of climate change impact on hydrological extremes in two source regions of the nile river basin. *Hydrol. Earth Syst. Sci.*, 15(1):209–222.

te Linde, A. H., Aerts, J. C. J. H., Bakker, A. M. R., and Kwadijk, J. C. J. (2010). Simulating low-probability peak discharges for the rhine basin using resampled climate modeling data. *Water Resour. Res.*, 46(3):n/a–n/a.

Teutschbein, C. and Seibert, J. (2012). Bias correction of regional climate model simulations for hydrological climate-change impact studies: Review and evaluation of different methods. *Journal of Hydrology*, 456-457:12 – 29.

Themeßl, M., Gobiet, A., and Leuprecht, A. (2011). Empirical-statistical downscaling and error correction of daily precipitation from regional climate models. *International Journal of Climatology*, 31(10):1530–1544.

Towler, E., Rajagopalan, B., Gilleland, E., Summers, R. S., Yates, D., and Katz, R. W. (2010). Modeling hydrologic and water quality extremes in a changing climate: A statistical approach based on extreme value theory. *Water Resour. Res.*, 46(11).

Tselioudis, G., Douvis, C., and Zerefos, C. (2012). Does dynamical downscaling introduce novel information in climate model simulations of precipitation change over a complex topography region? *International Journal of Climatology*, 32(10):1572–1578.

UN (2015). Making development sustainable: The future of disaster risk management. global assessment report on disaster risk reduction 2015. Technical Report 316p, Geneva, Switzerland: United Nations Office for Disaster Risk Reduction (UNISDR).

UNDP (2007). Human development report. fighting climate change: Human solidarity in a divided world. climate change and human development in viet nam. Technical Report 46, UNDP.

Uppala, S. M., KAllberg, P. W., Simmons, A. J., Andrae, U., Bechtold, V. D. C., Fiorino, M., Gibson, J. K., Haseler, J., Hernandez, A., Kelly, G. A., Li, X., Onogi, K., Saarinen, S., Sokka, N., Allan, R. P., Andersson, E., Arpe, K., Balmaseda, M. A., Beljaars, A. C. M., Berg, L. V. D., Bidlot, J., Bormann, N., Caires, S., Chevallier, F., Dethof, A., Dragosavac, M., Fisher, M., Fuentes, M., Hagemann, S., Holm, E., Hoskins, B. J., Isaksen, L., Janssen, P. A. E. M., Jenne, R., Mcnally, A. P., Mahfouf, J.-F., Morcrette, J.-J., Rayner, N. A., Saunders, R. W., Simon, P., Sterl, A., Trenberth, K. E., Untch, A., Vasiljevic, D., Viterbo, P., and Woollen, J. (2005). The era-40 re-analysis. *Quarterly Journal of the Royal Meteorological Society*, 131(612):2961–3012.

Van Genuchten, M. T. (1980). A closed frrom equation for predicting the hydraulic conductivity of unsaturated soils. *Soil Science Society*, 44:892–898.

van Pelt, S. C., Kabat, P., ter Maat, H. W., van den Hurk, B. J. J. M., and Weerts, A. H. (2009). Discharge simulations performed with a hydrological model using bias corrected regional climate model input. *Hydrol. Earth Syst. Sci.*, 13(12):2387–2397.

van Vuuren, D. P., Edmonds, J., Kainuma, M., Riahi, K., Thomson, A., Hibbard, K., Hurtt, G. C., Kram, T., Krey, V., Lamarque, J.-F., Masui, T., Meinshausen, M., Nakicenovic, N., Smith, S. J., and Rose, S. K. (2011). The representative concentration pathways: an overview. *Climatic Change*, 109(1):5.

Verbunt, M., Gurtz, J., Jasper, K., Lang, H., Warmerdam, P., and Zappa, M. (2003). The hydrological role of snow and glaciers in alpine river basins and their distributed modeling. *Journal of Hydrology*, 282(1-4):36 – 55. Mountain Hydrology and Water Resources.

Vogl, S., Laux, P., Qiu, W., Mao, G., and Kunstmann, H. (2012). Copula-based assimilation of radar and gauge information to derive bias-corrected precipitation fields. *Hydrol. Earth Syst. Sci.*, 16(7):2311–2328.

Vormoor, K., Lawrence, D., Heistermann, M., and Bronstert, A. (2015). Climate change impacts on the seasonality and generation processes of floods-projections and uncertainties for catchments with mixed snowmelt/rainfall regimes. *Hydrol. Earth Syst. Sci.*, 19(2):913–931.

Vu, M., Vo, N., Gourbesville, P., Raghavan, S., and Liong, S.-Y. (2017). Hydrometeorological drought assessment under climate change impact over the vu gia–thu bon river basin, vietnam. *Hydrological Sciences Journal*, 62(10):1654–1668.

Wagner, P. D., Fiener, P., Wilken, F., Kumar, S., and Schneider, K. (2012). Comparison and evaluation of spatial interpolation schemes for daily rainfall in data scarce regions. *Journal of Hydrology*, (464-465):388 – 400.

Wagner, S. (2008). *Water Balance in a Poorly Gauged Basin in West Africa Using Atmospheric Modelling and Remote Sensing Information*. PhD thesis, Institute for water research, University of Stuttgart. University of Stuttgart: H. 173.

Warscher, M. (2014). *Performance of Complex Snow Cover Descriptions in a Distributed Hydrological Model System and Simulation of Future Snow Cover and Discharge Characteristics.A Case Study for the High Alpine Terrain of the Berchtesgaden Alps*. PhD thesis, Faculty of Applied Computer Science, University of Augsburg.

WMO (2008). Manual on low-flow estimation and prediction. Operational hydrology report no. 50, World Meteorological Organization. WMO-No. 1029.

Xu, H., Taylor, R. G., and Xu, Y. (2011). Quantifying uncertainty in the impacts of climate change on river discharge in sub-catchments of the yangtze and yellow river basins, china. *Hydrol. Earth Syst. Sci.*, 15(1):333–344.

Yang, S., Zhang, Z., Kousky, V. E., Higgins, R. W., Yoo, S.-H., Liang, J., and Fan, Y. (2008). Simulations and seasonal prediction of the asian summer monsoon in the ncep climate forecast system. *Journal of Climate*, 21(15):3755–3775.

Zhang, Y., Tang, Q., Peng, S., Xing, D., Quin, J., Laza, R. C., and Punzalan, B. R. (2012). Water use efficiency and physiological response of rice cultivars under alternate wetting and drying conditions. *The Scientific World Journal*, 2012:10.

Curriculum Vitae

PERSONAL DATA

Name:	Dang Quang Thinh
Date of birth:	04.07.1978
Place of birth:	Nam Dinh, Vietnam
Nationality:	Vietnamese

EDUCATION

Oct 2013 - Mar 2017	PhD student Institute of Meteorology and Climate Research–Atmospheric Environmental Research (KIT/IMK-IFU), Campus Alpin Karlsruhe Institute of Technology, Garmisch-Partenkirchen and University of Augsburg, Augsburg, Germany
Oct 2008 - Apr 2010	Master of Science Institute for Water Education, UNESCO-IHE Delft, The Netherlands
Sep 1996 - Jun 2001	Bachelor of Hydrology and Environment Water Resources University Hanoi, Vietnam

LIST OF PUBLICATIONS

1. **T, Dang.**, R, Pedroso., P, Laux., H, Kunstmann. (2018). *Development of an integrated hydrological-irrigation optimization modelling system for a typical rice irrigation scheme in Central Vietnam.* Agricultural Water Management, 208(2018): 193-203.

2. **T, Dang.**, P, Laux., H, Kunstmann. (2017). *Future high and low flow estimations for Central Vietnam: A hydrometeorological modelling chain approach.* Hydrological Sciences Journal, 62(11):1867-1889.

3. Souvignet, M., Laux, P., Freer, J. E., Cloke, H., **T, Dang.**, T, Tran., Cullmann, J., Nauditt, A., Flugel, W. A., Kunstmann, H., and Ribbe, L. (2014). *Recent climatic trends and linkages to river discharge in Central Vietnam.* Hydrological Processes,

28(4):1587-1601.

WORKING EXPERIENCE

Apr 2017 - Present	Deputy Director Climate Change Research Center, Institute of Meteorology Hydrology and Climate Change, 23/62 Nguyen Chi Thanh, Dong Da, Hanoi, Vietnam
May 2012 - May 2013	Deputy Director Climate Change Research Center, Institute of Meteorology Hydrology and Climate Change, 23/62 Nguyen Chi Thanh, Dong Da, Hanoi, Vietnam
Aug 2011 - Apr 2012	Head Division for Adaptation Research to Climate Change Climate Change Research Center, Institute of Meteorology Hydrology and Environment, 23/62 Nguyen Chi Thanh, Dong Da, Hanoi, Vietnam
Jun 2010 - Jul 2011	Head Division of Hydrological Prediction Center for Hydrology and Water Resources, Institute of Meteorology Hydrology and Environment, 23/62 Nguyen Chi Thanh, Dong Da, Hanoi, Vietnam
Jun 2001 - Sep 2008	Assistant researcher Division of Hydrological Prediction Center for Hydrology and Water Resources, Institute of Meteorology Hydrology and Environment, 23/62 Nguyen Chi Thanh, Dong Da, Hanoi, Vietnam